To the Graduate Council:

I am submitting herewith a thesis written by James D. Selman, Jr. entitled "Computational Model of the Laser Induced Schlieren Technique in Sodium-Nitrogen Atmospheres." I have examined the final copy of this thesis for form and content and recommend that it be accepted in partial fulfillment of the requirements for the degree of Master of Science, with a major in Physics.

James W. L. Lewis, Major Professor

We have read this thesis
and recommend its acceptance:

Accepted for the Council:

The Graduate School

COMPUTATIONAL MODEL OF THE LASER INDUCED SCHLIEREN TECHNIQUE IN SODIUM-NITROGEN ATMOSPHERES

A Thesis

Presented for the

Master of Science

Degree

The University of Tennessee, Knoxville

James D. Selman, Jr.

December 1983

ACKNOWLEDGMENTS

During the progression of my research, I have found myself particularly indebted to my major professor and academic advisor, Dr. J. W. L. Lewis. His guidance and encouragement have been essential in the completion of this thesis. The patience and understanding of my wife, Pam, have also been instrumental in its completion. To Pam goes my thanks for the excellent work in typing the thesis. I would also like to acknowledge with thanks the UTSI computer center for the access to the computer necessary to verify the computational model.

ABSTRACT

An evaluation has been made of the feasibility of detecting trace species concentrations in a host gas mixture using a laser induced Schlieren Technique (LIST). A numerical prediction of the deflection of a probe laser beam intersecting the thermal lens caused by a resonantly absorbed laser pump beam which is tuned to a spectral line of the trace species has been found to be proportional to the concentration of the trace species at the intersection point of the two beams. Results from case studies are presented where the gas mixture is $Na-H_2O-N_2$ using Na as the absorbing trace species and H_2O as a nonabsorbing trace species. It is estimated that for the mixture with Mach numbers less than 0.1, the Na measurement sensitivity is on the order of 1 ppb for a 1 watt pump laser source with a 10^{-3} sec pulse width.

TABLE OF CONTENTS

LIST OF FIGURES

CHAPTER I

INTRODUCTION

Many application areas require the accurate measurement of trace gas contaminants in both static gas and flowfield environments. While several techniques are possible, most involve either disturbing the gas mixture or sacrificing real-time measurement. In some applications such as high temperature combustion studies or wind tunnel flows, probing of the mixture may be undesirable or difficult. In all applications where the gas density is variable, spatially-resolved and time-resolved measurements become essential.

To be successful, the measurement technique used should (1) be non-perturbing to the environment being measured, (2) yield results that are spatially and temporally resolvable, and (3) be capable of detecting exceedingly small concentrations of the trace species (on the order of 1 ppb). Several methods have developed into standard use, but have proven limited for measurement of trace gas species. For example, the accuracy of coherent anti-Stokes Raman scattering is degraded by signal contributions from the non-resonant electronic susceptibilities of the gas mixture [1]. Resonant flourescence scattering which requires quenching corrections [2], and absorption spectroscopy which is affected by line of sight temperature and density gradients are two other well-known techniques with bothersome limitations. Mass sampling probes perturb the gas mixture and are limited by calibration and mass resolution problems [3]. Use of opto-

acoustic spectroscopy (OAS) has had some success, but is limited by acoustic refraction effects [4].

A promising method which may satisfy the aforementioned requirements is the Laser Induced Schlieren Technique (LIST) proposed by Herman and Pohl [5]. LIST is a variation of opto-acoustic spectroscopy using the thermal lens effect caused by an absorbed laser traversing the gas mixture. This laser radiation, referred to as the pump radiation, is tuned to a spectral line of the trace species. The subsequent electronic (or vibrational) excitation energy caused by absorption of the pump is transferred from the trace species to the host gas molecule by electronic-(or vibrational) vibrational collisional exchanges. The energy then "relaxes" to translational energy by vibration-vibration (V-V), vibration-rotation (V-R), and vibration-translation (V-T) processes, and the transferred energy becomes measurable as a temperature rise (δT) in the host. The resulting temperature field along the path of the pump produces a change (δn) in the index of refraction (n_o) and creates a thermal lens. When a nonabsorbed probe laser beam intersects the thermal lens created by the pump beam, a deflection of the path of the probe beam results. Since the strength of the thermal lens effect is directly dependent on the temperature increase, and the temperature rise is directly dependent on the trace species' number density, the deflection of the probe would reasonably be expected to be a direct measure of the trace number density. The crossed beam arrangement is shown as Fig. 1.

LIST differs from OAS primarily in the time that the measurement is made. When the pump radiation enters the gas mixture, two time

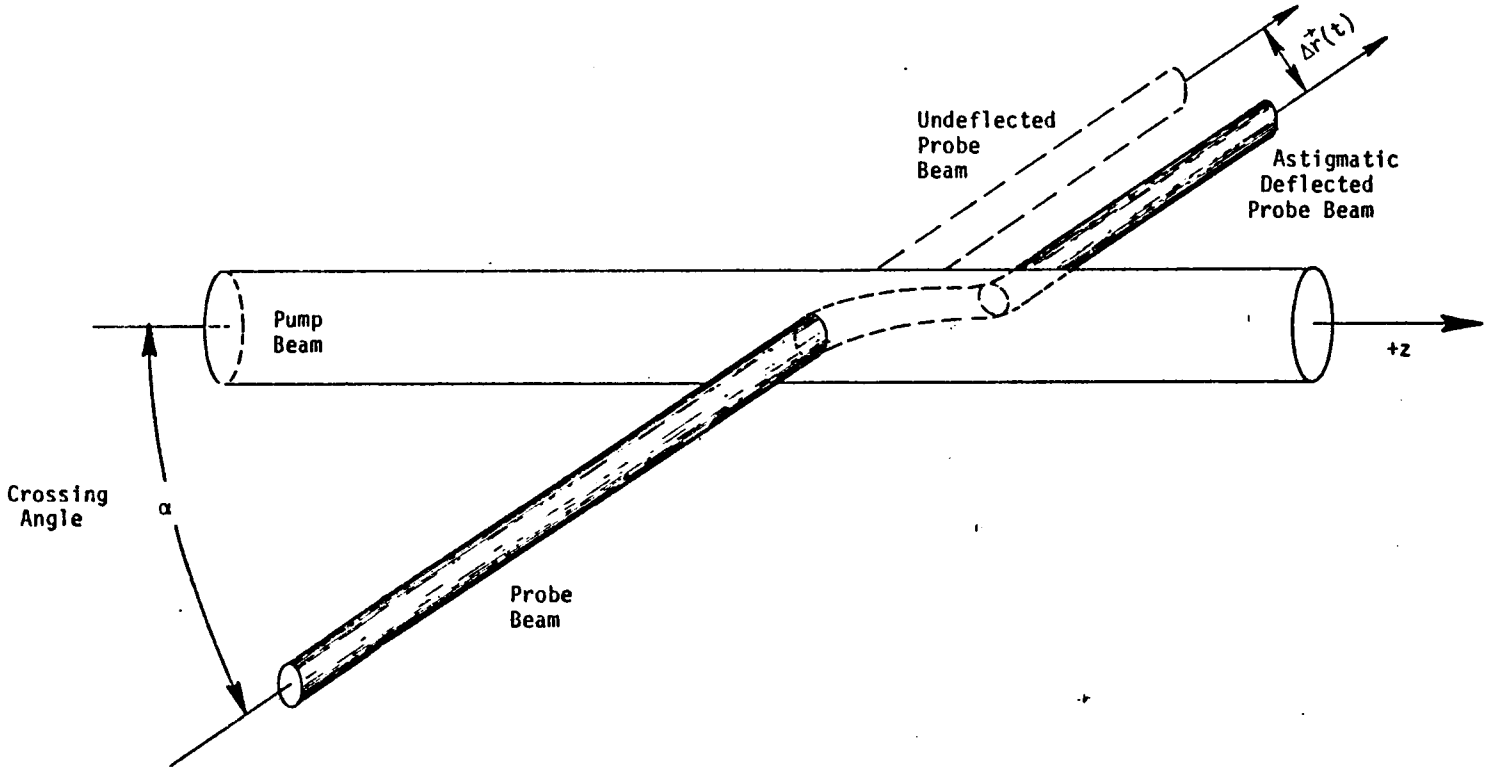

Figure 1. Crossing of Pump and Probe Beams.

domains are of importance. First, the accoustic domain is defined by the pressure wave generated by the initial transfer of energy to the trace species. The duration of this time region is of the order of magnitude of the time (τ_a) required for the acoustic pulse to travel across the pump beam. For an atmospheric pressure sample of N_2 at 300K and a beam radius of about 1mm, this time is on the order of 3 microseconds. After approximately 10-30 microseconds, isobaric conditions prevail within the thermal lens region; thus begins the second time (thermal) domain. The thermal domain lasts until the thermal lens either decays by conduction to ambient temperature or, by convection, is swept away by the flowfield. The mathematical difference in the two regions is that the opto-acoustic region requires solution of a wave equation, but the thermal region is found by solving the heat conduction equation.

Even though Hermann and later Bailey [6] both demonstrated that deflections do occur under such conditions, neither investigation examined the critical processes inherent in the LIST method. Specifically, these processes consist of the pumping scheme of the pump laser, the broadening characteristics of the gas, the radiational and collisional transfer mechanisms, and a time-dependent prediction of the deflection caused by a multiply-pulsed pump laser. Also not addressed in these reports are the limitations for a flowing gas sample.

For this work, a mixture of atomic sodium (Na) as the trace species and diatomic nitrogen (N_2) as the host species was assumed. The choice of gas species was made because the doublet sodium 3^2P electro-

nic levels are easily pumped and because the energy relaxation processes in N_2/Na mixtures are well known [7,8,9]. The molecular relaxation computer model (MRCM) written by D. H. Campbell [10] was modified to allow laser and line broadening processes and to utilize a more realistic pulse shape for the pump laser (see Appendix D). Inclusion of broadening processes produces a realistic model which is capable of describing the off-resonance pumping of both doublet levels.

The primary purpose of this work then becomes to investigate the feasibility of using LIST to measure trace species. To accomplish this goal, two secondary tasks must be accomplished. The spatial and temporal temperature field along the pump beam must be quantitatively calculated; the deflection of the probe beam must be predicted as a function of time and space. These tasks are accomplished by combining Campbell's MRCM with the temperature increase model of Bailey to describe the time-space behavior of the thermal lens produced by the pump beam. These results are then incorporated into an optical ray deflection computation to describe time dependent deflection of the probe beam. The following sections of this work describe the computational models of the pump and probe processes and the result of the computation. Finally, an assessment of the feasibility is presented for the use of LIST to measure the concentration of trace gas species.

CHAPTER II

THEORY

A. Theoretical Considerations

Deflection of any light ray requires simply a change in the index of refraction of the media through which it propagates. The ray's path of lengths may be quantitatively predicted by the eikonal equation [11]

$$\frac{d}{ds}\left(n\frac{d\vec{r}}{ds}\right) = \vec{\nabla}n$$

For present purposes, assume that the cartesian coordinate system is used and that the ray lies sufficiently close to the z axis that the paraxial ray approximation may be used. Using $\vec{r} = x\hat{i} + y\hat{i} + z\hat{k}$, the eikonal then becomes

$$d/dz\ \left[n\left((dx/dz)\hat{i} + (dy/dz)\hat{i} + \hat{k}\right)\right] = \vec{\nabla}n$$

If the beam is initially injected into a vacuum such that $n = n_o = 1.00$ then

$$(d^2x/dz^2)\hat{i} + (d^2y/dz^2)\hat{j} = 0$$

or

$$d^2x/dz^2 = 0$$

and

$$d^2y/dz^2 = 0$$

These two vector components describe a linear vector whose slope is constant, so that no deflection occurs. Replacing the vacuum with a medium of constant index of refraction (n_o) results in the two

components

$$\frac{d}{dz}\left(n_o \frac{dx}{dz}\right) = 0 \qquad \frac{d}{dz}\left(n_o \frac{dy}{dz}\right) = 0 \quad ,$$

and the results are similar with no deflection and constant slope.

Any variation in the index of refraction such that n becomes spatially dependent, n(x,y,z,t), will make the right side of the eikonal non-zero. Suppose the index of refraction now varies only along the z axis but is constant in x and y. Then the eikonal becomes

$$\left(dn(z)/dz\right)\left[(dx/dz)\hat{i} + (dy/dz)\hat{j} + \hat{k}\right] +$$
$$n(z)\left[(d^2x/dz^2)\hat{i} + (d^2y/dz^2)\hat{j}\right] = \left[dn(z)/dz\right]\hat{k}$$

giving the vector components

$$\left(\frac{dn}{dz}\right)\left(\frac{dx}{dz}\right) + n\left(\frac{d^2x}{dz^2}\right) = 0 \qquad \left(\frac{dn}{dz}\right)\left(\frac{dy}{dz}\right) + n\left(\frac{d^2y}{dz^2}\right) = 0$$

and

$$dn/dz = dn/dz \qquad \text{(an identity)} \quad .$$

A z dependent case which will illustrate one aspect of the temperature calculation in the following section is the propagation of the pump beam in an absorbing medium for which the transmitted intensity is described by Beer's law. In Beer's law absorption the media absorbs incident radiation according to the relation [12]

$$I = I_o e^{-\beta z}$$

where β is the absorption coefficient. Assume now that the change in index of refraction is directly dependent on the Beer's Law absorption process so that for a gas ($1 \leq n_o \leq n_o + C_o$) with $z_o \leq z \leq z_s$ where z_s is the z coordinate of the measurement

$$n(z) = n_o + C_o(1 - e^{-\beta z}) \quad .$$

C_o is a constant such that the behavior of the gas as $\beta \to \infty$ is known to be $n_o \to n_o + C_o$. The indicial equation representing the two components is given by

$$(dn/dz)(dx_i/dz) + n\,(d^2x_i/dz^2) = 0 \qquad \begin{matrix} x_{i=1} = x \\ x_{i=2} = y \end{matrix}$$

A general solution to this equation may be written immediately as

$$x_i = \left(A_i D_o/\left(\beta(n_o + C_o)\right)\right)[\beta z + \ln(n(z))] + B_i \ ,$$

or in vector notation, the deflected ray path $\vec{r}_d$ is given by

$$\vec{r}_d = \vec{A}_d\left(1/\beta(n_o + C_o)\right)[\beta z + \ln(n(z))] + \vec{B}_d \qquad \begin{matrix} \vec{A}_d = A_{xd}\hat{i} + A_{yd}\hat{j} \\ \vec{B}_d = B_{xd}\hat{i} + B_{yd}\,\hat{j} + B_{zd}\hat{k} \end{matrix}$$

The absolute deflection ($||\,\Delta\vec{r}\,||$) may be defined by the magnitude of the vector difference (see Fig. 1) of $\vec{r}_d$ and the incident beam path $\vec{r}_o$

$$||\,\Delta\vec{r}\,||^2 = |\,(\vec{r}_d - \vec{r}_o)\,|^2 = \vec{r}_d^{\,2} + \vec{r}_o^{\,2} - 2\beta(\vec{r}_o \cdot \vec{r}_d)$$

To illustrate the results obtainable from the eikonal formulation, let $\vec{r}_o$ and $\vec{r}_d$ have identical slopes at the initial starting position, $z = z_o$. The two vectors then become

$$\vec{r}_o = \vec{A}_o D_o(n_o z) + \vec{B}_o$$

$$\vec{r}_d = \frac{\vec{A}_o n_o}{\beta} D_o\left[\beta z_o + \frac{\beta(z - z_o) + \ln\left(n(z)/n(z_o)\right)}{\left(1 - C_o \exp(-\beta z_o)/n(z_o)\right)}\right] + \vec{B}_o$$

where $\vec{A}_o$ and $\vec{B}_o$ are constant vectors describing the initial position and slope of the two rays, D_o is a multiplicative constant (let $D_o \equiv 1$) and n_o is the initial index of refraction. By defining an intersection point along the z axis as (x_i, y_i, z_i) the use of the vector equation

$$(\vec{r} - \vec{r}_o) = k\vec{\Omega}$$

where k is a magnitude to be determined, yields the value of $\vec{A}_o$ and $\vec{B}_o$ as

$$\vec{A}_o = (\Delta x/\Delta z)\hat{i} + (\Delta y/\Delta z)\hat{j}$$

and

$$\vec{B}_o = \Delta x\hat{i} + \Delta y\hat{j} + \Delta z\hat{k}$$

where

$$\Delta x = x_i - x_o$$

$$\Delta y = y_i - y_o$$

$$\Delta z = z_i - z_o \quad .$$

The absolute deflection then becomes

$$||\Delta\vec{r}|| = \frac{n_o}{\beta}\left[\beta(z - z_o) + \frac{\beta(z - z_o) + \ln(n(z)/n(z_o))}{\beta\left(1 + C_o\exp(-\beta z_o)/n(z_o)\right)}\right]|\vec{A}_o| \quad .$$

For a specific case of N_2 at STP and $|\vec{A}_o| \equiv 1$, $z - z_o = 110$ cm, $C_o = -0.0003$ and $n_o = 1.0003$, a graph of $||\vec{\Delta r}||$ vs β for this case is given as Fig. 2.

It becomes obvious from this simple case that as the ray traverses the gas, the deflection is dependent on the index of refraction. What is not so obvious is the dependence of the deflection on the density and temperature. It will be shown in the following section that for the isobaric thermal wave domain, the temperature and index of refraction are related by

$$\delta n = -\Lambda\left(\frac{n_o - 1}{T}\right)\delta T$$

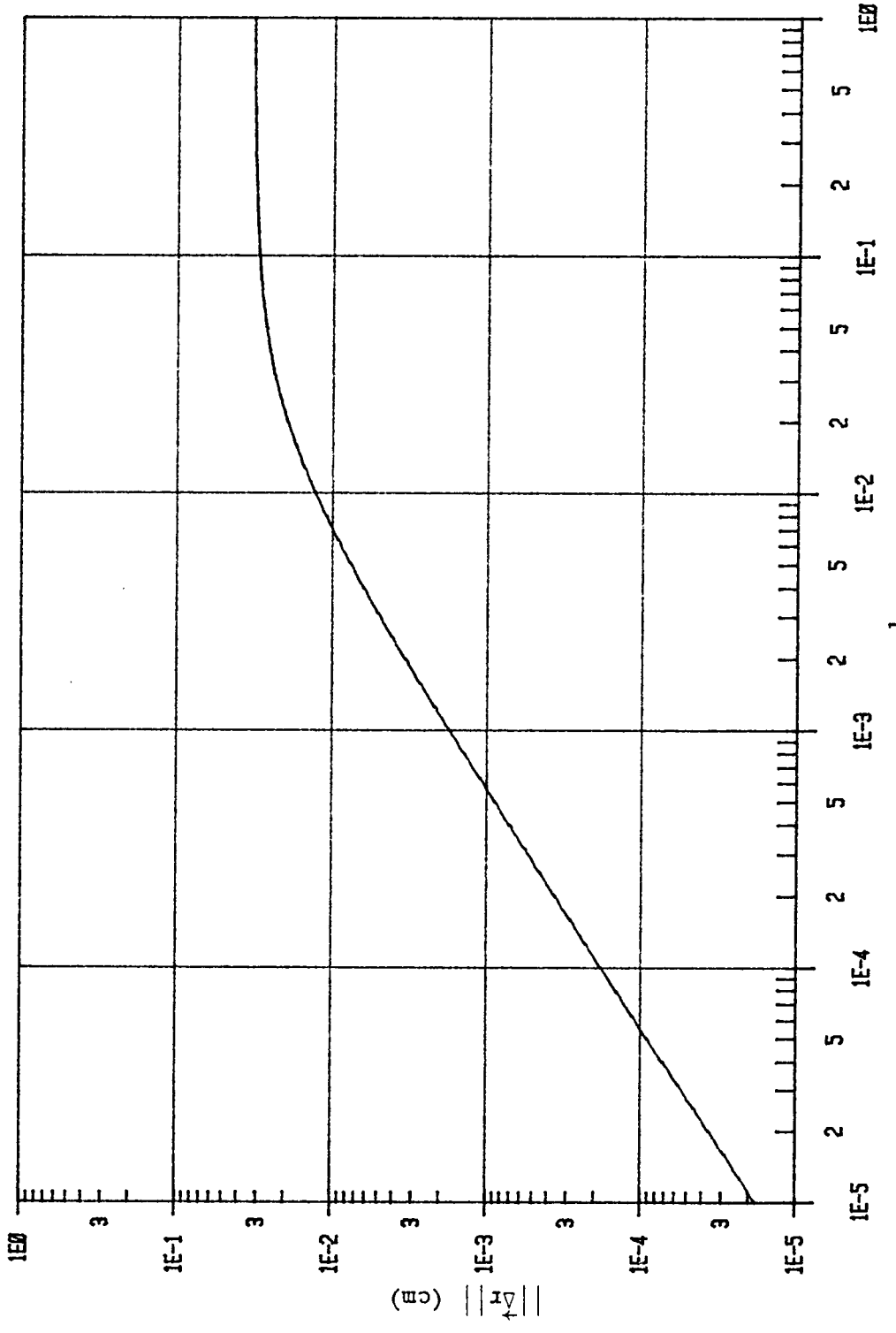

Figure 2. Beer's Law Absorption and Deflection.

where $\Lambda \equiv 1.00$ for an ideal gas and δT may be a function of space and time.

Herman and Pohl [5] have demonstrated that for a Gaussian beam spatial profile and a parabolic spatial approximation to δn, the solution of the eikonal yields the following

$$\delta y = -2(y_i/w)^3 w(\delta n/\Theta^2)$$

and

$$x'(z) = 2(\delta n/\Theta)(y_i/w)(x_i/w)$$

as the displacement, δy, and divergence, $x'(z)$, where Θ is the intersection angle and (x_i, y_i) are the intersection coordinates in the xy plane. Using these equations in the δn equation for an ideal gas yields

$$\delta y = 2(y_i/w)^3 (w/\Theta^2)(n_o - 1)(\delta T/T)$$

and

$$x'(z) = -2(y_i/w)(x_i/w)(n_o - 1)(1/\Theta)(\delta T/T)$$

with the restrictions given by Herman and Pohl that

$$(\delta n/\Theta^2) \ll 1 \qquad \text{and} \qquad (\delta T/T) \ll 1 \quad .$$

Taking $\delta T/T \simeq 0.1$ and realizing that for a gas sample, $n_o - 1 = 0(10^{-4})$ the order of magnitude of the deflection becomes

$$\delta y \simeq w/5 \quad \text{(maximum)}$$

and the divergence is

$$x'(z) \simeq 10^{-3}$$

if y_i/w and x_i/w are approximately 1.0. For a beam of radius $w = 1$ mm, δy is then on the order of 0.2 mm. Taking $\Delta z = z_s - z_o \simeq 100$ cm, the spatial divergence then becomes

$$\Delta x = (10^{-3})(100 \text{ cm}) = .1 \text{ cm}$$

If the medium through which the ray passes is selectively heated by a source of radiation such as a laser, δT will be nonzero in a volume defined by the beam. For a binary mixture heated by a laser beam of energy E_o and cross sectional area A_o, the ratio $\delta T/T$ may be approximated by

$$\delta T/T = X_1(M_1/M_2)(\gamma - 1)(\sigma_{abs}/A_o)(E_o/kT)$$

where X_1 is the mole fraction of the species that absorbs the laser radiation, M_1 is its molecular weight and σ_{abs} is its absorption cross section. The host species in the mixture is assumed to be of molecular weight M_2, predominant in number density, and to have a ratio of specific heats, γ. If the sodium $3S1/2 \rightarrow 3^2P1/2$ transition is the absorbing transition and the laser energy is 1 mJ with a beam radius of 1 mm, $\delta T/T$ is on the order of 0.1 at 300K. Since laser powers of 1 mJ are quite reasonable, measurable deflections should be calculable and observable.

For flowfields the lifetime of the thermal lens effect severely limits the use of LIST. In a flowfield, the thermal lens of characteristic diameter, $2r_g$, decays with a characteristic convection time $\tau_{cc} = 2r_g/V_\infty$, where V_∞ is the flow velocity component perpendicular to the axis of the cylindrical thermal lens. If the flow speed is large, the lens is greatly distorted or swept away entirely [13]. Therefore, use of a multiply-pulsed beam of sufficient power and sufficiently short pulse length is necessary to maximize heating and minimize convective heat loss. For a flow field, the LIST deflection measurement becomes limited to a narrow region in time. The initial time, t_i, of the deflection measurement must be much longer than the characteristic

acoustic time ($t_i >> \tau_a$), and the time, t_f, at which the measurement is concluded must be less than the characteristic flow time (τ_{cc}) relative to V_∞ (see fig. 3). Combining the two restrictions limits the flow speeds to $M_\infty \leq 0.1$ (where M_∞ is the flow Mach number) for the isobaric thermal region of the pulse (LIST). Supersonic flows could be observed by allowing the deflection times to enter the acoustic region of the pulse. However, as stated above, the solution would become the solution to a wave equation (rather than the heat conduction equation), and sensitivity to the gas molecular relaxation processes can be expected to increase, which for an unknown host gas constituency is undesirable.

Although increased laser power produces a larger gas temperature increase, sufficiently high pump powers result in saturation of the absorbing gas species. When saturated, the trace species' absorption coefficient goes to zero and gain in the media is possible. Little energy is absorbed, but a large amount of radiant energy is released in the form of fluorescence. Fluorescence is included in the MRCM calculation, but contributes to the thermal lensing process only by further absorption, and such multiple photon-atom collision processes are ignored in this work. Pump laser powers, therefore, will be kept below saturation in the LIST calculations.

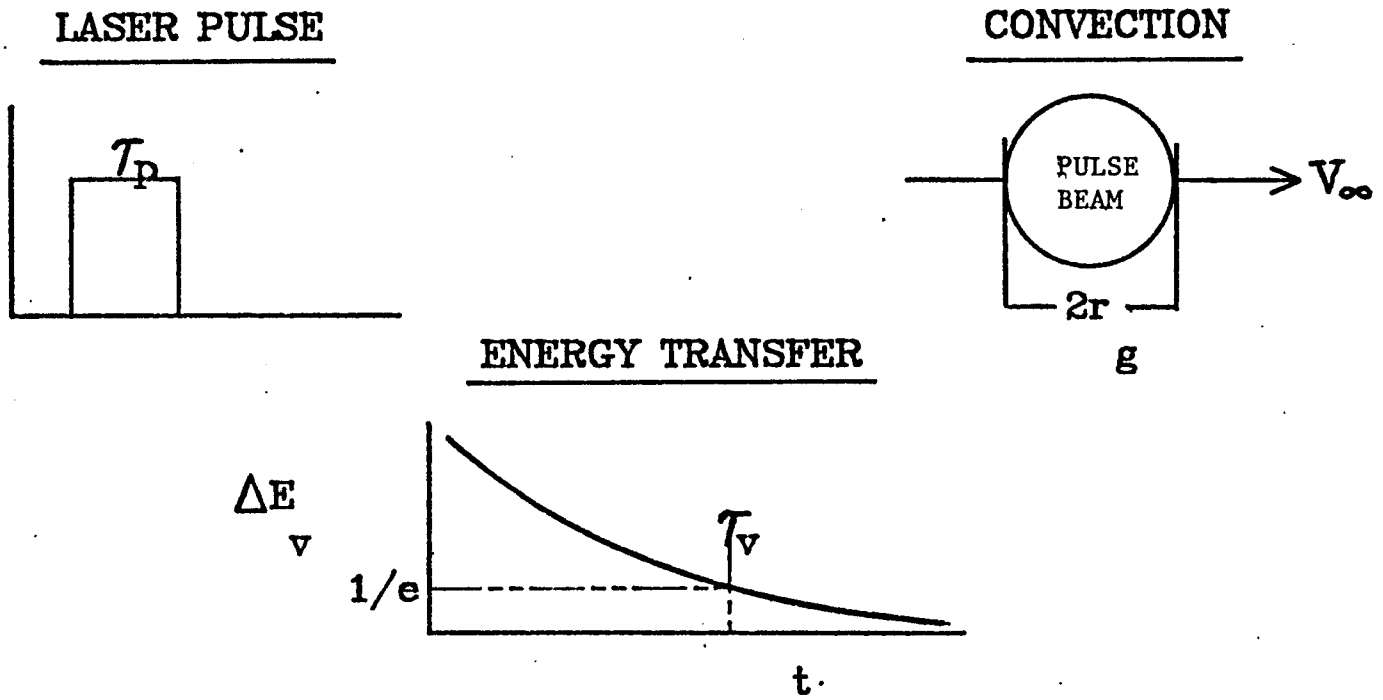

Acoustic $\tau_a = 2r_g / C$

Convection $\tau_{cc} = 2r_g / V_\infty$

Conduction $\tau_C = a^2 (r_g)^2 / 4$

Figure 3. Characteristic Times.

B. Temperature Field Theory

Transfer of the pump laser's radiant energy to kinetic energy in the host species produces the temperature rise in the gas mixture. Three physical processes are involved in this transfer. The first process is absorption of the radiation by the trace species' electronic levels. Transfer of the trace species' electronic energy to the host species' vibrational energy levels is the second process. The final process is relaxation of the vibrational energy into translational energy in the host species. All three processes are well-documented for the Na-N_2 mixture and the general theory for molecular energy relaxation is complete [7,8,9,14]. A brief overview of each process would be beneficial, however, to the understanding of the entire method.

By neglecting hyperfine structure, sodium may be represented by a three-level model (see Fig. 4) [10]. The most spectrally predominant of sodium's many electronic energy levels are the doublet 3^2P levels ($3^2P1/2$, $3^2P3/2$). The $3^2P1/2$ level lies 16,956.1 cm^{-1} above the ground state ($3S1/2$) and may be excited by radiation at 589.59 nm. Similarly, the $3^2P3/2$ level lies 17.19 cm^{-1} above the $3^2P1/2$ level and may be excited by radiation at 588.99 nm [15]. Laser radiation impinging on the sodium atom at either of the two frequencies will cause electron transitions to the appropriate upper level. After about 20 nsec, the sodium atom would lose its excess energy by spontaneous emission. Before spontaneous emission occurs, however, one of two events could possibly happen to cause premature decay. Stimulated emission may cause the electronic energy to be released as radiation, or collisions

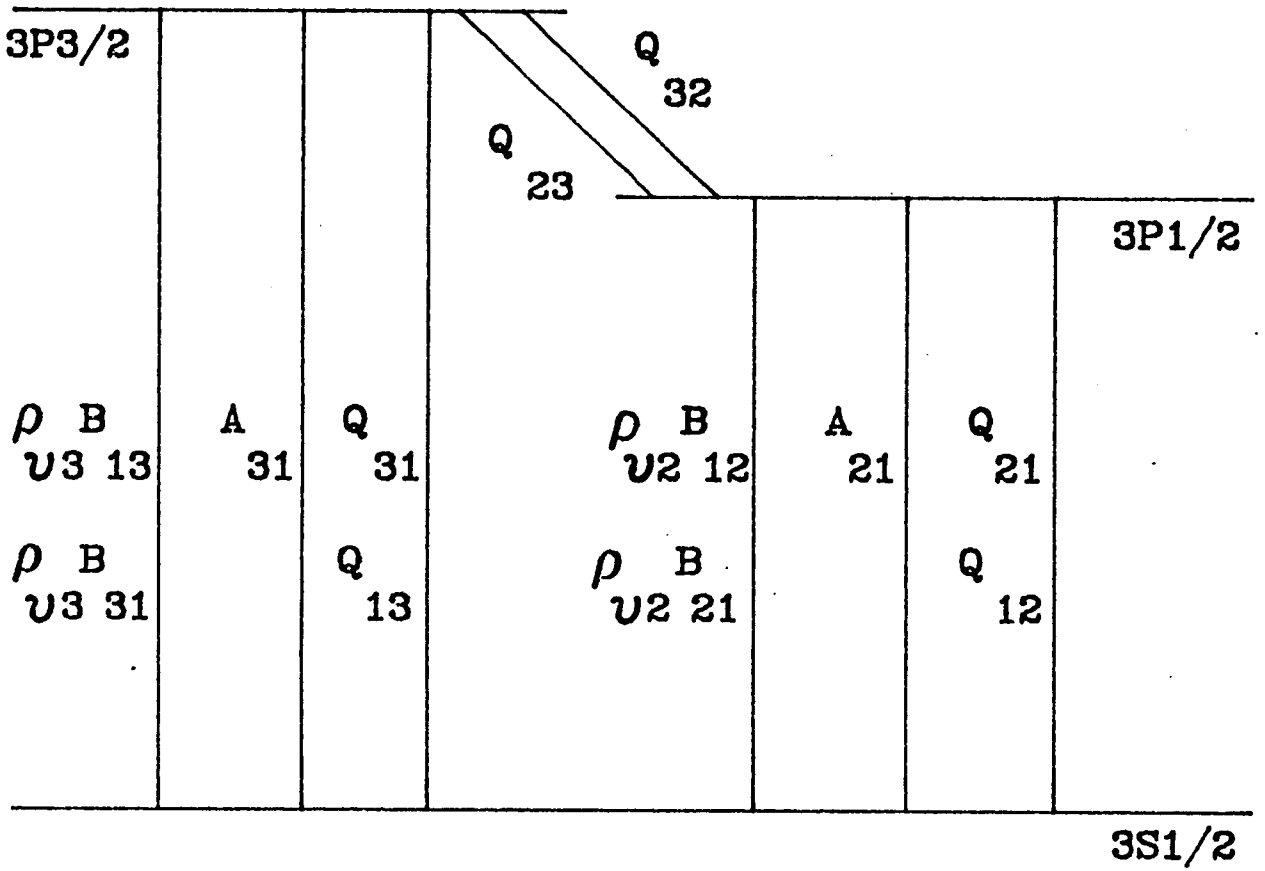

Figure 4. Three Level Pumping Model for Sodium.

with other atoms or molecules could cause the atom to return to the $3S1/2$ state.

Two collisional mechanisms occur. If the sodium atom interacts with another sodium atom, the most likely energy transfer is from one electronic level of one atom to an electronic level of the collision partner. The level-to-level transfer probabilities or quenching rates are determined experimentally and are reported in previous works [7,8]. Rate equations which describe the number density distribution functions are determined by detail balancing of the level energy transfer mechanisms [9]. In particular, when both levels are pumped by a laser with linecenter $\nu_{o\ell}$, and the gas sample is broadened by a Voight profile, the rate equations for Na - N_2 energy transfer (to the 3^2P levels) become [10]

$$dn_2/dt = -[B_{21}\rho_{\nu 2} + A_{21} + Q_{21} + Q_{23}]n_2 + [B_{12}\rho_{\nu 2} + Q_{12}]n_1 + Q_{32}n_2$$

and

$$dn_3/dt = -[B_{31}\rho_{\nu 3} + A_{31} + Q_{31} + Q_{32}]n_3 + [B_{13}\rho_{\nu 3} + Q_{13}]n_1 + Q_{23}n_2$$

where A_{ij} and B_{ij} are the appropriate Einstein coefficients, Q_{ij} is the quenching rate probability for the i^{th} to the j^{th} level and $\rho_{\nu i}$ is the energy density for pumping the i^{th} level given by

$$\rho_{\nu i} = F(\nu_{o\ell}, \nu_{og}^{(i)})\rho_{\nu o}$$

(see Appendix C). Quantum effects are ignored by this formulation, and it is assumed that the temperature is sufficiently low that higher-lying electronic states are not populated either thermally or by collisional excitation with the 3^2P species. Complexity of the

relaxation problem increases with the excitation of four or more of the atom's electronic levels. Information concerning phase relationships between the electronic states is not retained by the rate equation formulation. Although important in studies involving the interaction of coherent light sources (such as coherent Raman scattering) it is assumed in this work that the electronic state phase relationships are ignorable. To include phase relationships would require formulating a density matrix for each number density utilizing its complex, quantum wave function. In the three level model, each energy level is described by its own rate equation forming a set of three coupled, first-order differential equations to be solved for the number densities as a function of time. The other collisional mechanism is Na-N_2 collisional quenching. Comparison of the energy levels of Na to N_2 (see Fig. 5) indicates that resonant transfer of electronic energy should occur between Na 3^2P levels and the v = 7,8 vibrational levels. Previous experimental investigations have determined, however, that due to a strongly nonresonant, electronic to vibrational coupling in N_2 - Na collisions, the energy transfer is most likely at the v = 3,4 levels [8]. A graph of the probability distribution is given as Fig. 6 for the 3^2P electronic-vibrational energy transition. To describe these atom-molecule collisional energy exchanges, the rate equations above must be expanded. The quenching rates (Q_{ij}) given above become dependent on the vibrational population distribution of the colliding molecule such that

$$Q_{21} = \sum_{v} \nu_v \sum_{w>v} k_{vw}$$

Figure 5. Energy Level Diagram Calculated from Herzberg. Units are cm^{-1}.

Reference: Herzberg, Gerhard; Spectra of Diatomic Molecules, D. Van Nostrand Co., Inc., Princeton, N.J., p.88ff (1964)

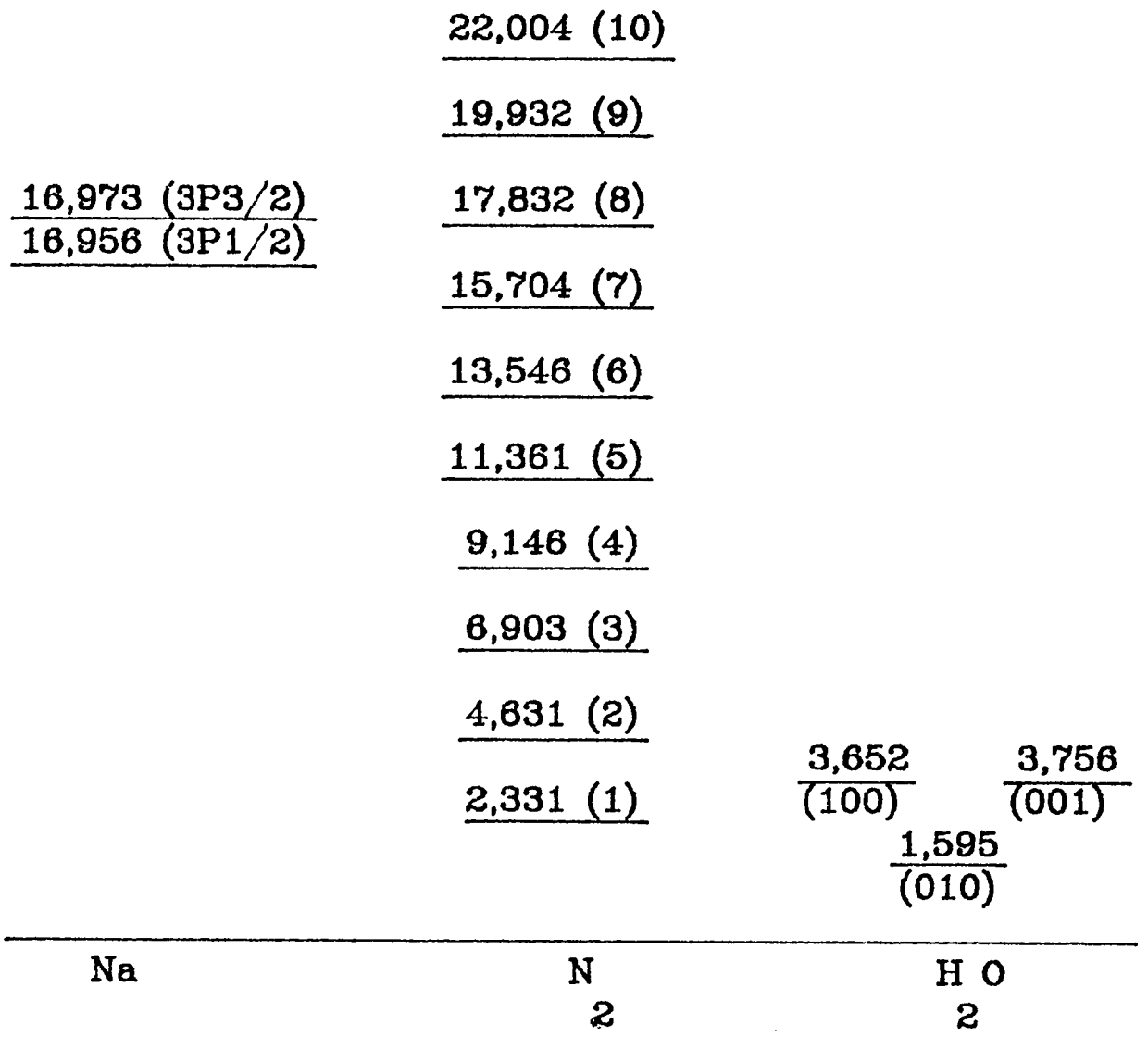
22,004 (10)
19,932 (9)
16,973 (3P3/2)
16,956 (3P1/2)
17,832 (8)
15,704 (7)
13,546 (6)
11,361 (5)
9,146 (4)
6,903 (3)
4,631 (2)
2,331 (1)
3,652
(100)
3,756
(001)
1,595
(010)
Na
N
2
H O
2

Figure 5.

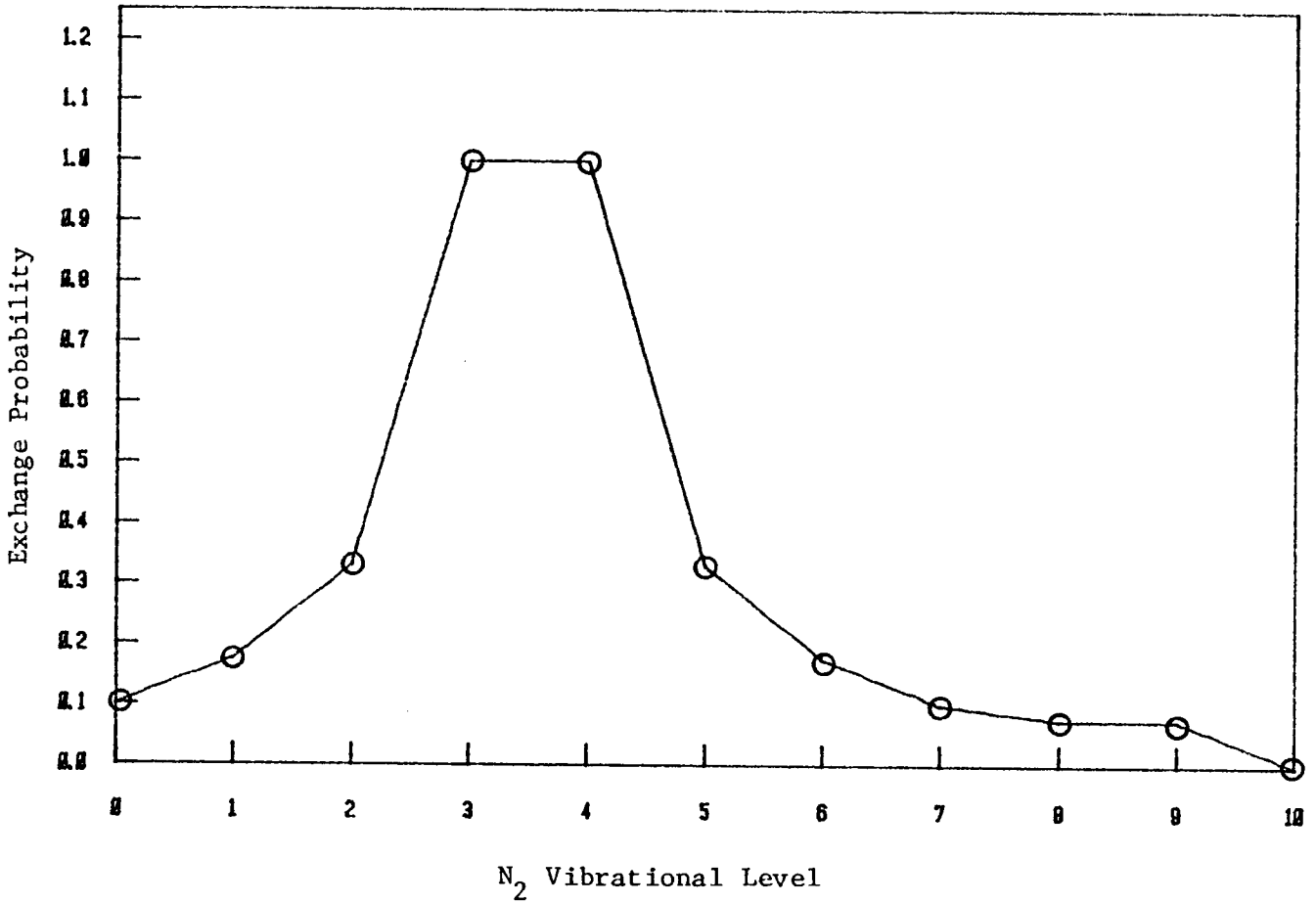

Figure 6. Relative Exchange Probabilities of Na - N_2.

Reference: Campbell, D. H. and Lewis, J. W. L.; "Detailed Temporal Behavior of Laser Excited Sodium Tracer in Nitrogen and Application to Nitrogen Number Density Measurements at Low Densities", Applied Optics, vol. 20 pp. 4102-4109 (1981)

$$Q_{12} = \sum_{w} n_w \sum_{v<w} k'_{wv}$$

$$Q_{31} = \sum_{v} n_v \sum_{w>v} k_{vw}$$

$$Q_{13} = \sum_{v} n_v \sum_{w>v} k''_{vw}$$

$$Q_{23} = n_3 k_{23} + n_T k'_{23}$$

and

$$Q_{32} = n_2 k_{32} + n_T k'_{32}$$

where in the notation of Campbell and Lewis [10], k_{32} and k_{23} are P-level exchange rate constants for collisions with Na atoms in the ground state (level 1), k'_{32} and k'_{23} are exchange rate constants for collision with N_2 molecules of total number density N_T, k_{vw} is the exchange rate constant for an upward vibrational transition causing a downward Na transition (quenching), and k'_{wv} is the exchange rate constant for a downward vibrational transition causing an upward Na tranition (reverse quenching). The relation between k_{vw} and k'_{wv} is given by

$$k_{wv} = k_{vw}(g_2/g_1)\exp[-(\Delta E_{21} - \Delta E_{vw})/kT] \quad .$$

In this work quenching rate constants which are assumed equal for both P-levels are only valid for two-body collisions. An increase in $n(N_2)$ also increases the probability of three body collisions ocurring. Three body quenching rates are not well known and are needed for number densities much above $2 \times 10^{20} cm^{-3}$. For this reason, $n(N_2)$ will be assumed less than $2 \times 10^{20} cm^{-3}$ (approximately 10 atmospheres at

300K). The constraining equation for the solution of the N_1, N_2, and N_3 rate equations is

$$n_{total(Na)} = n_1(t) + n_2(t) + n_3(t) = \text{a constant}$$

The final physical process is the relaxation of the vibrational energy into translational energy. The overall process involves two mechanisms, but both result from collisions between molecules of the host gas. Energy can be transferred by vibration-vibration (V-V) transfer; that is, vibrational energy exchanges which occur between colliding host species molecules. These collisions usually result in only part of the original vibrational energy going directly into vibrational modes of the collision partner. After collision, both partners may still be in vibrational modes, one higher than before the collision, the other lower than before the collision. The other mechanism may also occur in the collision such that little or no energy goes into the vibrational modes of the colliding partner, but, instead goes into translational or motional energy (V-T energy transfer). These collisions (V-V and V-T) are also represented by rate equations where the dependent variable becomes the vibrational level number density, n_v. For m nitrogen vibrational levels, there are m rate equations describing the transitions. These m rate equations are then solved simultaneously with the three sodium rate equations to produce temporal number density distributions. Since the actual mechanism of the nitrogen vibrational rate equations is of lesser interest to this report than those of the sodium which contain the broadening mechanism, the reader is referred to Campbell and

Lewis [10] for a detailed description of the vibrational level rate equations. The MRCM of Ref. 10 is a numerical routine to solve the simultaneous rate equations yielding number density solutions as a function of time. Typical distributions of $n(N_2)$ vibration levels are shown as Fig. 7 and for n(Na) electronic levels in the results. Use of the MRCM, with some modification, is the first step in calculating the time-dependent temperature field of the laser.

Modifications made to the MRCM of Ref. 10 were two-fold. Where it was originally assumed that the entire laser pulse was available to pump the entire spectral line of only one level, the realistic method is to convolve the Voight broadening function of the gas mixture with the pump laser lineshape. The second modification is to use a more versatile (and realistic) pulse-shape.

Convolving the laser and Voight lineshapes produces spectral fractions that can be used to calculate the spectral absorption coefficient [16] and modify the energy density, $\rho_{\nu o}$, in the rate equations. The broadening parameter, $B(\nu,\nu_{o\ell},\nu_{og})$, is given by the product of two functions

$$B(\nu,\nu_{o\ell},\nu_{og}) = L(\nu,\nu_{o\ell})\ g\ (\nu,\nu_{og})$$

where

$$L(\nu,\nu_{o\ell}) = C_L \exp\left(- (\nu - \nu_{o\ell})^2/\Delta\nu_L^2\right)$$

and

$$g(\nu,\nu_{og}) = C_V \int_{-\infty}^{\infty} \frac{\exp(-(\nu'/\Delta\nu_g)^2)}{[\Delta\nu_s^2 + (\nu - \nu_{og} - \nu')^2]}\, d\nu'$$

Here $g(\nu,\nu_{og})$ is the Voight function given by Kielkopf [17]. $L(\nu,\nu_{o\ell})$ is the expression for a laser with a Gaussian frequency distribution

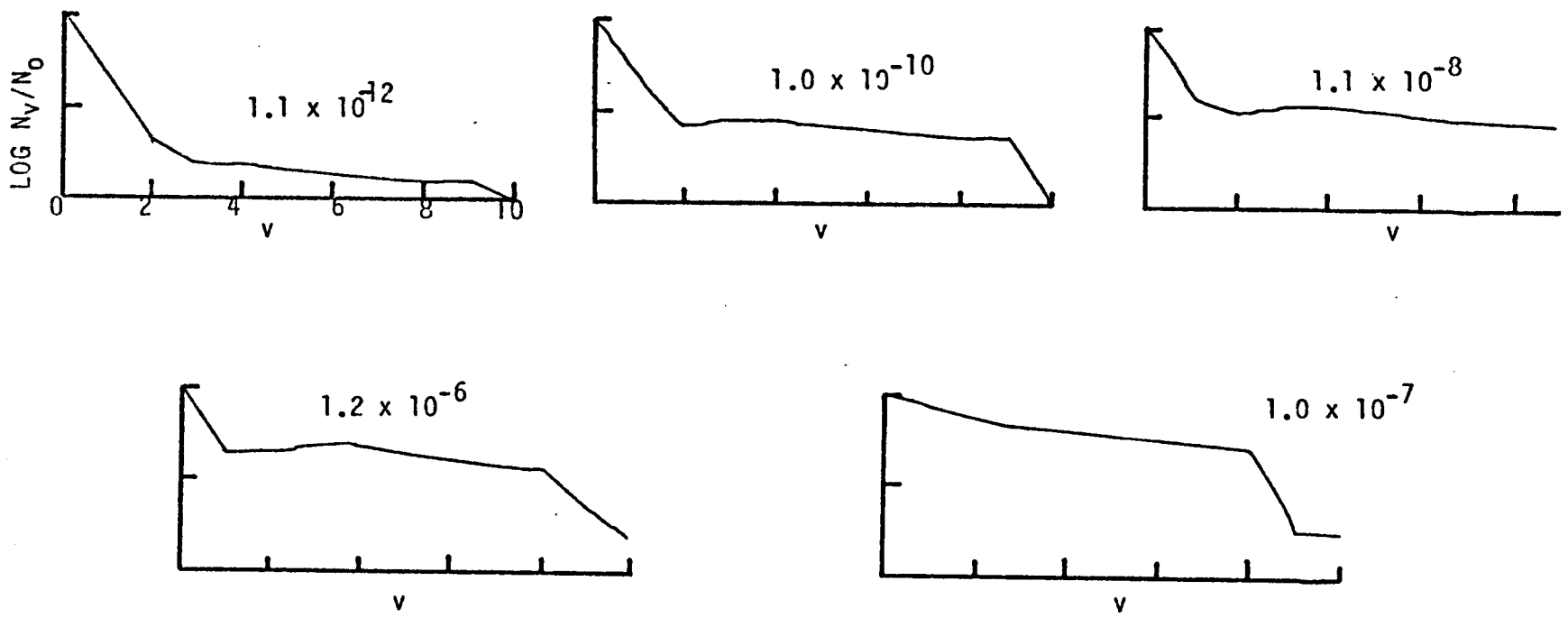

Figure 7. Time Dependent N_2 Vibrational Distributions.

Reference:Campbell, D. H. and Lewis, J. W. L.; "Detailed Temporal Behavior of Laser Excited Sodium Tracer in Nitrogen and Application to Nitrogen Number Density Measurements at Low Densities", Applied Optics, vol. 20 pp. 4102-4109 (1981)

of line width $\Delta\nu_L$ centered about $\nu_{o\ell}$. $\Delta\nu_s$ is the Lorentzian linewidth given by the sum of $\Delta\nu_p$ and $\Delta\nu_N$, the pressure broadened linewidth and natural broadened linewidth respectively. For the convolution to be properly normalized, C_L and C_ν must be such that

$$\int_{-\infty}^{\infty} L(\nu,\nu_{o\ell})g(\nu,\nu_{og})d\nu \equiv 1 \quad .$$

Therefore, $C_L = \frac{1}{\Delta\nu_L\sqrt{\pi}}$, and $C_\nu = \frac{\Delta\nu_s/\pi}{\Delta\nu_g\sqrt{\pi}}$, and

the resulting function is

$$B(\nu,\nu_{o\ell},\nu_{og}) = \frac{\Delta\nu_s}{\Delta\nu_L\Delta\nu_g\pi^2}\int_{-\infty}^{\infty}\frac{\exp(-(\nu - \nu_{o\ell})^2/\Delta\nu_L^2)\exp(-(\nu'/\Delta\nu_g)^2)}{[\Delta\nu_s^2 + (\nu - \nu_{og} - \nu')^2]}d\nu \quad .$$

Computing this function for a given laser linewidth ($\Delta\nu_L$) and laser line center ($\nu_{o\ell}$) at each spectral line center (ν_{og}) and integrating over all frequencies gives

$$F(\nu_{o\ell},\nu_{og}) = \frac{\Delta\nu_s}{\Delta\nu_L\Delta\nu_g\pi^2}\int_{-\infty}^{\infty}\int\frac{\exp(-(\nu - \nu_{o\ell})^2/\Delta\nu_L^2)\exp(-(\nu'/\Delta\nu)^2)}{[\Delta\nu_s^2 + (\nu - \nu_{og} - \nu')^2]}d\nu'd\nu \quad .$$

This fraction then modifies $\rho_{\nu o}$ and the absorption coefficient for each spectral absorption linecenter. Figures 8 through 10 present the Voight/laser profile as a function of several temperatures. $F(\nu_{o\ell},\nu_{og})$ cannot be determined analytically; results must be obtained either as an approximation or as a numerical integration [18] (see Appendix C). Both methods were used in order to cover the entire range of broadening effects. In Appendix C the various linewidths are shown to be functions of the temperature. For $\delta T/T < 0.1$, changes in the temper-

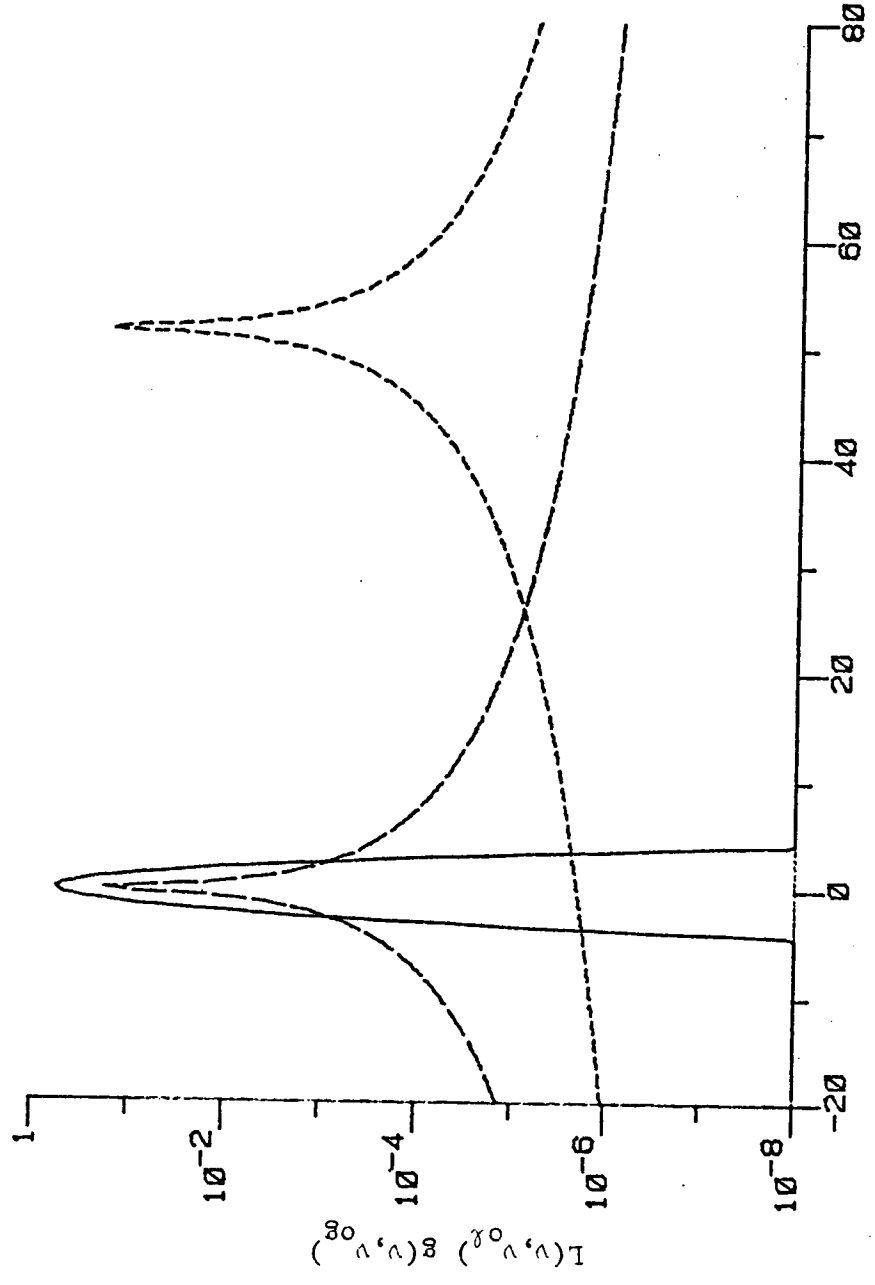

Figure 8. Voight/Laser Lineshape for $n(N_2) = 10^{19}$ and T = 300K. Solid line represents the Gaussian frequency distribution of the pump laser. Long broken line is the $3^2P1/2$ Voight lineshape. Short broken line is the $3^2P3/2$ Voight lineshape. $3^2P1/2$ state excited. $\Delta\nu_L = 10^{10}$ hertz

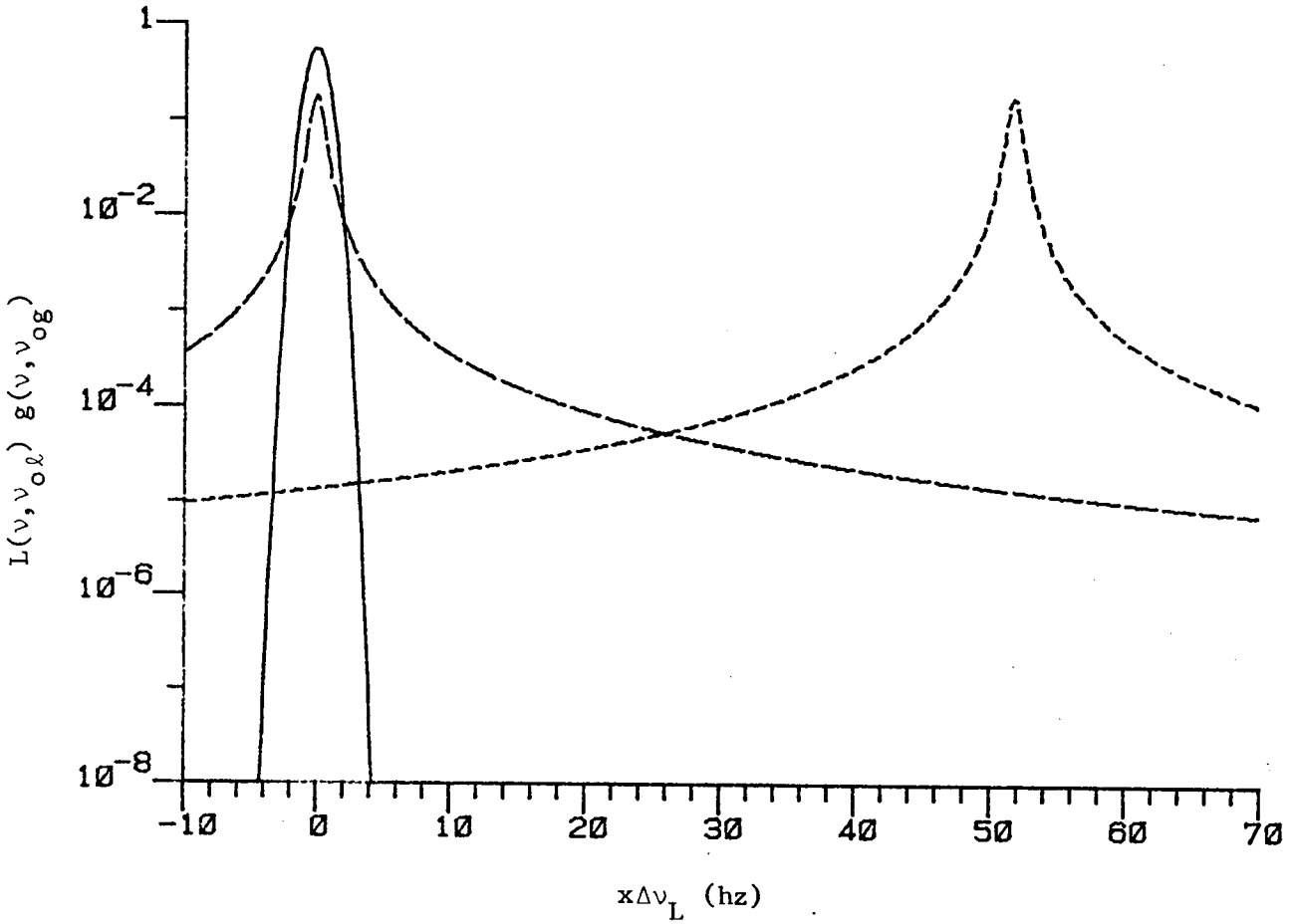

Figure 9. Voight/Laser Lineshape for $n(N_2) = 10^{19}$ and T = 2000K. Solid line represents the Gaussian frequency distribution of the pump laser. Long broken line is the $3^2P1/2$ Voight lineshape. Short broken line is the $3^2P3/2$ Voight lineshape. $3^2P1/2$ state excited. $\Delta\nu_L = 10^{10}$ hertz.

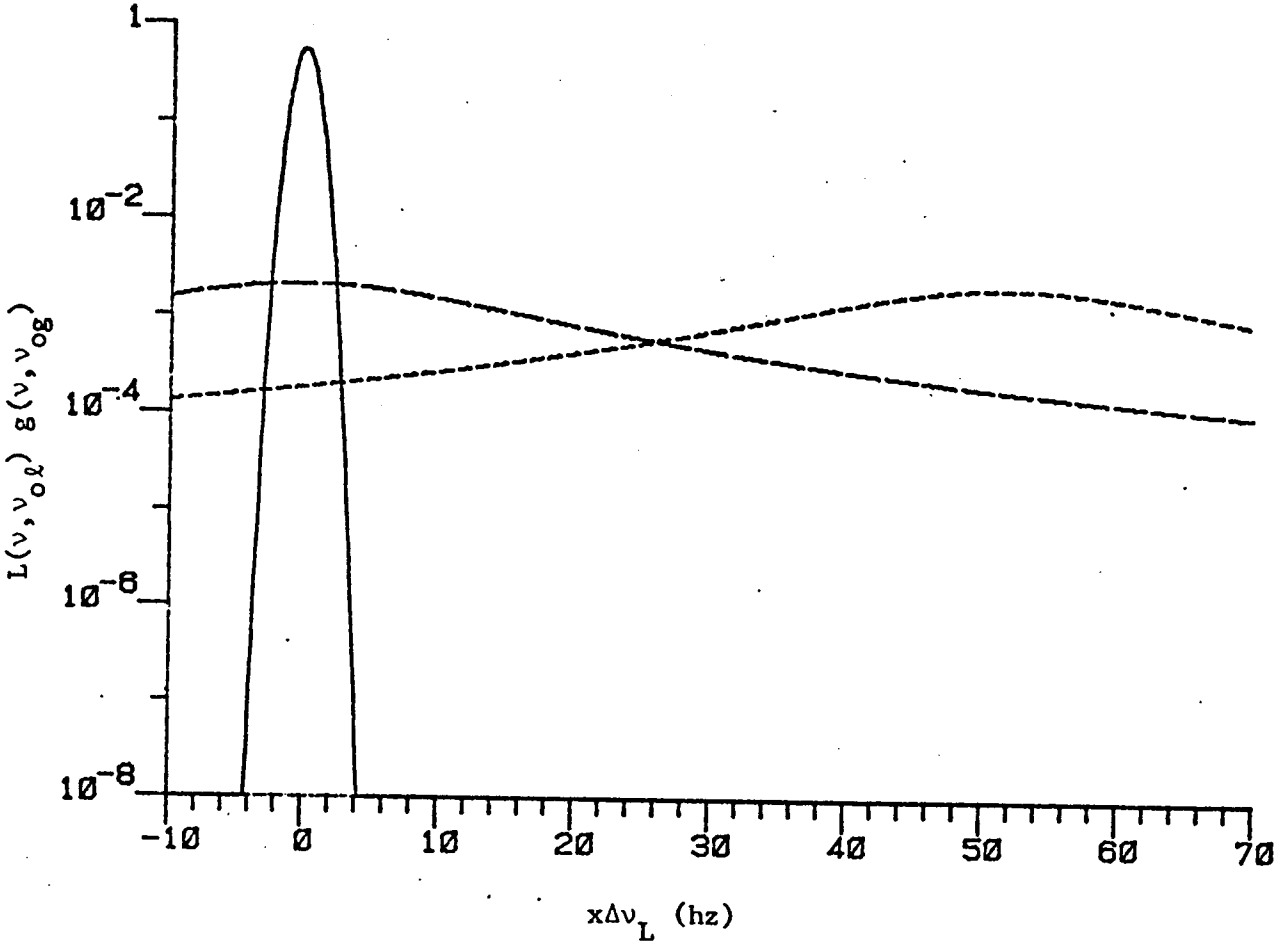

Figure 10. Voight/Laser Lineshape for $n(N_2) = 10^{21}$ and T = 300K. Solid line represents the Gaussian frequency distribution of the pump laser. Long broken line is the $3^2P1/2$ Voight lineshape. Short broken line is the $3^2P3/2$ Voight lineshape. $3^2P1/2$ state excited. $\Delta\nu_L = 10^{10}$ hertz.

ature-dependent linewidths ($\Delta\nu_p$,$\Delta\nu_g$) are less than 5 percent; therefore, $\Delta\nu_s$, $\Delta\nu_g$, and $\Delta\nu_p$ were treated as constants in the calculation.

Using time dependent number densities calculated directly from the rate equations, the total absorption coefficient ($\beta_{\nu o}$) was calculated for each 3^2P level. For level i this became

$$\beta_{\nu o}^{(i)} = \frac{c^2 A_{il}}{8\pi\nu^2}\left(1 - (g_l/g_i)N_i\right)N_l \quad .$$

The spectral absorption coefficient of the i^{th} level was then obtained from

$$\beta(\nu_{og}^{(i)},\nu_{o\ell}) = F(\nu_{o\ell},\nu_{og}^{(i)})\beta_{\nu o}^{(i)}$$

where $\nu_{og}^{(i)}$ is the spectral line frequency of the i^{th} level.

Laser energy densities at the spectral linecenters were calculated in like manner such that for each rate equation $\rho_{\nu o}$ became for the i^{th} level

$$\rho_{\nu i} = F(\nu_{o\ell},\nu_{og}^{(i)})\rho_{\nu o}$$

thereby allowing both levels to be pumped if the various linewidths allowed such pumping.

The second modification of the MRCM changed the pulseshape to a function formed by the difference of two Heaviside functions. This pulse shape was normalized to a minimum and a maximum of 0.00 and 1.00, respectively, and was used to determine the amplitude of the pulse as a function of time. A weighting variable in the pulse function produced a wide range of pulse shapes (see Appendix D).

The crux of the LIST is the two-fold task of determining the temperature increase caused by the pump beam as it passes through the absorbing mixture and obtaining the relationship between this temperature increase and the change which it produces in the index of refraction of the gas. The time dependent temperature field, $\delta T(\vec{r},t)$, calculation will be presented in a subsequent section where the uses will be made evident of the parameters derived from the MRCM, such as $\beta_{\nu o}(t)$ and τ . The next derivation will focus on the relationship of the change of the index of refraction due to gas heating.

Jackson shows that the index of refraction is related to the molecular polarizability by the Lorenz-Lorenz relation [19] given by

$$\gamma_{mol} = \frac{3}{4\pi\rho}\left(\frac{n^2 - 1}{n^2 + 2}\right)$$

where ρ is the density in molecules cm^{-3} and γ_{mol} is computed on a molar basis. For gases n^2 is $\simeq$ 1.0, therefore

$$4\pi\rho\gamma_{mol} = n2 - 1 = (n + 1)(n - 1)$$

or

$$n - 1 = 2\pi\rho\gamma_{mol} \quad .$$

If $2\pi\gamma_{mol} = K$ this relation is essentially a constant for a given gas species and can be written as

$$(n - 1)/\rho = K \quad .$$

At another density, ρ', the index of refraction becomes n' while K remains constant to yield

$$(n' - 1)/\rho' = K \quad .$$

Now write

$$\delta n = n_o - n' \quad \text{and} \quad \delta\rho = \rho_o - \rho'$$

so that

$$(n_o - 1)/\rho_o = (n' - 1)/\rho' = (n_o - \delta n - 1)/(\rho_o - \delta\rho)$$

or

$$\delta\rho/\rho_o = \delta n/(n_o - 1)$$

which is the Gladstone-Dale equation [20].

For imperfect gases, the equation of state can be written as a virial expansion

$$p/kT = \rho(1 + B_2(T)\rho + B_3(T)\rho^2 + \ldots) \qquad [21]$$

where $B_i(T)$ is the i^{th} virial coefficient. Several works give experimental results for the virial coefficient [21,22,23]. For pressures less than 50 atmospheres (approximately 10^{21} molecules per cm^3 at 300K), virial coefficients higher than the second may be ignored. Proof of this comes from Fig. 12-6 in McQuarry where the third virial coefficient for N_2 ($300K \leq T \leq 2000K$) is approximately

$$B_3 = 0.3b_o^2 \quad .$$

The factor b_o is a hard-sphere potential result used to normalize B_3 and is given by

$$b_o^2 = [2\pi\sigma^3/3]^2 \quad .$$

For N_2, Ref. 23 gives $\sigma = 3.7 \times 10^{-8}$ cm so that

$$b_o^2 = 1.126 \times 10^{-44} cm^6$$

and

$$B_3 = 3.38 \times 10^{-44} cm^6 \quad .$$

The third virial coefficient's contribution to the equation of state then becomes the dimensionless quantity,

$$B_3\rho^2 = 0.0034 \text{ for } \rho = 10^{21} \text{ cm}^{-3}$$

which is small compared to the contribution from the second virial coefficient (see below). Neglecting virial coefficients higher than the second (B_2), the equation of state becomes

$$p/kT = \rho + B_2(T)\rho^2$$

where for spherically symmetric interaction potentials, u(r),

$$B_2(T) = -2\pi \int_0^\infty [e^{-u(r)/kT} - 1]r^2 dr \quad .$$

McQuarrie shows that for available experimental results, the Lennard-Jones potential function [21]

$$u(r) = 4E_o[(\sigma/r)^{12} - (\sigma/r)^6]$$

is a good approximation with $\sigma = 3.7 \times 10^{-8}$cm and $E_o/k = T_c = 95.2$K for N_2. Including u(r) and setting $x = r/\sigma$ gives the second virial coefficient as

$$B_2(T) = 2\pi\sigma^3 \int_0^\infty \{\exp[-(4T_c/T)(x^{-12} - x^{-6})] - 1\}x^2 dx$$

which can be evaluated to yield

$$B(T) = b_o \sum_{j=o}^{\infty} \left[\left(\frac{-2^{j+1/2}}{4j!}\right) \Gamma\left(\frac{2j-1}{4}\right) \right] (T/T_c)^{-(2j+1)/4} \quad .$$

Calculating the isobaric density change yields

$$-(P/kT^2)\delta T = \delta\rho + 2\rho B_2(T)\delta\rho + \rho^2(\partial B_2(T)/\partial T)_p \delta T$$

or

$$-[p/kT^2 + \rho^2(\partial B_2(T)/\partial T)]\delta T = (1 + 2\rho B_2(T))\delta\rho \quad ,$$

but

$$(\partial B_2/\partial T)_p = -2\pi\sigma^3 \int_0^\infty (-4T_c/T^2)(x^{-12} - x^{-6})\exp[-4T_c/T(x^{-12} - x^{-6})]x^2 dx$$

which becomes

$$(\partial B_2/\partial T)_p = dB_2/dT = b_o \sum_{j=o}^{\infty} \left(\frac{2j + 1}{4}\right)\left(\frac{2^{j+1/2}}{4j!}\right) \Gamma\left(\frac{2j - 1}{4}\right)(T/T_c)^{-(2j + 5)/4} .$$

Letting

$$B_2'(T) = 8\pi\sigma^3 T_c \int_o^{\infty} (x^{-12} - x^{-6})\exp[-4T_c/T*(x^{-12} - x^{-6})]x^2 dx ,$$

the density change equation becomes

$$-[P/kT^2 + \rho^2 B_2'(T)/T^2]\delta T = \left(1 + 2\rho B_2(T)\right)\delta\rho ,$$

and dividing both sides by ρ and rearranging terms yields

$$-[1 + \rho B_2'(T)]\delta T/T = [1 + 2\rho B_2(T)]\delta\rho/\rho .$$

Setting

$$\Lambda = [\left(1 + \rho B_2'(T)\right)/\left(1 + 2\rho B_2(T)\right)]$$

yields the relation

$$\delta\rho/\rho = - \Lambda(\delta T/T)$$

for the isobaric density change where only the second virial coefficient is significant. From the Gladstone-Dale equation above

$$\delta n/(n_o - 1) = \delta\rho/\rho \equiv - \Lambda(\delta T/T)$$

then

$$\delta n = -\Lambda(n_o - 1)(\delta T/T)$$

where $\Lambda = 1.0$ for an ideal gas. Evaluating Λ at 300K with number densities of 10^{18}cm^{-3} and 10^{19} cm^{-3} gives values of 0.999 and 0.995, respectively. Increasing the number density to 10^{21}cm^{-3} at 300K gives $\Lambda = 0.677$, a significant change.

Herman and Pohl [5] stated this relationship for an ideal gas ($\Lambda = 1.0$), but did not calculate δT. For their calculations, δn was assumed to be a parabolic function and δT was not needed.

Having obtained the relationship between δn and δT for isobaric heating of an imperfect gas, attenuation is now turned to the computation of the temperature field $\delta T(\vec{r},t)$. A detailed treatment of the temperature rise is given by Bailey [6]. Bailey's derivation has four significant limitations, however. Use of semi-infinite boundaries in the Green's function is a special case of finite boundaries (see Appendix B). No provision is made for thermal gradients along the path of the pump beam. Only one pulse is assumed, and the shape of the pulse is that of a Dirac-delta function. Finally, Bailey's gas sample is assumed to be static. For the case at hand only the pulse-shape restriction becomes truly restrictive.

For a medium of molar density, $\bar{\rho}$, thermal conductivity, K, and molar specific heat C_p, the heat conduction equation is given by

$$\frac{\partial(\delta T)}{\partial t} - \frac{1}{a^2}\nabla^2(\delta T) = \Theta(r,t)$$

where

$$1/a^2 = K/C_p\bar{\rho} = \text{thermal diffusivity}$$

and $\theta(r,t)$ is the heat source function. Appendix B shows that for the semi-infinite boundaries $0 < r < \infty$ and $0 < z < \infty$ the Green's function,

$$G(\vec{r},t \mid \vec{r}',t') = \left(\frac{a}{2\left(\pi(t - t')\right)^{1/2}} \right)^3 \exp\left(- \frac{a^2(\vec{r} - \vec{r}')^2}{4(t - t')} \right)$$

solves the homogeneous partial differential equation ($\Theta \equiv 0$). Assum-

ing a uniform initial temperature distribution, the solution to the inhomogeneous partial differential equation with $\theta(\vec{r},t)$ becomes

$$\delta T(\vec{r},t) = \int_0^t dt' \int_v d\vec{r}' \; G(\vec{r},t \mid \vec{r}',t')\theta(\vec{r}',t) \quad .$$

With the volume integral separable into radial and axial parts, and no angular dependence assumed,

$$\delta T(\vec{r},t) = \int_0^t dt' \int_0^\infty dr'r'G(r,t \mid r',t') \int_0^\infty dz' \; G(z,t \mid z',t')\theta(r',z''\tau').$$

Bailey asserts that the only axial contribution to the temperature rise comes from evaluating the source function at the z coordinate; i.e., that

$$\int_0^\infty dz'G(z,t \mid z',t')\theta(r'z',t)$$

actually becomes

$$\int_0^\infty dz'\delta(z - z')\theta(r',z',t') \equiv \theta(r',z,t') \quad .$$

This assertion ignores axial gradients; i.e., it is assumed that $\partial(\delta T)/\partial z \equiv 0$) in the temperature calculation which, in effect, reduces the problem to one of determining the radial temperature variation in a series of circular planes perpendicular to the z axis. The temperature rise in this case then becomes

$$\delta T(r,z,t) = \int_0^t dt' \int_0^\infty dr'r'G(r,t \mid r',t')\theta(r',z',t')$$

where now

$$G(r,t \mid r',t') = \left(\frac{a}{2[\pi(t - t')]^{1/2}} \right)^2 \exp \left[- \frac{a^2(r - r')^2}{4(t - t')} \right] .$$

For slight absorption along the z-axis, as before, a Beer's law attenuation process may be assumed

$$I = I_o e^{-\beta z} ,$$

and Bailey shows that an appropriate source function incorporating the Beer's law attenuation, the time release of energy into translational motion, and the radial flow of temperature is a Gaussian source given by

$$\Theta(r',z,t') = \left(\frac{1}{C_p \bar{\rho} r_g^2}\right) \beta E_o \exp(-\beta z) \exp(-r'^2/r_g^2) \psi(t') .$$

$\psi(t')$ is the function yielding the rate of heat production in the environment, E_o is the pump laser energy such that $\rho_{vo} = E_o/(c\pi r_g^2)$, c is the speed of light in vacuum and r is the Gaussian limit of the pump beam. Bailey suggests that by modeling a single laser pulse such that its entire energy is imparted to the gas before the temperature begins to rise, a first-order approximation for $\psi(t')$ is

$$\psi(t') = \frac{1}{\tau_v} \exp\left(- \frac{t'}{\tau_v}\right)$$

where τ_v is the characteristic vibrational relaxation time. The validity of the source term is verified by the MRCM calculation. Figure 11 compares $\psi(t')$ with the shape of the relaxation curve calculated by the MRCM. The broken line is $\Delta E_v/\Delta E_{max}$ vs t and the solid line is $\psi(t')\tau_v$ vs t. ΔE_v is the total vibrational energy difference

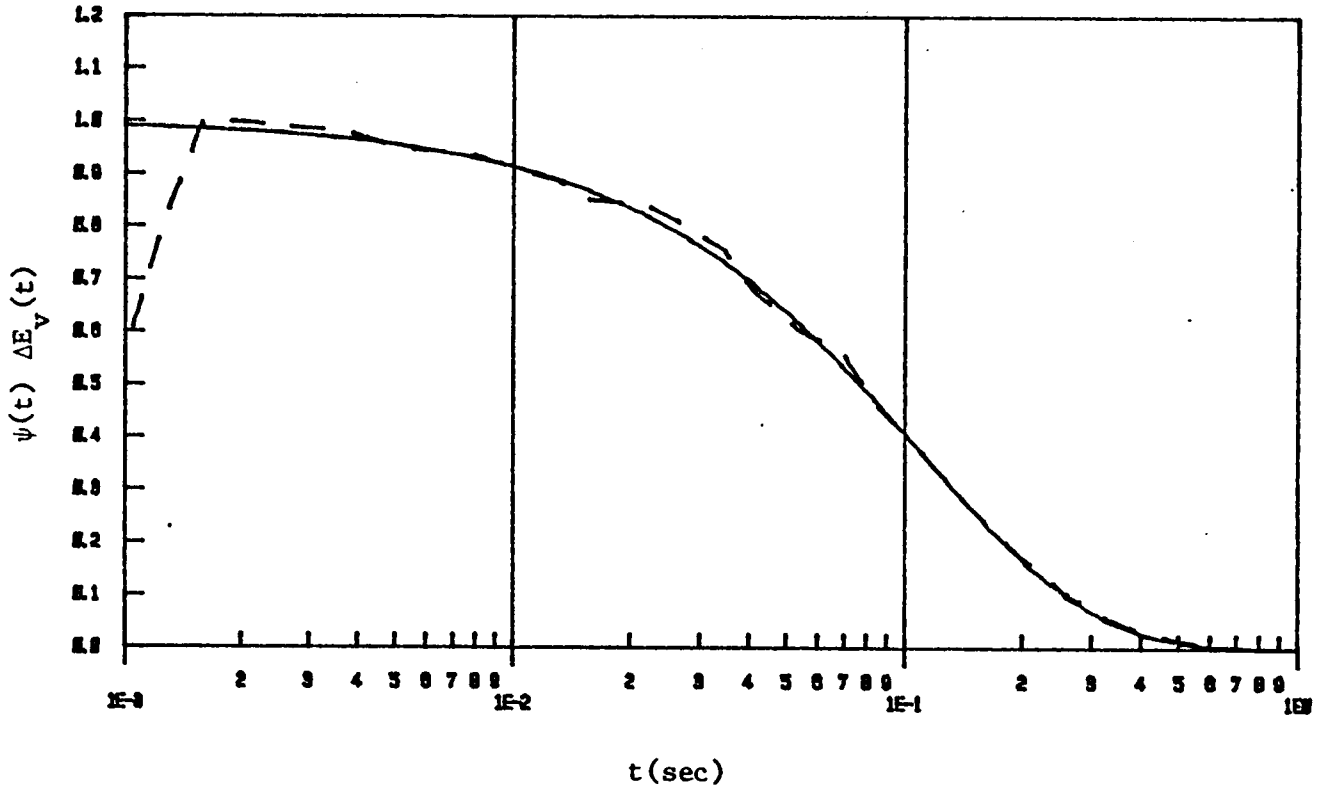

Figure 11. Heat Conduction Equation Source Term Comparison with MRCM Results. Standard Model vibration relaxation shown as broken line. Source term plot shown as solid line.

between the vibrational states of the diatomic species (N_2) at time t and its ground state vibrational energy at time t = 0. ΔE_{max} is the maximum vibrational energy difference. τ_v is taken to be the time at which $\Delta E_v/\Delta E_{max} = 1/e$. The entire source function then becomes

$$\Theta(r',z,t') = \left(\frac{1}{C_p\bar{\rho}\pi\tau_v r_g^2}\right)\beta E_o \exp(-\beta z)\exp(-r'^2/r_g^2)\exp\left(-\frac{t'}{\tau_v}\right)$$

giving

$$\delta T(r,z,t) = -\left(\frac{a}{4\pi}\right)\left(\frac{\beta}{C_p\bar{\rho}\pi\tau_v r_g^2}\right)E_o\exp(-\beta z)\int_o^t dt' \int_o^\infty dr' r'\left[\frac{\exp(-t'/\tau_v)}{(t-t')}\right] \quad (x)$$

$$\left[\exp(-r'^2/r_g^2)\exp\left(-\frac{a^2(r-r')^2}{4(t-t')}\right)\right] \quad .$$

The integral over r', can be calculated using Bessel functions to yield the final temperature rise prediction

$$\delta T(r,z,t) = -\left(\frac{a^2}{4\pi C_p\bar{\rho}\tau_v}\right)\beta\exp(-\beta z)E_o\int_o^t dt'\left(\frac{\exp(-t'/\tau_v)}{(t - t' + a^2 r_g^2/4)}\right) \quad (x)$$

$$\exp\left(-\frac{a^2r^2}{4(t - t' + a^2 r_g^2/4)}\right) \quad .$$

Using $\tau_c = a^2 r_g^2/4$ (the heat conduction relaxation time) and r_g as a characteristic time and length, respectively, and $\hat{\tau}_v = \tau_v/\tau_c$ this equation can be written as

$$\delta T(r,z,t) = \left(\frac{\beta}{\pi C_p\bar{\rho} r_g^2\hat{\tau}_v}\right)E_o\exp(-\beta z)\int_o^{\hat{t}} \frac{\exp(-\hat{t}'/\hat{\tau}_v)\exp\left(-\hat{r}^2/(\hat{t}-\hat{t}'+1)\right)d\hat{t}}{(\hat{t}-\hat{t}'+1)} \quad .$$

Bailey's derivation using a single, delta-function shaped pulse as stated above, is not obviously applicable to a multiply pulsed pump

laser. The extension may be made by introducing the normalized Heaviside difference function, $\tilde{A}(t)$, of Appendix D into the calculation. If each pulse of the pump laser is assumed to consist of m Dirac-delta function shaped pulses, an envelope using $\tilde{A}(t)$ may be constructed to enclose the peaks (see Fig. 12).

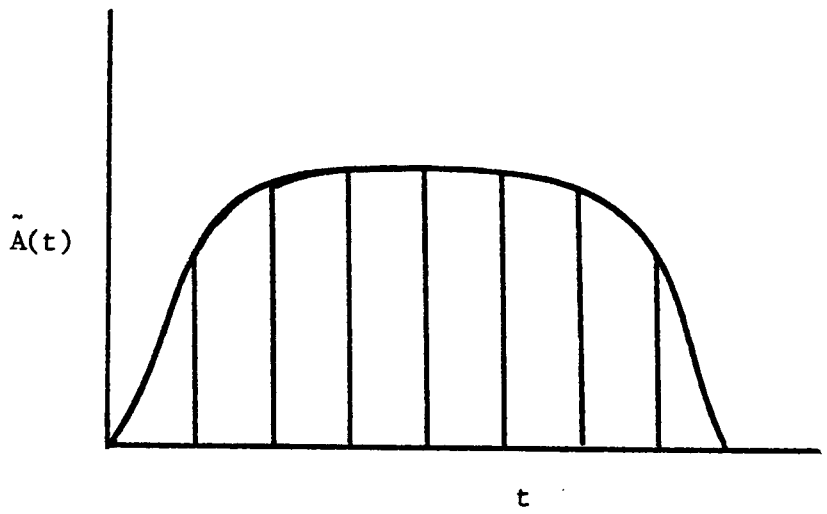

Figure 12. Heaviside envelope and delta function pulses.

The time between the i^{th} and the $(i - 1)^{th}$ pulse is simply $t_i - t_{i-1}$. During this time interval the energy from the $(i - 1)^{th}$ pulse attenuates according to $\psi(t_i - t_{i-1})$ given above. A pulse function of the form

$$\sum_{i=1}^{n} \tilde{A}(\hat{t}_i)\hat{t}_i \exp\left(\frac{-(\hat{t}_i - \hat{t}_{i-1})}{\hat{\tau}_v}\right)$$

where $n \leq m$ was devised with $\tilde{A}(t_i)$ given in Appendix D. Using this

in the Bailey δT expression gives

$$\delta T_n(1) = \left(\frac{\beta_n^{(1)}}{\pi C_p \rho r_g^{\hat{2}} \hat{\tau}_v^{\hat{2}}}\right) \exp(-\beta_n^{(1)} z) E_o \quad (x)$$

$$\sum_{i=1}^{n} \tilde{A}(\hat{t}_i^{(1)}) \hat{t}_i \exp\left(\frac{-(\hat{t}_i^{(1)} - \hat{t}_{i-1}^{(1)})}{\hat{\tau}_v}\right) \quad (x)$$

$$\int_{o}^{\hat{t}_n^{(1)}} dt' \frac{\exp(-\hat{t}'/\hat{\tau}_v) \exp\left(-\hat{r}^2/(\hat{t}_n^{(1)} - \hat{t}' + 1)\right)}{(\hat{t}_n^{(1)} - \hat{t}' + 1)}$$

where $\hat{t}_n^{(1)}$ is the non-dimensional time ($\hat{t}_n^{(1)} \leq \hat{t}_m^{(1)}$) for which $\delta T_n^{(1)}$ is being calculated, $\beta_n^{(1)}$ denotes the absorption coefficient at $t_n^{(1)}$, and (1) denotes the first pulse.

For the case of multiple pulses, the pulse shape is taken to be invariant. Summing the temperature increases ($\delta T_n^{(1)}$) for k pulses where $t_n^{(j)}$ denotes the n^{th} time in the j^{th} pulse yields

$$\delta T(t) = \sum_{j=1}^{k} \delta T_n^{(j)}$$

and the n^{th} interior time in the j^{th} pulse is given by

$$t_n^{(j)} = t - (j - 1)(\tau_{ps})$$

where j is the integer number of the pulse ($1 \leq j \leq k$) and τ_{ps} is the total time spanned by one pulse (including the separation time between pulses).

At time t, the total temperature rise is given by,

$$\delta T(r,z,t) = [\pi C_p \rho \hat{\tau}_v r_g^2]^{-1} E_o \sum_{j=1}^{k} \beta_n^{(j)} \exp[-\beta_n^{(j)} z] \quad (x)$$

$$\sum_{i=1}^{n} [\tilde{A}(\hat{t}_i^{(j)}) \hat{t}_i^{(j)} \exp(\frac{-(\hat{t}_i^{(j)} - \hat{t}_{i-1}^{(j)})}{\hat{\tau}_v})] \quad (x)$$

$$\int_o^{\hat{t}_n^{(j)}} d\hat{t}' \frac{\exp(-\hat{t}'/\hat{\tau}_v) \exp(-a^2 \hat{r}^2/(\hat{t}_n^{(j)} - \hat{t}' + 1))}{(\hat{t}_n^{(j)} - \hat{t}' + 1)}$$

where $\hat{t}_i^{(j)}$ represents the non-dimensionalized time of the i^{th} Dirac-function subpulse in the j^{th} pump laser pulse ($0 < \hat{t}_i^{(j)} < \hat{t}_n^{(j)}$). The factor

$$E_o \sum_{i=1}^{n} \tilde{A}(\hat{t}_i^{(j)}) \hat{t}_i^{(j)} \exp(\frac{-(\hat{t}_i^{(j)} - \hat{t}_{i-1}^{(j)})}{\hat{\tau}_v})$$

is the total energy made available to the trace species at time, t, by the j^{th} pulse. The index n may be deleted from the expression by use of

$$\hat{t}_n^{(j)} = \hat{t} - (j - 1)\hat{\tau}_{ps}$$

but is retained for clarity. The absorption coefficient is the sum of the absorption coefficients for each of the doublet 3^2P levels. Graphs of this function as a function of r and z, and as a function of r and t are given as Fig. 13 and Fig. 14 respectively. Behaviour of $\delta T(r,z,t)$ for times on the order of $5\tau_v$ is shown as Fig. 15.

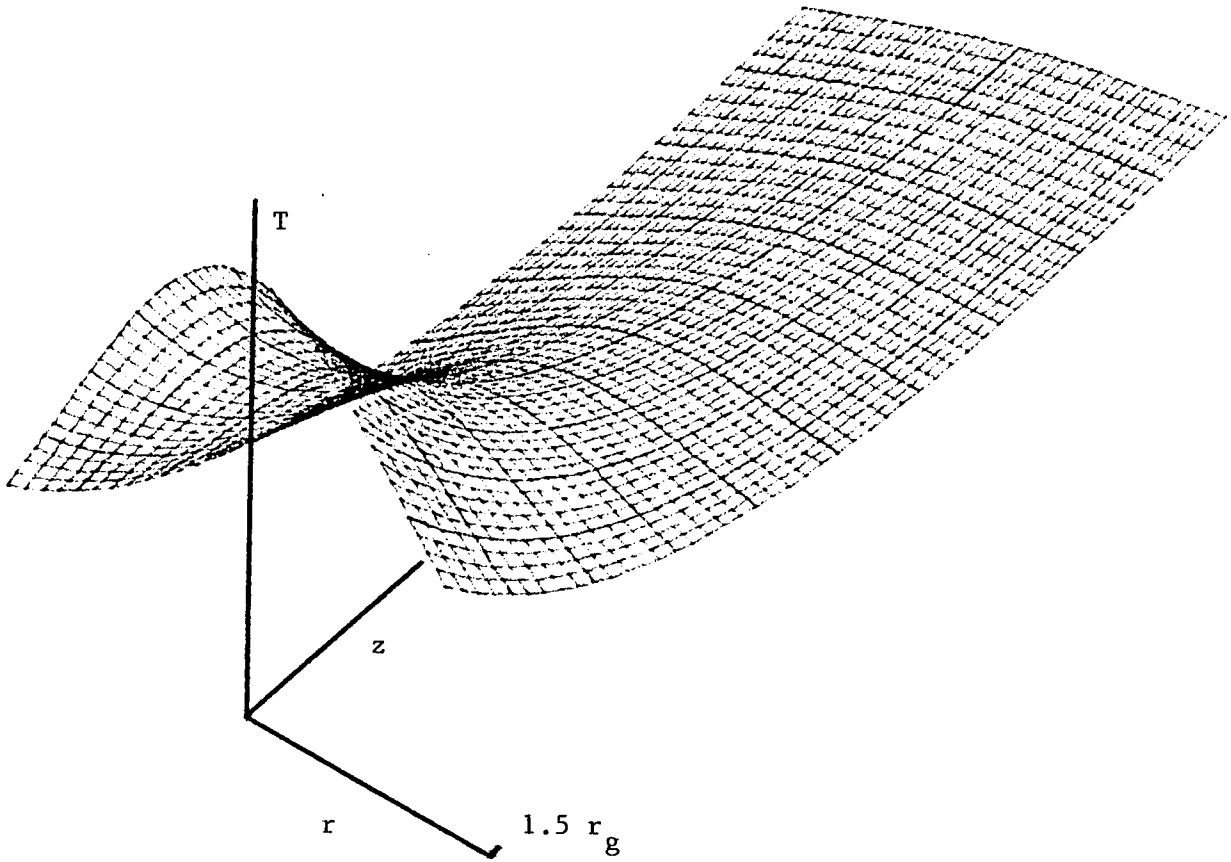

Figure 13. Plot of r vs Z vs δT at t = 63.1 mS for Standard Model.

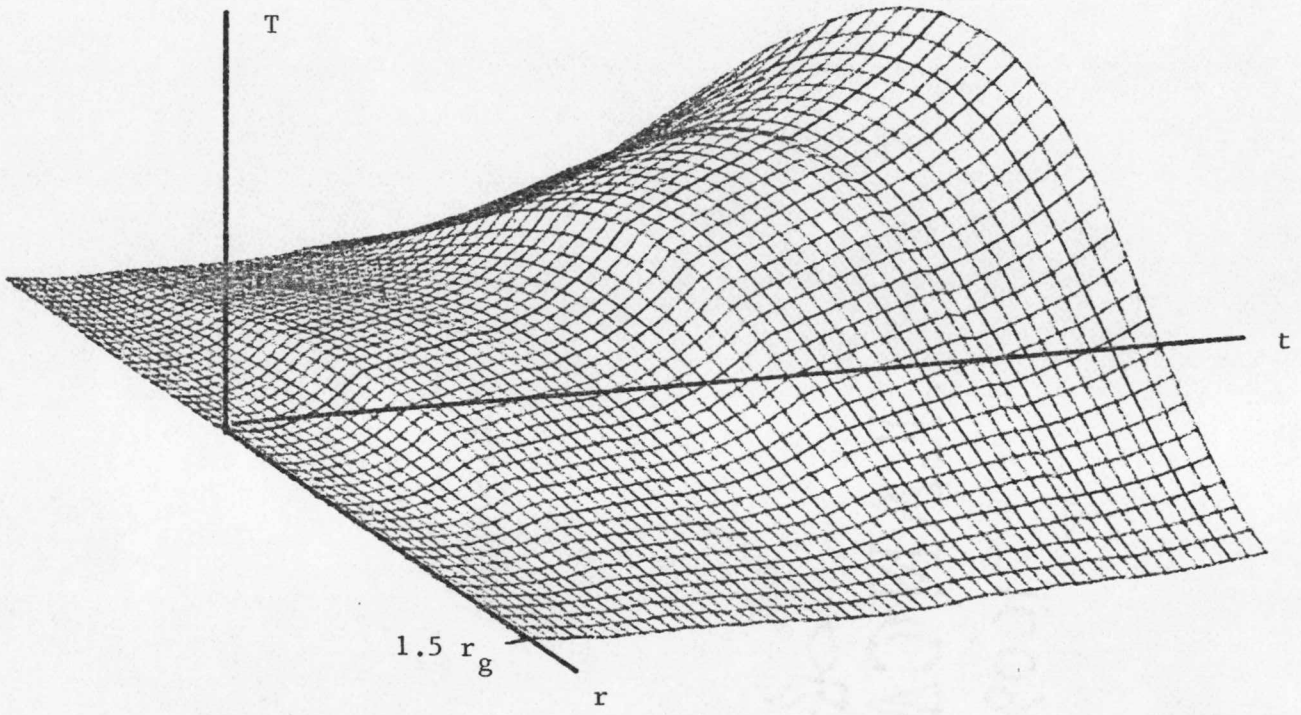

Figure 14. Plot of r vs t vs δT at z = 10 cm into the sample, 10^{-4} sec ≤ t ≤ $5x10^{-3}$ sec. Standard Model used.

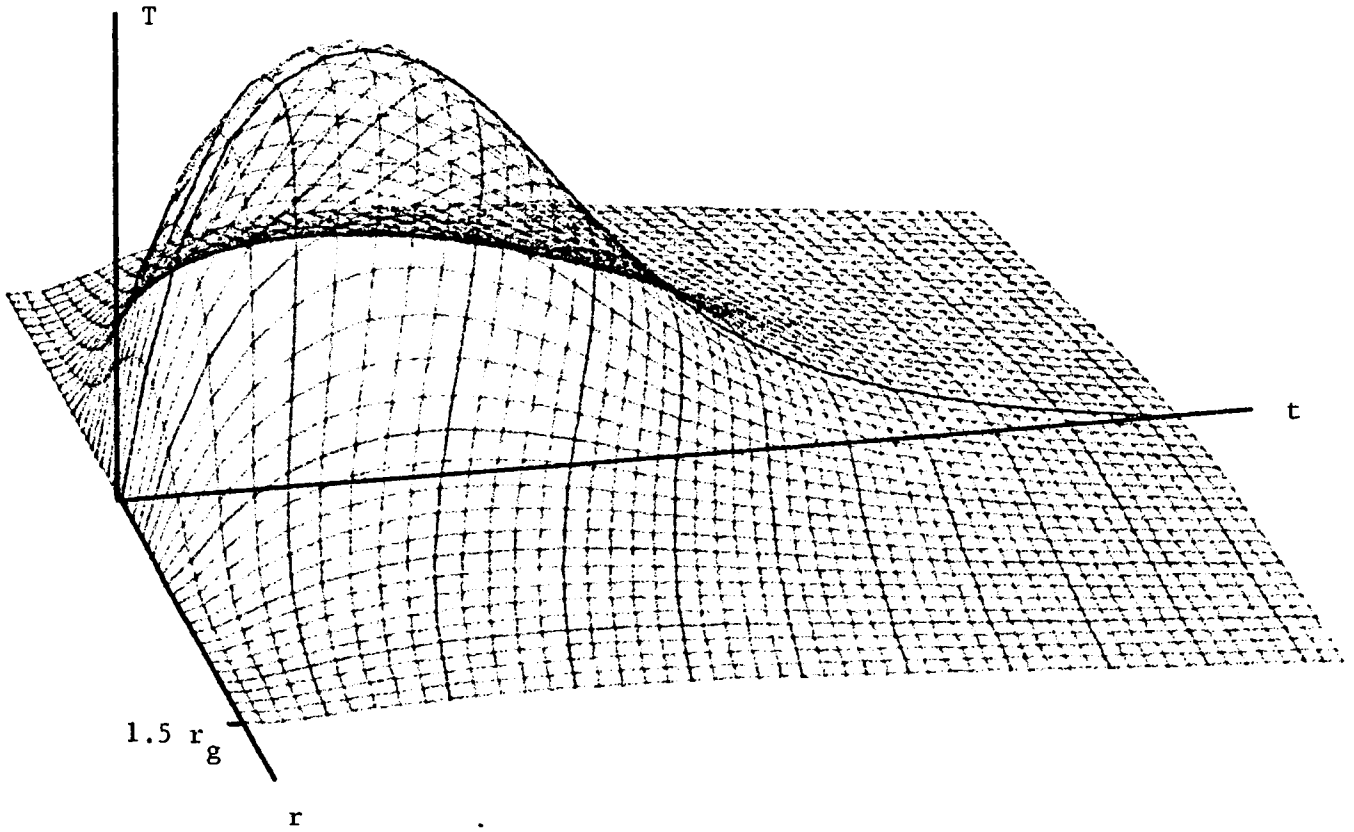

Figure 15. Plot of r vs t vs δT at z = 10 cm into the sample, 10^{-4} sec $\leq$ t $\leq$ $5\tau_v$. Standard Model used.

C. Beam Deflection Theory

Having calculated the two-dimensional, axially symmetric temperature rise $\delta T(r,z,t)$ at any point along the beam length, the change in index of refraction (δn) can be obtained for the thermal conduction domain from the Gladstone-Dale equation

$$\delta n/(n_o-1) = -\delta T/T$$

The path of light through any medium with varying index of refraction is given by the eikonal equation,

$$d/ds\left(n(d\vec{r}/ds)\right) = \vec{\nabla}n$$

where s is the path length and $n = n(r,\theta,z,t)$.

For an incident pump beam along the z axis, the paraxial ray approximation to the eikonal equation is

$$d/dz\left(n(d\vec{r}/dz)\right) = \vec{\nabla}n$$

A sketch of the beam geometry is shown as Fig. 16.

As shown in Appendix A, for axially symmetric conditions, cylindrical coordinates allows the eikonal equation to be written as a set of four coupled, first-order differential equations

$$df_\rho/dt = A(\delta T)f_\rho + \rho f_\theta^2 - B(\delta T)$$

$$df_\theta/dz = A(\delta T)f_\theta - (2/\rho)f_\rho f_r$$

$$d\rho/dz = f_\rho \qquad d\theta/dz = f_\theta \quad .$$

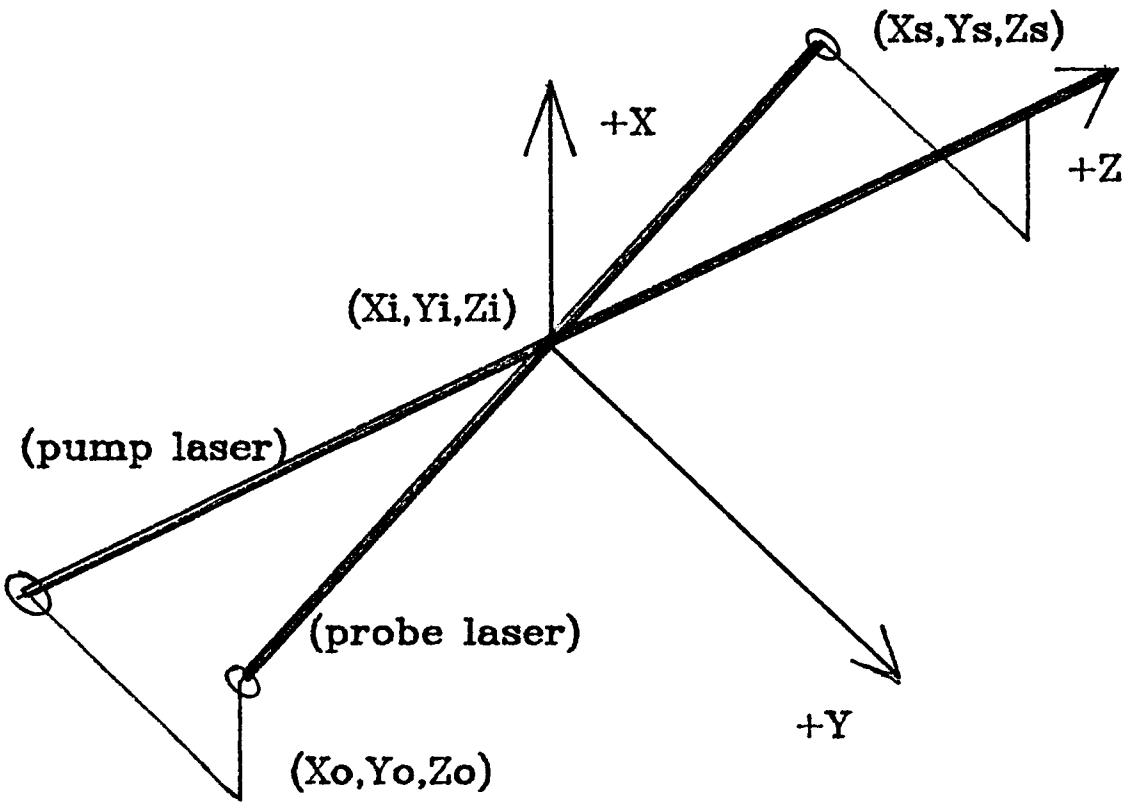

Figure 16. Beam Geometry and Coordinate System.

Solving these equations for the deflection ($||\vec{\Delta r}||$) is not straight-forward, however. One difficulty arises when a temporal calculation is desired and δn is proportional to $\delta T(t)$. Since the eikonal equation does not contain the time explicitly, a separate solution must be determined for each time of interest . Another difficulty arises in just solving the differential equation for a specific time. Essentially these equations are integro-differential equations for which no analytical solution exists. Further, the boundary conditions on the temperature calculation are semi-infinite so that at all points past the entry point of the pump beam into the gas mixture a non-zero temperature field theoretically exists. The final difficulty lies in determining exactly what constitutes the deflection of a probe beam that is finite in width.

To solve the eikonal differential equations and provide the time dependence requires a numerical analysis. A deflection computer code (DCM) was written using the Gear multistep method [24] to integrate the spatial equations. Temporal dependence of the deflection was accomplished by incrementing the time variable in the DCM producing a full set of solutions for each time increment. Merging the MRCM and DCM then produced a realistic model in which the temporal population changes of the sodium 3^2P level, the Voight broadening function of the gas, and the frequency distribution of the laser provided the temporal and spatial temperature field (and consequent deflection) at each point along the path of a light ray.

Since each solution of the DCM calculated the deflection of only one ray of light contained in the probe beam, it was necessary to

devise a method whereby the deflection of the entire probe could be defined. To include a finite width for the probe beam required solving the DCM for enough rays to lend shape to the probe beam. For the sake of clarity in observing the deflection and astigmatic distortion of the probe beam at the screen position, an elliptical Gaussian beam shape was assumed. The length of the semi-major axis of the ellipse varied with the intersection angle, α, to insure that the undeflected beam at the screen position would be Gaussian (and near circular) in shape. Figure 17a shows the circular projection of the beam on the xy plane and Figures 17b, c, and d show the necessary shape of the elliptical beam to produce the circular projection at several intersection angles. The equation of the ellipse necessary to produce the circular image becomes

$$r_e^2 = \frac{r^2 \cos^2\alpha}{(\sin^2\theta + \cos^2\theta \cos^2\alpha)}$$

where r,θ are the polar coordinates in the circular projection. Eccentricity of the ellipse is simply $\sin\alpha$. The Gaussian radius, r_{ep}, of the ellipse for a circular projection of Gaussian radius, r_p, is then

$$r_{ep}^2 = \frac{r_p^2 \cos^2\alpha}{(\sin^2\theta + \cos^2\theta \cos^2\alpha)}$$

and the intensity plot for the elliptical, Gaussian probe beam becomes

$$I/I_o = \exp\left(-(r_e/r_{ep})^2\right)$$

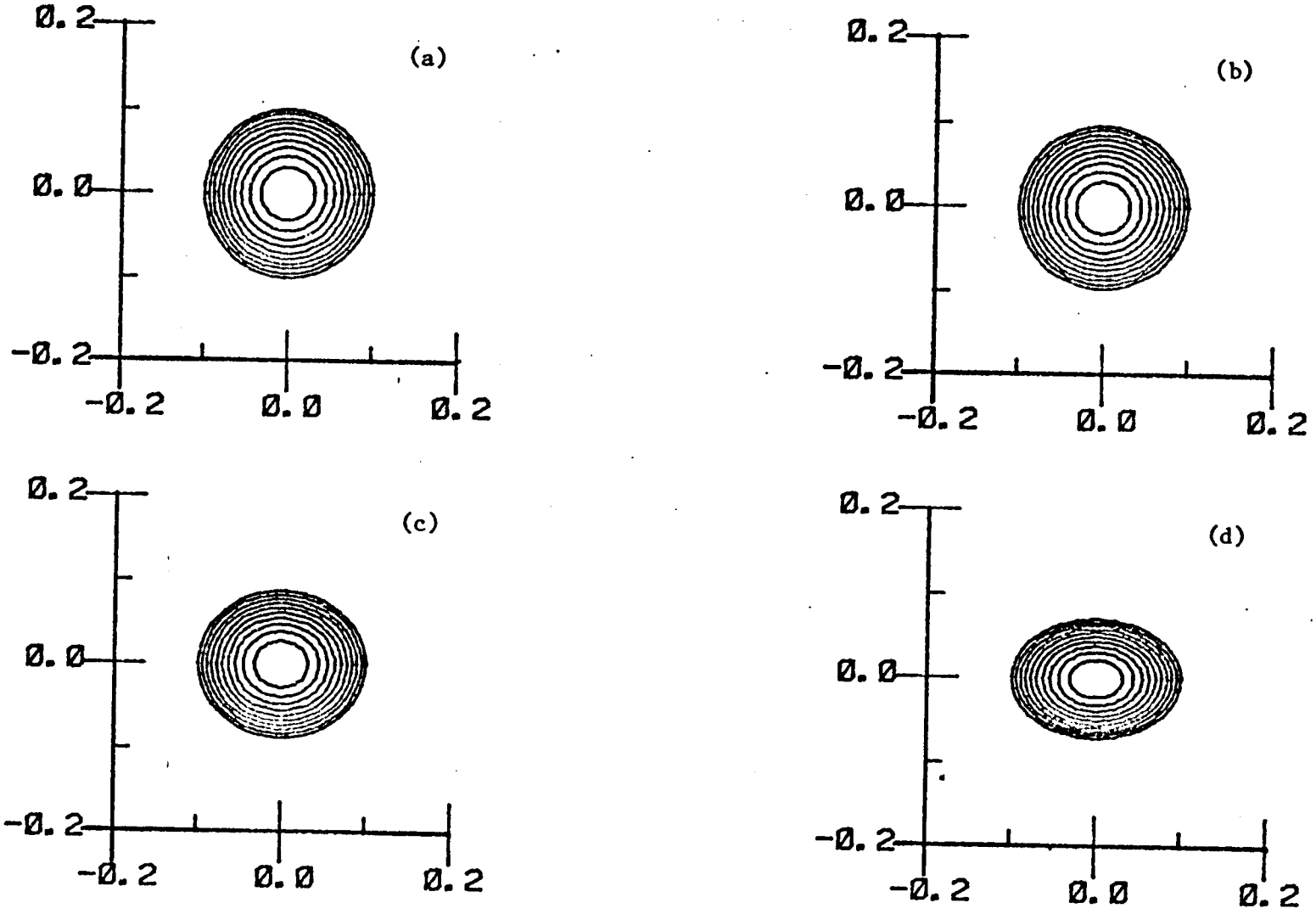

Figure 17. Elliptical Gaussian Shape of the Probe Beam. All axes are in mm. (a) Image of probe beam on xy plane. Elliptical shape of the beam for crossing angles of (b) 15°, (c) 30°, (d) 45°.

to produce a corresponding Gaussian intensity distribution of

$$I/I_o = \exp\left(-(r/r_p)^2\right)$$

on the xy plane. Taking n rays within the probe beam, one ray at the center, the balance spaced around the perimeter at the Gaussian radius, r_{ep}, required n solutions of the eikonal, but produced plots dramatically illustrating the computed deflection (see Fig.20 as an example).

The final two questions to arise are (1) the validity of using the intensity distribution of such an elliptical beam to experimentally determine the deflection, and (2) the experimental feasibility of producing such a beam.

Since the beam is of finite width, precisely determining a deflection that may be less than or approximately .001 r_p can be done only if the intensity distribution is predictable after deflection occurs. To be predictable, the deflected beam must also be the same intensity distribution as the undeflected beam. For example, a Gaussian undeflected beam must produce a Gaussian deflected beam. For $\delta T/T < 0.1$, the absolute deflection, $||\vec{\Delta r}||$, of each computed ray comprising the beam model in the DCM was equal (see Fig. 18). Constant deflection with respect to the width of the xy projection of the undeflected probe indicates that a Gaussian, circular intensity region before deflection will map into a Gaussian region after deflection. Because of astigmatic effects, the deflected image will not necessarily be circular. Using a photo-sensitive array capable of detecting variations on the order of 1 μm, a digital integration by

standard laboratory equipment could be performed over the area of both the deflected and undeflected images. Comparison of the areas covered on the array by the spot intensity would give the deflection, $||\vec{\Delta r}||$. If the probe beam is taken to be non-Gaussian, but of constant intensity, the projection of the elliptical shape would again be circular, but of constant intensity. The digital integration technique mentioned above would again be valid.

The final procedure to be established is the ability to construct such an angle-varying, elliptical beam in the laboratory. Once the shape and cross sectional area of the probe beam is determined, a circular aperature with radius, r_p, centered at the (x_o,y_o,z_o) point and overfilled by the probe beam would produce the desired elliptical shape within the gas sample. All intersection angles, α, defined by (x_o,y_o,z_o) and (x_i,y_i,z_i) would be restricted to values such that the paraxial ray approximation is valid ($\tan \alpha \simeq \alpha$). Since the deflection is a measure of the absolute difference in position across the area of the beam intensity, the actual intensity distribution at the initial entry point (x_o,y_o,z_o) is not critical, The only requirement for the probe laser intensity distribution is that it be constant during the time that the deflection measurement is taken.

CHAPTER III

RESULTS

To provide a reference, a standard model (SM) was devised using the constraints and concepts developed in the paragraphs above. Specific data for the SM is shown in Table 1. To insure that the calculations were truly being made in the isobaric region, pulse lengths of 1 msec were used. All models used to quantify deflection effects assumed four, 1 msec pulses of a pump laser with r_g = 0.1 cm centered on the $3^2P1/2$ spectral line of sodium (589.59nm) and with linewidth, $\Delta\nu_L$ of 10^9 hz. Voight broadening then allowed both spectral lines of the sodium to be pumped and the degree of pumping of each line varied with the assumed ambient temperature and number density of the gas. As an example, ratios of spectral pumping for the $3^2P1/2$ to $3^2P3/2$ lines are 1:1.2 x 10^{-5} at 300K, 1:4 x 10^{-5} at 1000K, and 1:7.5 x 10^{-5} at 2000K. For all calculations, the intersection angle, α, was taken to be approximately 14° (0.245 radians) with the intersection point of the two beams lying 10 cm into the gas sample. Deflections were calculated assuming a distance of 100 cm from intersection point to screen position. Length of this "moment arm" had a direct effect on the value (and detectability) of the deflection.

An initial run of the SM with only nitrogen as the host species and sodium as the trace species produced a V-T relaxation time (τ_v) in excess of 10^2 seconds. This was predictable from the empirical results given by Anderson.[32] Extremely long relaxation times produced virtually no temperature rise in the gas mixture and, consequently, no

Table 1. Standard Model (SM) Parameters

A. Pump Laser Parameters:

E_o (energy) = 1.00×10^7 ergs

r_g (Gaussian radius) = 1.0 mm

τ_p (FWHM of pulse time) = 1.0 msec

τ_{ps} (FWHM + pulse separation time) = 2.0 msec

I_p (no. of pulses) = 4

$\Delta\nu_L$ (Linewidth) = 1.0×10^9 hz

$\nu_{o\ell}$ (Linecenter) = 589.59 nm

B. Atmosphere Parameters:

$n(N_2)$ (host number density) = 1×10^{19} molecules/cm^3

n(Na) (trace number density) = 1×10^{10} molecules/cm^3

τ_c (heat conduction time) = 4.649 msec

τ_v (vibrational relaxation time = 111.2 msec

n_o (index of refraction) = 1.0003

K (thermal conduct.) = 2.598×10^3 ergs/(cm - k)

C_p (specific heat) = 2.910×10^8 ergs/(g-mole k)

ρ (molar density) = 1.550×10^{-5} g-mole/cm^3

$\Delta\nu_g$ (Doppler Linewidth) = 1.066×10^9 hz

$\Delta\nu_s$ (Lorentzian linewidth) = 1.606×10^9 hz

C. Interception parameters:

(x_o, y_o, z_o) (initial probe beam coordinate) = (4,4,-10) (cm)

(x_i, y_i, z_i) (beam intersection point) = (0,0,0) (cm)

deflection. To decrease the relaxation times by about three orders of magnitude (to about 100 msec), introduced into the Na | N_2 mixture was a third gas whose selection had to meet two criteria. No spectral absorption could take place at or near the sodium 3P levels. Vibrational resonances must occur at or near the predominant levels of the nitrogen with the energy quickly relaxing into translational energy. A common gas meeting both criteria proved to be water vapor [21]. Vibrational levels of water vapor are shown juxtaposed with those of nitrogen in Fig. 5. By introducing a number density of water vapor equivalent to approximately 10 ppm, the V-T relaxation time was decreased to approximately 100 msec, and significant heating of the gas mixture occured with this V-T relaxation time. Using SM computations yielded a maximum temperature rise of 15.1K at a time of about 63.1 mS for four (4), millisecond pulses. The calculated deflection was quite satisfactory (see Fig. 18) and was of the order of approximately 500 μm.

To obtain a region of validity for the LIST, initial computational runs of the MRCM and DCM were made for a $n(N_2)$ of 10^{19} per cm^3 (approximately 0.4 atm. at 300K) and n(Na) ranging by decades from 1 part per trillion (1 ppt) to 100 ppb. For each value of n(Na), pump laser energies, E_o, ranging from 10^4 ergs to 10^9 ergs were used. To investigate the effect of varying $n(N_2)$ on the deflection, selected calculations were also performed for 10^{18} per cm^3 (approximately 0.04 atmospheres at 300K) and 10^{21} per cm^3 (approximately 40 atmospheres at 300K). As mentioned previously, the accuracy of the calculations for 10^{21} per cm^3 of nitrogen suffer from the lack of three body quenching

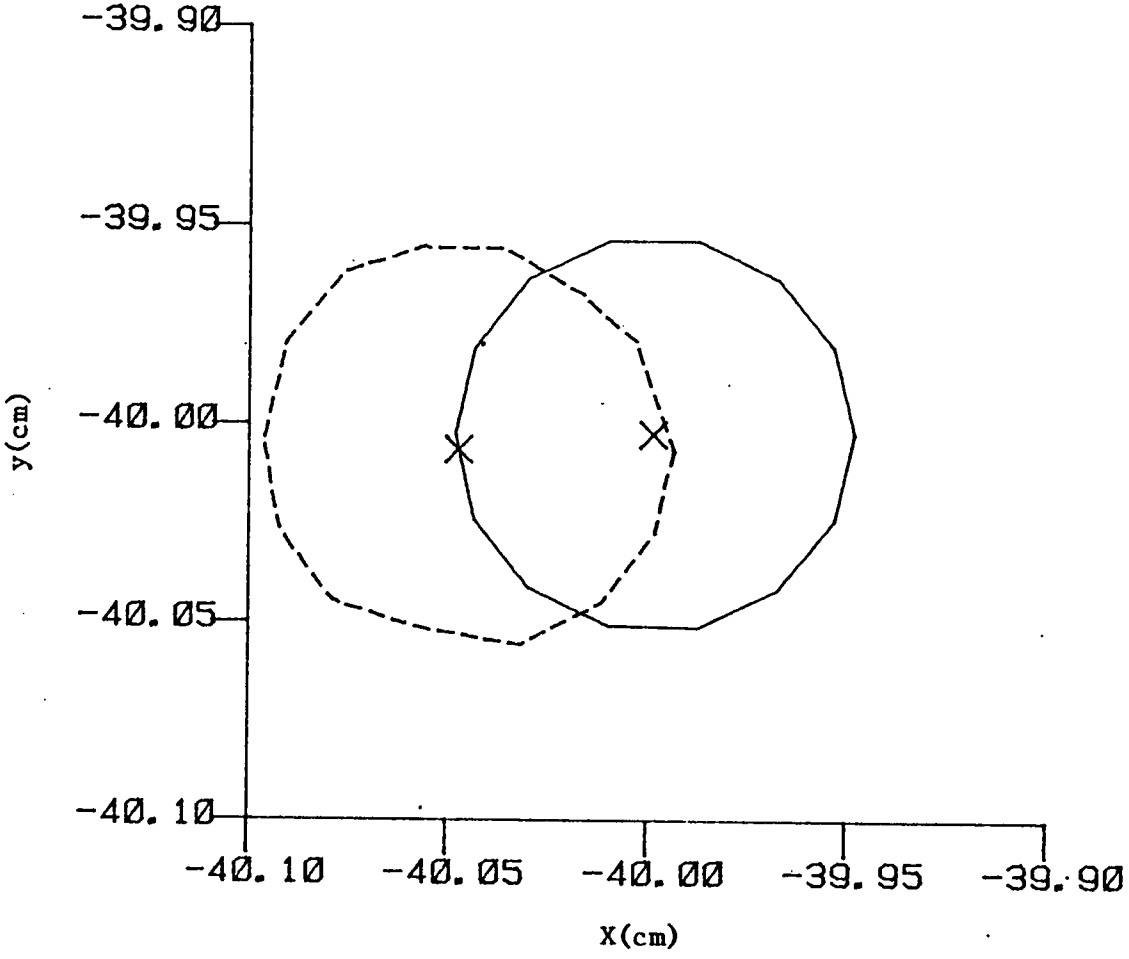

Figure 18. Deflection Plot Showing Point-to-Point Deflection

rates in the MRCM, but the deflection results may be used to indicate a trend.

Figure 19 graphically displays the results of $||\vec{\Delta r}||$ vs n(Na) (10^{19} cm^{-3} of nitrogen at 300K, $E_o = 10^7$ ergs, and $\tau_v = 113.5$ mS). Figure 20 displays the change in the sodium levels as a function of time. As expected low n(Na) allowed little absorption of the pump laser radiation with virtually no deflection of the probe. Figure 21 displays the calculated xy projections of the deflection of the probe beam for the indicated number densities at $t/\tau_v \simeq 0.55$, the time ratio for maximum δT. Increases in the astigmatic distortion as $||\vec{\Delta r}||$ increases are easily seen. Maximum deflection for $n(N_2) = 10^{19}$ cm^{-3} occured at or near the SM (1 ppb of sodium) with $||\vec{\Delta r}||$ rapidly dropping for $n(Na)/n(N_2)$ greater than 10 ppb. Above 100 ppb the deflection from 10^7 ergs of laser energy is again virtually undetectable. The decrease in $||\vec{\Delta r}||$ at the 100 ppb number density is attributable to the increased absorption cross section of the sodium and the attendant rise in the absorption coefficient from .0263 cm^{-1} to 2.63 cm^{-1} (see Fig. 22). The gas becomes optically thick with little energy available for absorption at the intersection of the beams.

Varying E_o produced an exponential increase in the deflection at $t/\tau_v \simeq 0.55$ for 10^{19} cm^{-3} of nitrogen and 1 ppb of sodium. The condition that $\delta T/T < .1$ was quickly violated once E_o exceeded approximately 10^8 ergs, although the DCM computed deflections of nearly 50,000 μm (5 cm) at $t/\tau_v \simeq 0.55$ for the 10^9 ergs case. Increasing the pump power increased the population of the two sodium 3^2P levels as shown by Fig. 23. Saturation was nearly reached at 10^8 ergs. Figure 24

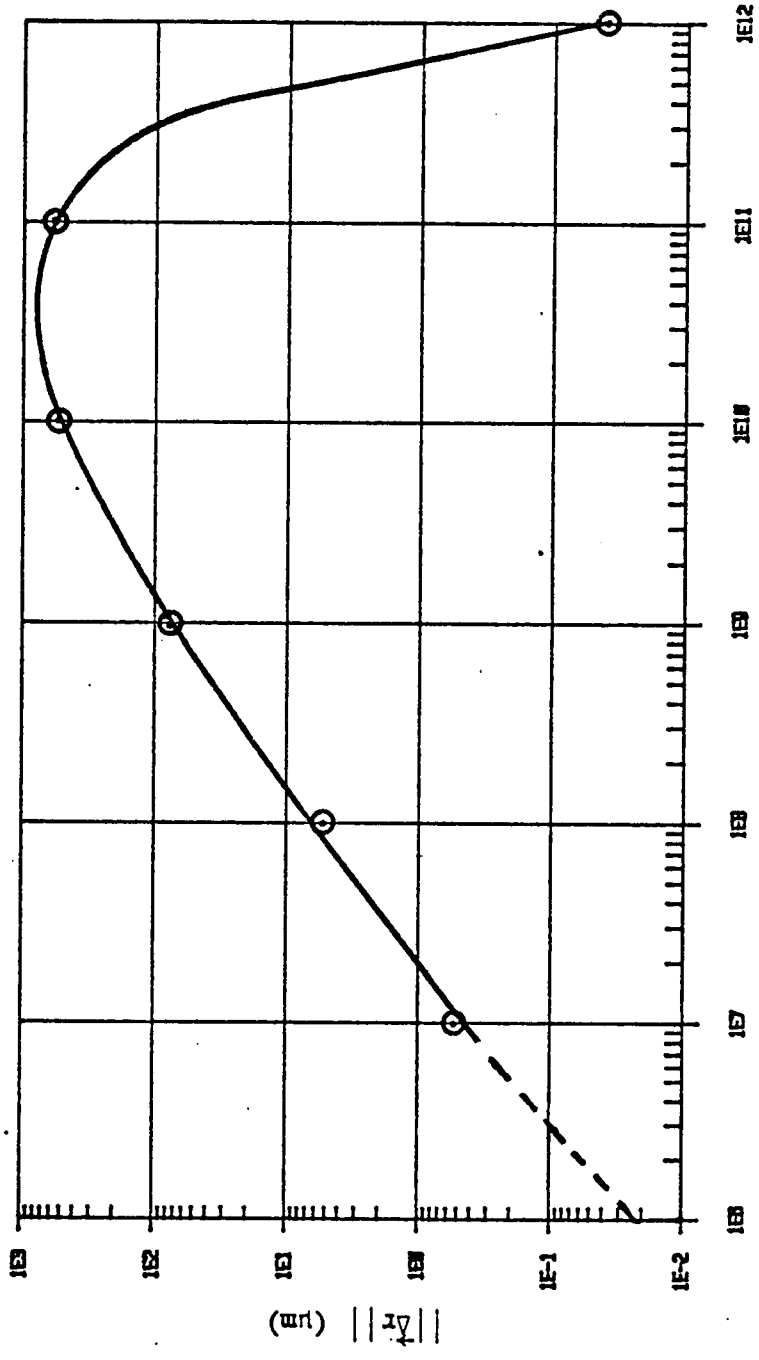

Figure 19. Line Plot showing $||\vec{\Delta r}||$ vs n(Na) for $n(N_2) = 10^{19}$ cm^{-3}.

Figure 20. Number Density Variations of Sodium Electron Levels for constant E_o, solid line is $3S1/2$, short broken line is $3^2P3/2$ and long broken line is $3^2P1/2$. $n(N_2) = 10^{19}$ cm^{-3}, $E_o = 10^7$ ergs, (a) n(Na) = 10^9 cm^{-3}, (b) n(Na) = 10^{10} cm^{-3}, (c) n(Na) = 10^{11} cm^{-3}, (d) n(na) = 10^{12} cm^{-3} .

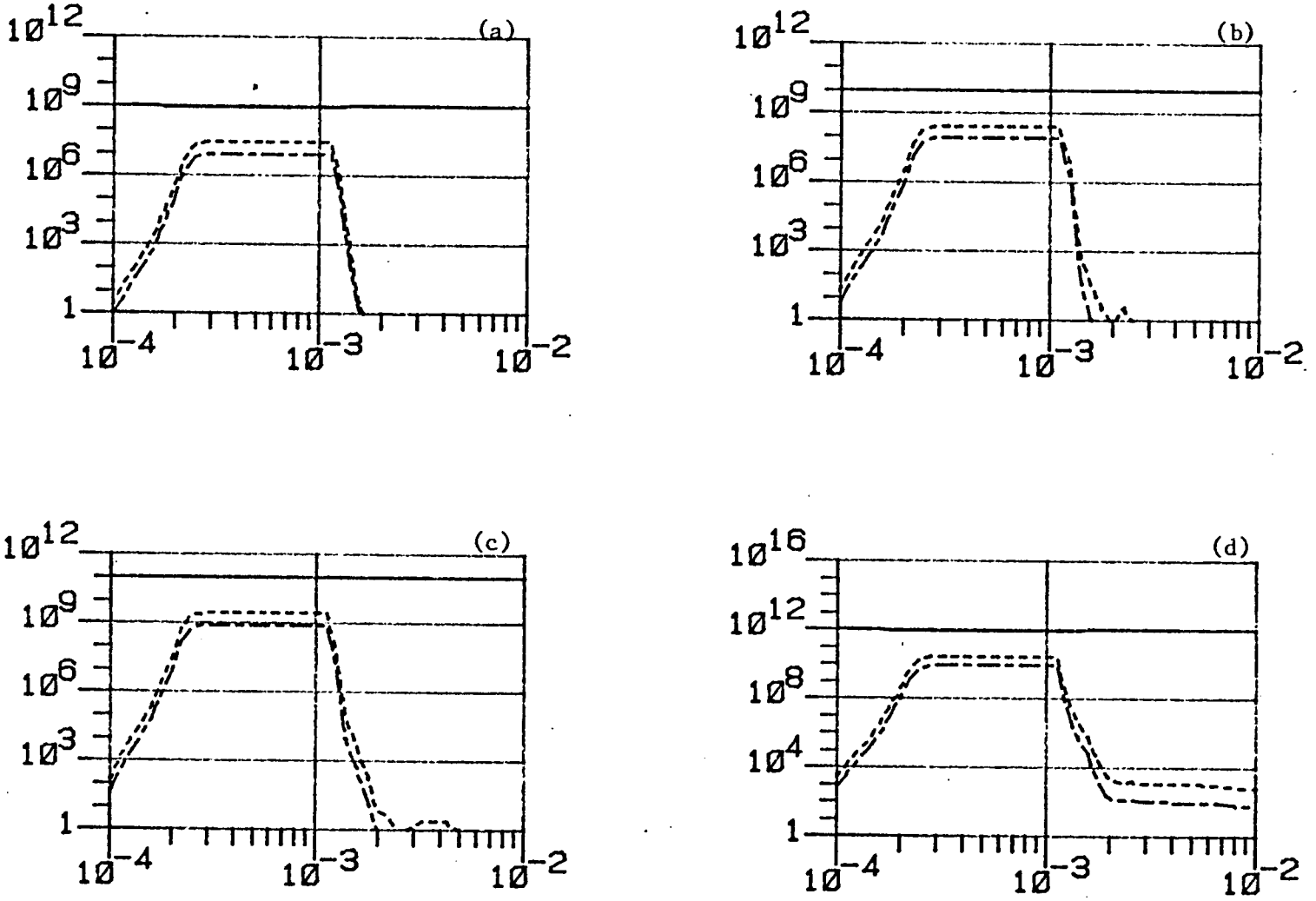
(a)
10^{12}
10^{9}
10^{6}
10^{3}
1
10^{-4}
10^{-3}
10^{-2}
(b)
10^{12}
10^{9}
10^{6}
10^{3}
1
10^{-4}
10^{-3}
10^{-2}
(c)
10^{12}
10^{9}
10^{6}
10^{3}
1
10^{-4}
10^{-3}
10^{-2}
(d)
10^{16}
10^{12}
10^{8}
10^{4}
1
10^{-4}
10^{-3}
10^{-2}

Figure 20

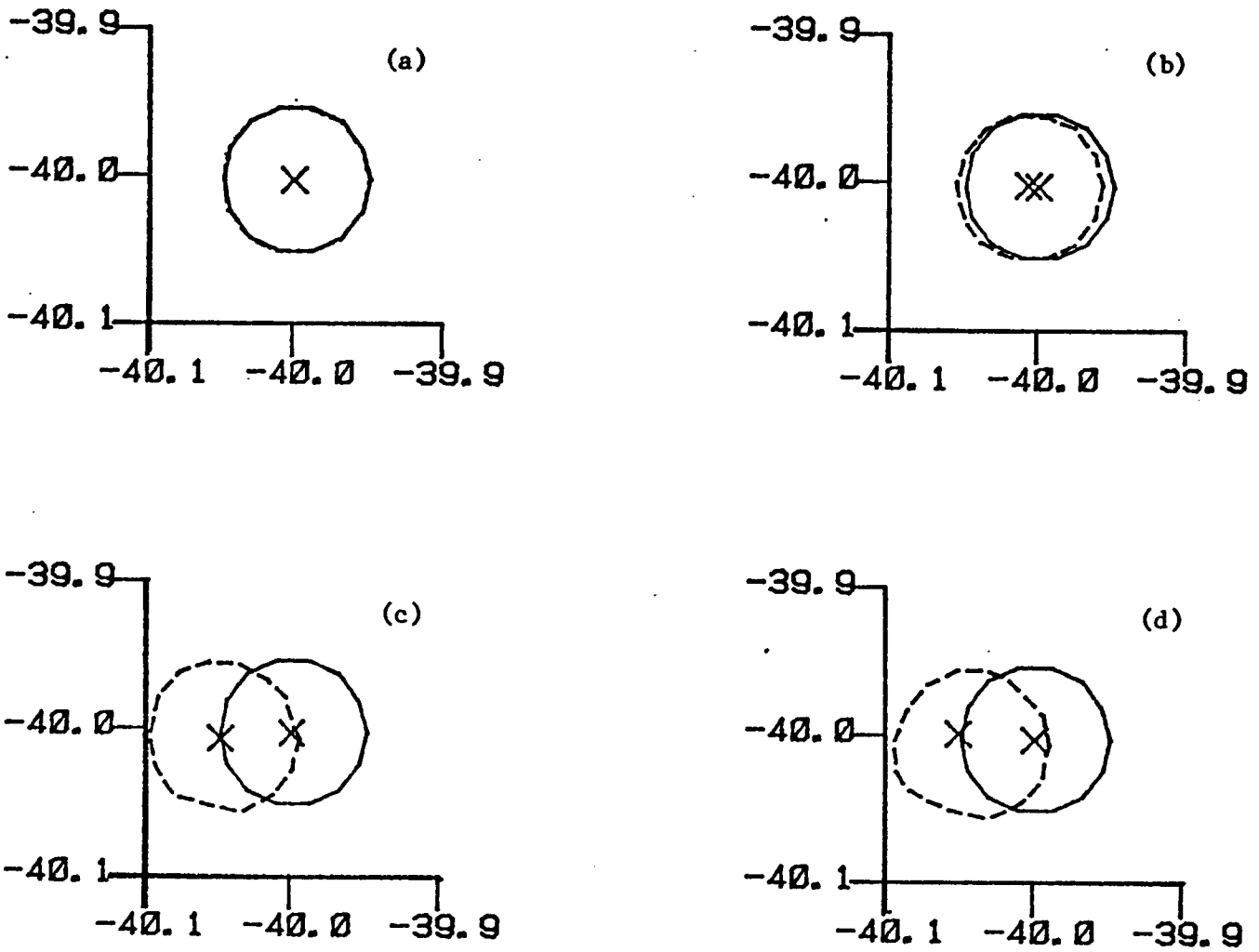

Figure 21. Circular Deflection Plot for $n(N_2) = 10^{19}$, $E_o = 10^7$ergs. (a) $n(Na) = 10^8$ cm^{-3}, (b) $n(Na) = 10^9$ cm^{-3}, (c) $n(Na) = 10^{10}$ cm^{-3} (5M), (d) $n(Na) = 10^{11}$ cm^{-3}. Axes are in cm.

Figure 22. Absorption Coefficient for $n(N_2) = 10^{19}$ and $E_o = 10^7$ ergs. (a) $n(Na) = 10^9$ cm^{-3}, (b) $n(Na) = 10^{10}$ cm^{-3}, (c) $n(Na) = 10^{11}$ cm^{-3}, (d) $n(Na) = 10^{12}$ cm^{-3}.

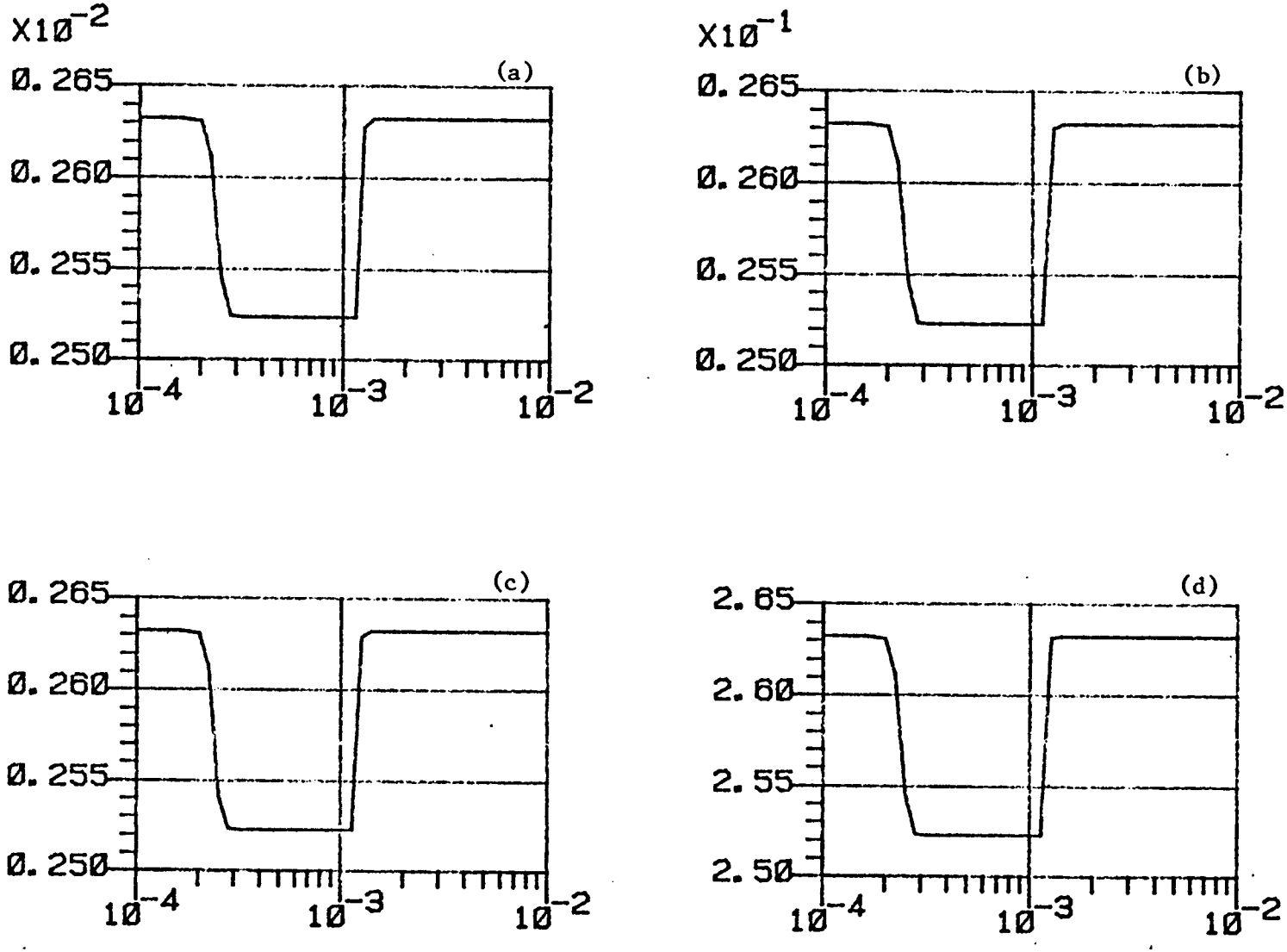
X10-2
0.265
0.260
0.255
0.250
10-4
10-3
10-2
(a)
X10-1
0.265
0.260
0.255
0.250
10-4
10-3
10-2
(b)
0.265
0.260
0.255
0.250
10-4
10-3
10-2
(c)
2.65
2.60
2.55
2.50
10-4
10-3
10-2
(d)

Figure 22.

Figure 23. Number density Variation of Sodium Electronic levels for varying E_o, solid line is $3S1/2$, short broken line is $3^2P3/2$ and long broken line is $3^2P1/2$. $n(N_2) = 10^{19}$ cm^{-3} and $n(Na) = 10^{10}$ cm^{-3} (a) $E_o = 10^5$ ergs, (b) $E_o = 10^6$ ergs, (c) $E_o = 10^7$ ergs (SM), (d) $E_o = 10^8$ ergs.

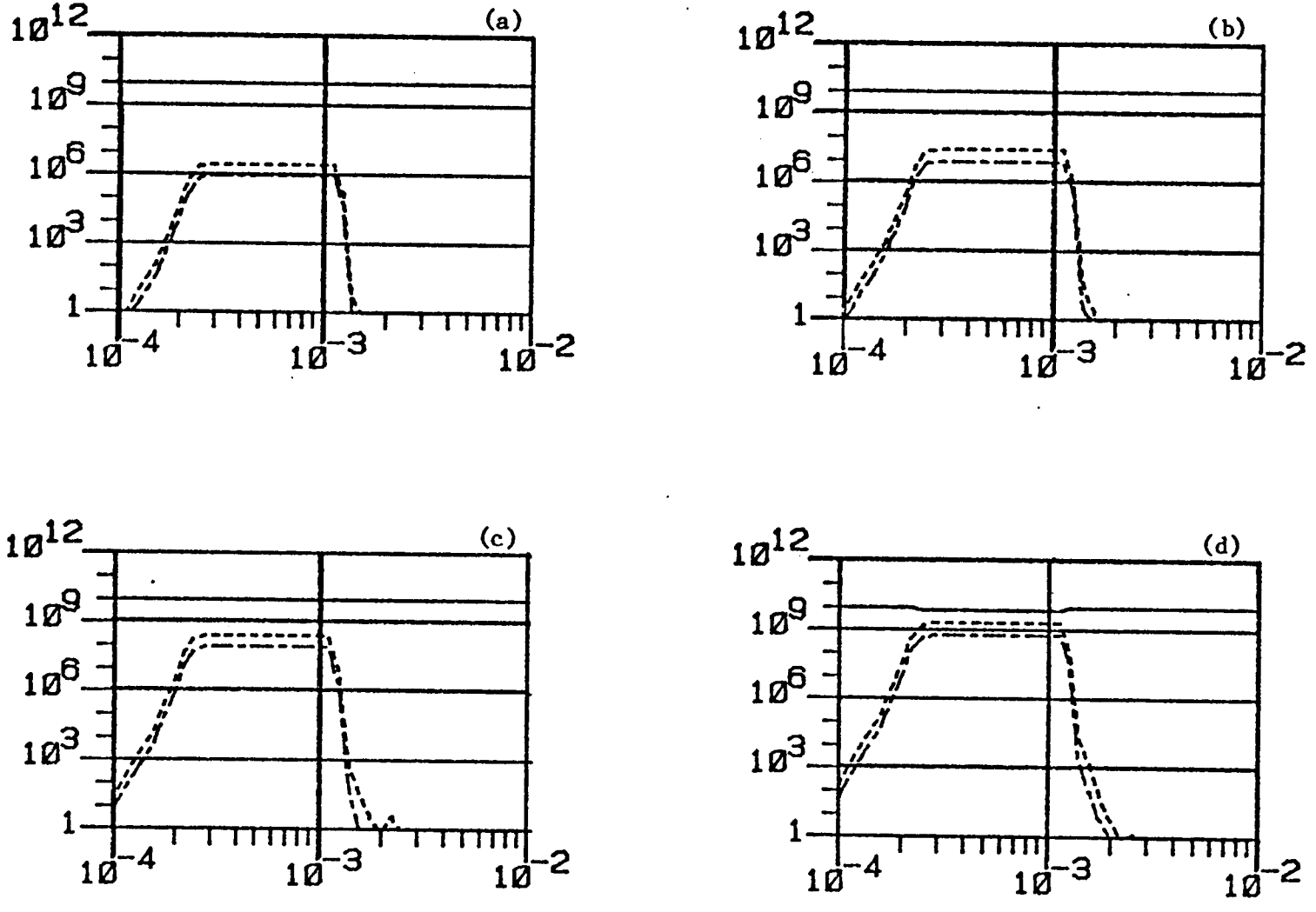

Figure 23.

Figure 24. Absorption Coefficient for $n(N_2) = 10^{19}$ cm^{-3}, $n(Na) = 10^{10}$ cm^{-3} and varying E_o. (a) $E_o = 10^5$ ergs, (b) $E_o = 10^6$ ergs, (c) $E_o = 10^7$ ergs (SM), (d) $E_o = 10^8$ ergs .

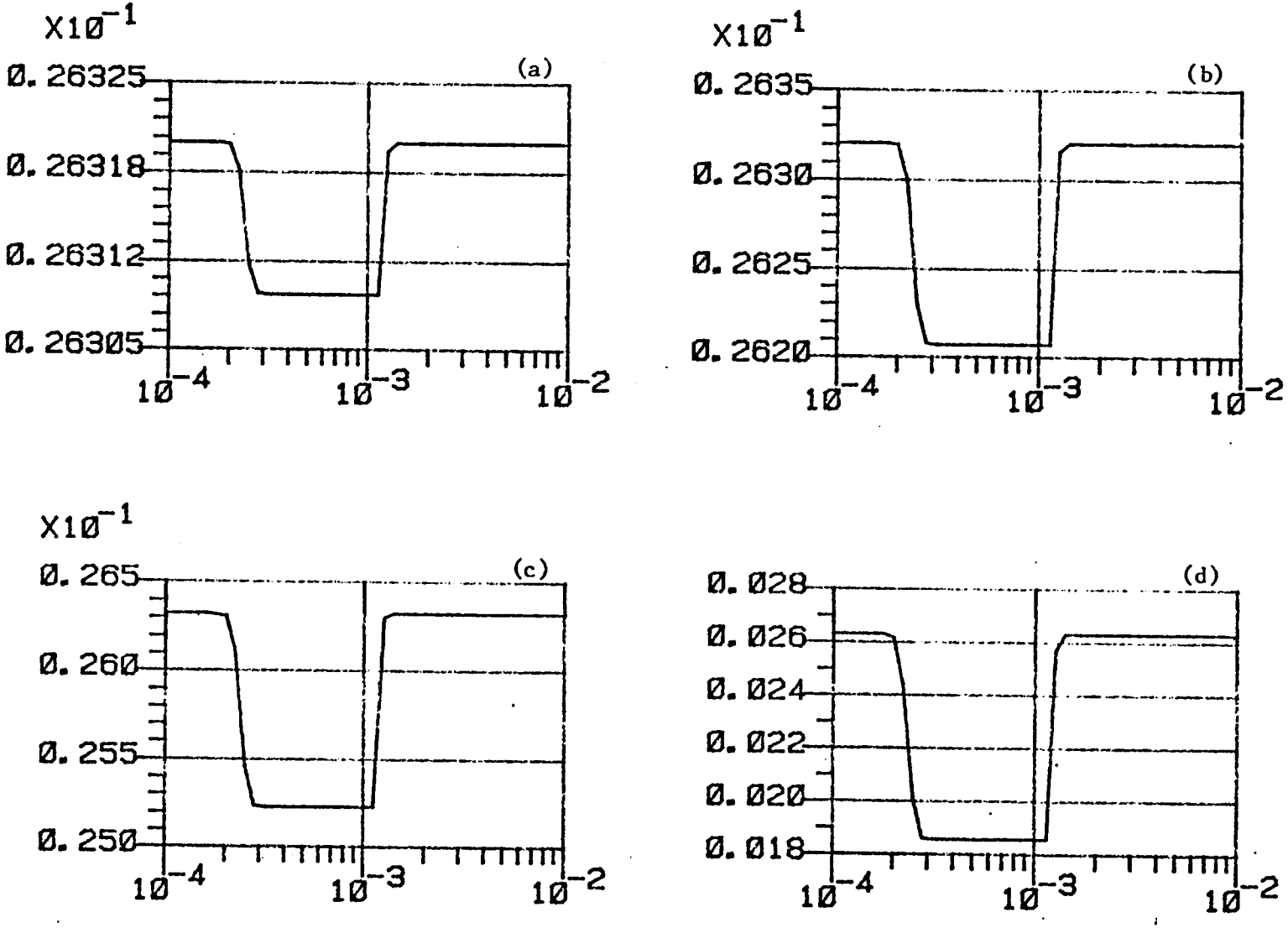
X10⁻¹
0.26325
0.26318
0.26312
0.26305
10⁻⁴
10⁻³
10⁻²
(a)
X10⁻¹
0.2635
0.2630
0.2625
0.2620
10⁻⁴
10⁻³
10⁻²
(b)
X10⁻¹
0.265
0.260
0.255
0.250
10⁻⁴
10⁻³
10⁻²
(c)
0.028
0.026
0.024
0.022
0.020
0.018
10⁻⁴
10⁻³
10⁻²
(d)

Figure 24.

shows the changing absorption coefficient. Restricting the $\delta T/T$ ratio to the upper end of its range of validity at the 10^8 ergs and 10^9 ergs values of E_o predicted reasonable deflection measurements of approximately 500 μm at $t/\tau_v = 0.022$ ($\delta T/T \simeq 0.08$). Deflection versus E_o projection plots, shown as Fig. 25, are chosen for time regions where $\delta T/T < 0.1$. A graph of $||\vec{\Delta r}||$ vs E_o is given as Figure 26.

Increasing $n(N_2)$ to 10^{21} per cm^3 decreased τ_v to approximately 2.0 msec. The temperature peaks occurred approximately 50 msec sooner than in the lower $n(N_2)$ case, but for $n(N_2) = 10^{21}$ per cm^3 $t/\tau_v = 7.9$ for the peak while at $n(N_2) = 10^{19}$ per cm^3 $t/\tau_v = 0.55$. The difference in t/τ_v ratios can be attributed to the increased dependence on the heat conduction time (τ_c) in the gas since for the $n(N_2) = 10^{21}$ per cm^3 runs, $\tau_v/\tau_c \simeq 0.005$ while for the $n(N_2) = 10^{19}$ per cm^3 runs, $\tau_v/\tau_c \simeq 25.0$. Even though the molecular collision processes increased the absolute rate at which the vibrational energy relaxed in the higher $n(N_2)$ case, the heat conduction time which is proportional to ρ^2 moderates the τ_v/τ_c ratio. Although not entirely valid because of the preponderance of three-body collisions in the gas sample, the higher $n(N_2)$ illustrates the increased dependence of the energy transfer mechanisms on the collisional relaxation times. Reasonable deflections seem possible at the higher value of $n(N_2)$ with a n(Na) range of 0.1 ppt to 1 ppb, but pump laser energies of 10^7 ergs or greater would be required. Since saturation effects begin to dominate at higher pump energies, the upper limit on useable E_o would be less than 10^9 ergs. Figure 27 depicts the deflection versus n(Na) for $n(N_2) = 10^{21}$ cm^{-3} of nitrogen, $E_o = 10^7$ ergs, and four 1 mS pulses.

Figure 25. Circular Deflection Plots for Varying E_o, n(Na) = 10^{10} cm^{-3}, $n(N_2)$ = 10^{19} cm^{-3}. $\delta T/T$ not violated. (a) E_o = 10^5 ergs, (b) E_o = 10^6 ergs, (c) E_o = 10^7 ergs (SM), (d) E_o = 10^8 ergs. All axes in cm.

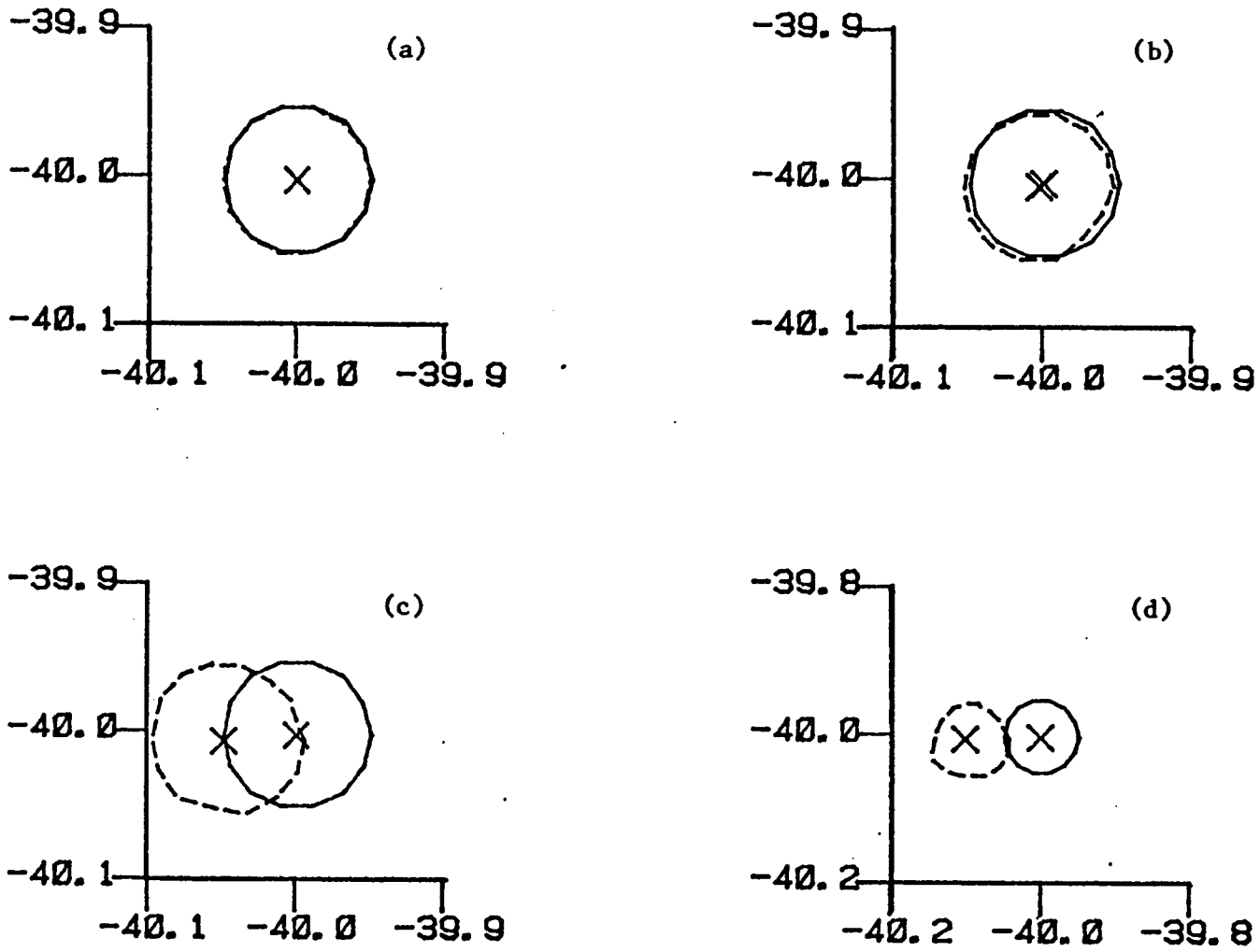
(a)
-39.9
-40.0
-40.1
-40.1
-40.0
-39.9
(b)
-39.9
-40.0
-40.1
-40.1
-40.0
-39.9
(c)
-39.9
-40.0
-40.1
-40.1
-40.0
-39.9
(d)
-39.8
-40.0
-40.2
-40.2
-40.0
-39.8

Figure 25.

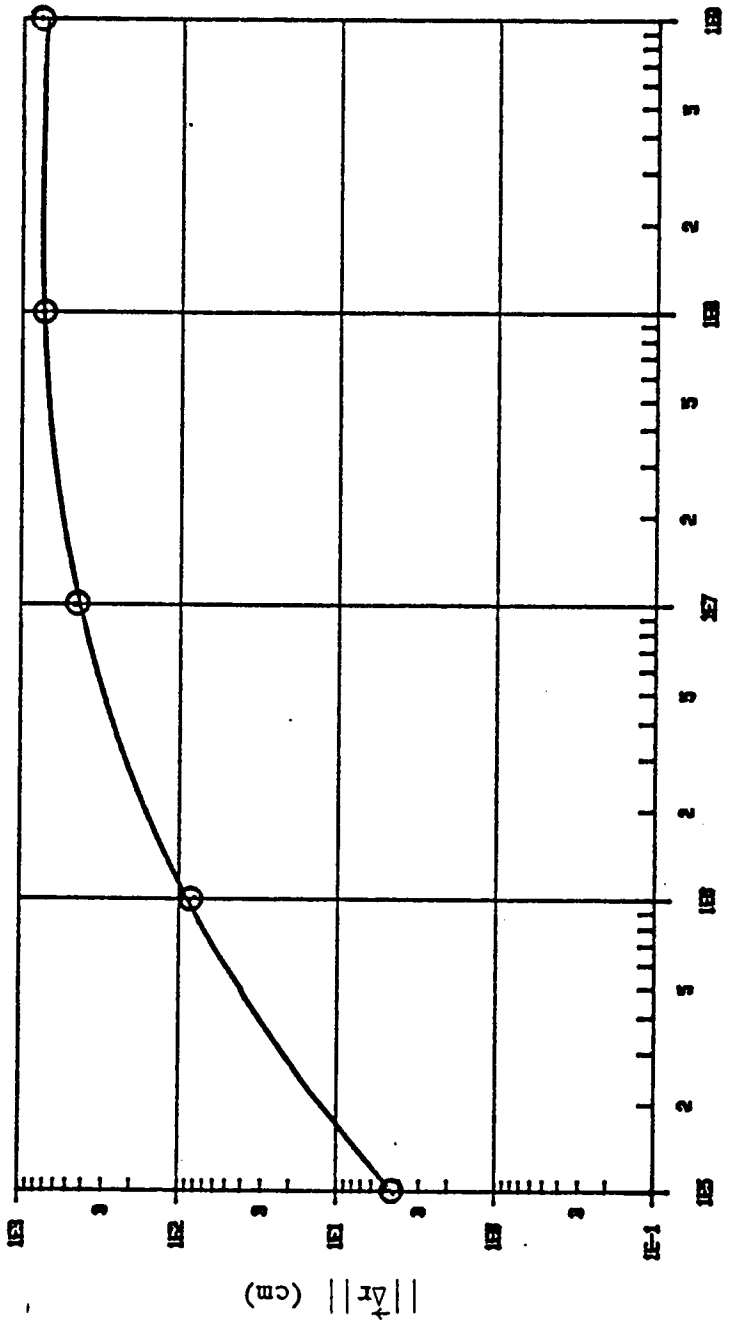

Figure 26. Line plot of $||\vec{\Delta r}||$ vs E_o, $n(Na) = 10^{10}$ cm^{-3}, $n(N_2) = 10^{19}$ cm^{-3}.

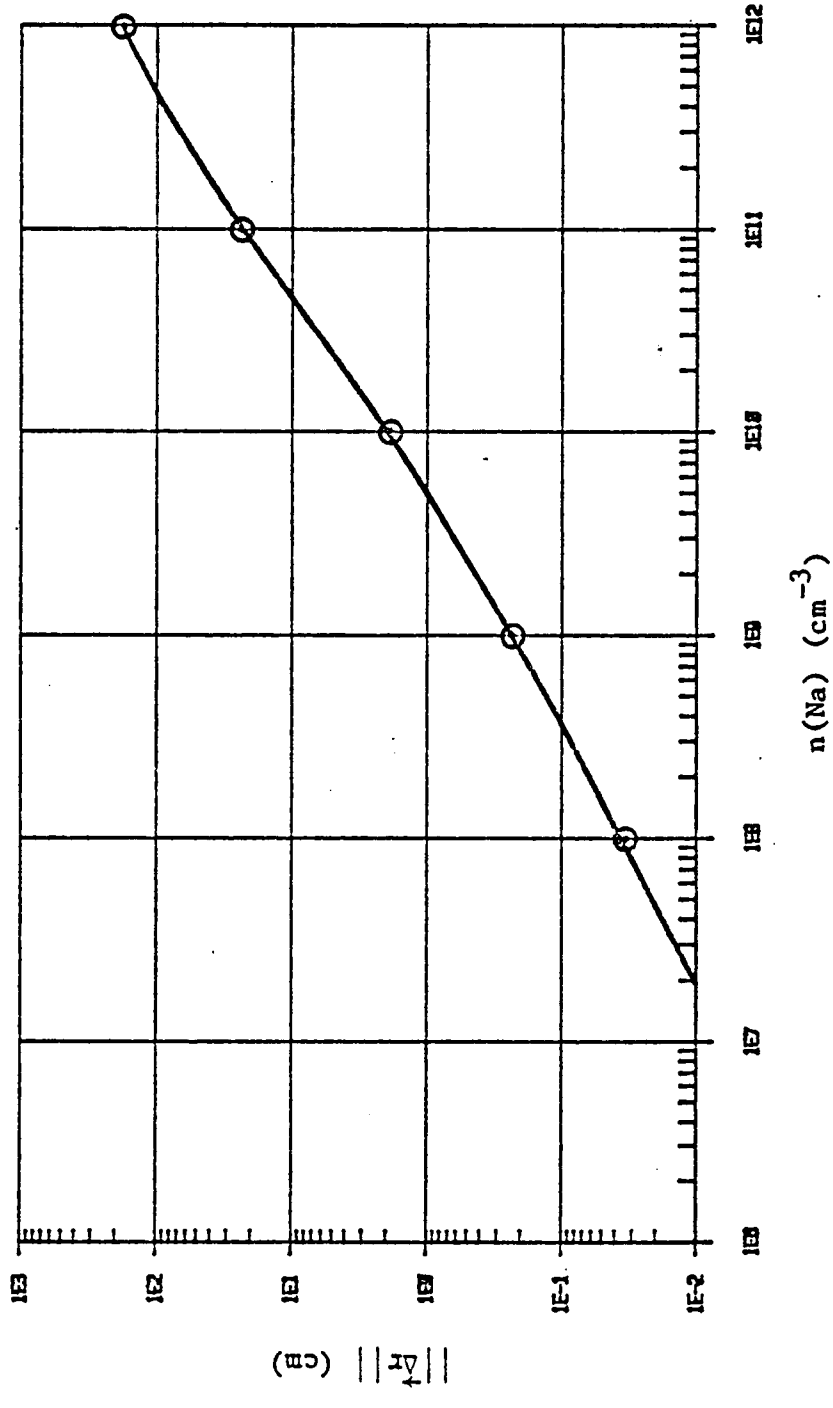

Figure 27. Line Plot of $||\vec{\Delta r}||$ vs n(Na) for $n(N_2) = 10^{21} cm^{-3}$, $E_o = 10^7$ ergs.

When the $n(N_2)$ was decreased to 10^{18} per cm^3 at 300K, the vibrational relaxation time, τ_v, increased to approximately 1.125 seconds. Temperature peaks occurred at ratios $t/\tau_v \simeq 0.09$, a significant decrease from the SM ratio. τ_v/τ_c increased to approximately 2450. Figure 28 is a graph showing $||\vec{\Delta r}||$ as a function of n(Na) for a nitrogen number density of 10^{18} per cm^3 and 1 watt of pump laser power. Measurable deflections ($>$ 1 μm) are calculated for n(Na) greater than 10^7 cm^{-3} (.01 ppb) peaking at approximately 10 ppb, and then decreasing quickly to non-measurable quantities for sodium number density ratios greater than 100 ppb.

From the data presented in Figures 19-28 and compiled as Tables 2-4, efficiency of the LIST method peaks at approximately $n(N_2) = 10^{19}$ cm^{-3}. Deflection peaks occur at about 10 ppb for $n(N_2) = 10^{18}$ cm^{-3}, 1 ppb for $n(N_2) = 10^{19}$ cm^{-3}, and about 1 ppb for $n(N_2) = 10^{21}$ cm^{-3} for those times where $\delta T/T < 0.1$ and with 10^7 ergs of pump laser energy. Efficiency can be improved by increasing pump laser energy, however saturation effects quickly begin to dominate at energies greater than 10^8 ergs violating the $\delta T/T$ restriction and decreasing the time in which the deflection measurement can be made.

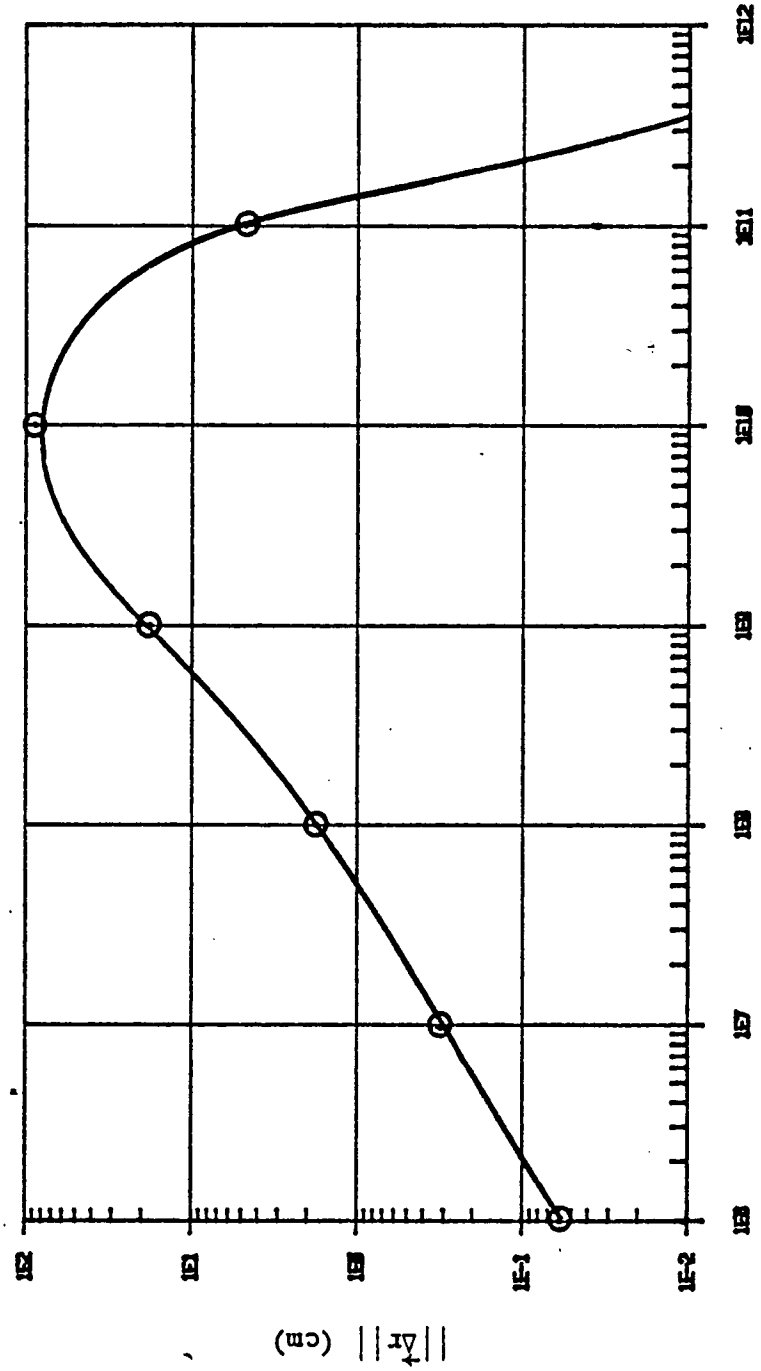

Figure 28. Line Plot of $||\vec{\Delta r}||$ vs n(Na) for $n(N_2) = 10^{18} cm^{-3}$, $E_o = 10^7$ ergs.

TABLE 2. Deflection Data for $n(N_2) = 10^{19}$ cm^{-3} and $E_o = 10^7$ ergs.

$n(Na)(cm^{-3})$	10^7	10^8	10^9	10^{10}	10^{11}	10^{12}
(ppb)	(.001)	(.01)	(.1)	(1.0)	(10.0)	(100.0)
t/τ_v	0.589	0.580	0.574	0.567	0.553	0.514
$\delta T/T$	6.62(-5)	6.67(-4)	6.16(-3)	5.02(-2)	4.62(-2)	2.27(-11)
τ_v/τ_c	23.0	23.4	23.7	23.9	24.5	26.4
$\|\| \vec{\Delta r} \|\|$	0.396	6.53	72.5	4.89(+2)	5.07(+2)	2.81(-7)

TABLE 3. Deflection Data for $n(N_2) = 10^{18}$ cm^{-3} and $E_o = 10^7$ ergs.

$n(Na)(cm^{-3})$	10^7	10^8	10^9	10^{10}	10^{11}
(ppb)	(0.01)	(0.1)	(1.0)	(10.0)	(100.0)
t/τ_v	9.85(-2)	9.49(-2)	8.89(-2)	8.78(-2)	8.63(-2)
$\delta T/T$	3.87(-5)	3.50(-4)	3.32(-3)	1.95(-2)	1.07(-3)
τ_v/τ_c	2.18(+3)	2.27(+3)	2.42(+3)	2.45(+3)	2.49(+3)
$\|\|\vec{\Delta r}\|\|$ (μm)	0.201	1.72	17.2	89.6	5.54

TABLE 4. Deflection Data for $n(N_2) = 10^{21}$ cm^{-3} and $E_o = 10^7$ ergs.

$n(Na)(cm^{-3})$	10^8	10^9	10^{10}	10^{11}	10^{12}
(ppb)	(.0001)	(.001)	(.01)	(.1)	(1.0)
t/τ_v	10.9	10.6	9.92	7.10	6.69
$\delta T/T$	1.24(-6)	1.24(15)	1.24(-4)	1.19(-3)	8.35(-3)
τ_v/τ_c	3.49(-3)	3.21(-3)	3.44(-3)	4.80(-3)	5.09(-3)
$\|\| \vec{\Delta r} \|\|$ (μm)	0.0307	0.2295	1.80	23.55	1.53(+2)

CHAPTER IV

CONCLUSIONS

An evaluation of LIST's feasibility in measuring trace species number density (n(trace)) may now be made using the theoretical calculations presented in this work. Results graphically presented in Fig. 18 through 23 and in Tables 2 through 4 demonstrate that LIST is theoretically capable of detecting a range of 0.001 ppb to 10 ppb of Na in an atmosphere which is predominately N_2. Similar sensitivities could be expected for any gas mixture where the pump laser is tunable to a spectral line of the trace species.

LIST calculations using the MRCM and DCM developed in this work are applicable to $n(N_2)$ values less than approximately $10^{20}cm^{-3}$. Its use is indicated especially for low $n(N_2)$ ($< 10^{19}cm^{-3}$) where the vibrational relaxation time, τ_v, ranges from 1 mS $< \tau_v <$ 1 sec. For N_2, this range of τ_v can be accomplished by introducing approximately 10 ppm of H_2O vapor into the atmosphere. Resonant energy transfer then reduces τ_v from a value in excess of 10^2 seconds to values in the desired range. A comparison of Tables 2, 3, and 4 indicates that as $n(N_2)$ increases by an order of magnitude, τ_v decreases and the heat conduction time, τ_c, each increase by an order of magnitude. Ratios of τ_v/τ_c decrease correspondingly indicating an increased dependence on the host gas relaxation processes. Large values of $n(N_2) > 10^{20}cm^{-3}$ enter the region where three-body collisions dominate; the two-body quenching rates used in the MRCM become invalid. Severe

decreases in τ_v which may occur in large $n(N_2)$ and high temperatures could shift the calculation into the acoustic domain of the pulse.

Laser radiation energy densities must remain below saturation energy for the given $n(N_2)$ to avoid population inversions. Restricting energy densities to the minimum required to produce a measurable deflection would also reduce the likelihood of a $\delta T/T$ violation. The LIST formulation requires that for large laser radiation energies ($> 10^8$ ergs/cm^3), deflection measurements must be made at times where $\delta T/T \leq 0.1$ is not violated. This decreases the time available for the measurement and introduces an unnecessary degree of uncertainty. Measurement times much below approximately 100 μs would approach the (forbidden) acoustic domain of the pulse.

As presented in the introduction, LIST in the thermal domain is also limited to static or slowly flowing gas samples. Convective transfer for $V_\infty \geq 0.1$ would distort the temperature field of the pump laser causing unpredictable deflection behaviour. Large values of V_∞ could be observed by decreasing τ_p and entering the acoustic domain of the pulse.

The method of applying LIST (composed of the MRCM and DCM) to a practical measurement of the number density n(trace) of a general trace species would be similar to the approach used in this paper. For given n(host) and pump laser characteristics, a set of deflection curves would be generated by varying n(trace) in the calculation. These curves could then be used to compare deflection measurements and obtain a measure of n(trace). Scanning the gas sample with a variable frequency laser source would allow a series of plots of laser fre-

quency versus deflection in the known n(host) at a measured time. Comparison of the deflection magnitudes at the respective laser frequency could then be used to determine both the amount and identity of the trace species in the sample.

Even though this work concentrated on the use of LIST for measurement of trace species number densities, the results could be of more general interest. Any procedure or technique which involves the intersection of laser beams could benefit from the temperature field calculations and deflection predictions. Spatial errors caused by deflections could be anticipated, predicted, and eliminated by the LIST technique.

BIBLIOGRAPHY

BIBLIOGRAPHY

1. Levenson, M. D. Introduction to Nonlinear Spectroscopy, Academic Press, New York 1982

2. Omenetto, N.; Analytical Laser Spectroscopy, Lohn Wiley and Sons, New York 1979

3. French, B. J.; "Continuum Source Molecular Beams", AIAA Journal, 3, 993-1000 (1965)

4. Pao, Y-H; Optoacoustic Spectroscopy and Detection, Academic Press, New York (1977)

5. Hermann, W. and Pohl, D. W.; "Trace Analysis in Gases by Laser-Induced Schlieren Technique", Infrared Physics, 19, 455-459, (1979)

6. Bailey, R. T. et al; "Pulsed Source Thermal Lens", J.C.S. Faraday II, 76, 633-647 (1980)

7. Kibble, B. P. et al; "Inelastic Collisions Between Excited Alkali Atoms and Molecules", Physicle Review, 159 no. 1, 11-13 (1967)

8. Hertel, I. V. et al; "Electronic to Vibrational Energy Transfer in the Differential Scattering of Na* by N_2 Molecules", Physical Review Letters, 36 no. 15, 861-863 (April 1976)

9. Anderson, John D.; Gasdynamic Lasers: An Introduction, Academic Press, New York (1976)

10. Campbell, D. H. and Lewis, J. W. L.; "Detailed Temporal Behavior of Laser Excited Sodium Tracer in Nitrogen and Application to Nitrogen Number Density Measurements at Low Densities", Applied Optics, 20, 4102-4109 (1981)

11. Born, M. and Wolf E.; Principles of Optics, Pergamon Press, New York (1975)

12. Barrow, Gordon M.; Introduction to Molecular Spectroscopy, McGraw Hill, New York, pp. 70-71 (1962)

13. Wallace, J. and Lilly, J. Q.; "Thermal Blooming of Repetively Pulsed Laser Beams", JOSA, 64, vol. 20, 1651-1655 (1974)

14. Taylor, R. L. and Bitterman, S.; "Survey of Vibrational Relaxation Processes Important in the CO_2-N_2 Laser System", Reviews of Modern Physics, 41 no. 1, (1967)

15. Kuhn, H. G.; Atomic Spectra, p. 152 ff., Academic Press, New York (1961)

16. Mitchell, Allan G. and Zenansky, Mark W.; Resonance Radiation and Excited Atoms, Cambridge Press, London (1961).

17. Kielkopf, J. F.; "New Approximation to the Voight Function with Applications to Spectral Line Profits Analysis", Journal of the Optical Society of America, 63 no. 8 (1973)

18. Drayson, S. R.; "Rapid Computation of the Voight Profile", Journal of Quantitative Spectroscopy and Radiational Transfer, 16, 611-614 (1976)

19. Jackson, J. D.; Classical Electrodynamics, John Wiley & Sons, New York, p. 155 (1975)

10. Vasil'ev, Lev A. (tans. by A. Baruch); Schlieren Methods, Ketter, Inc. (1971)

21. McQuarrie, D. A.; Statistical Mechanics, Harper & Row, New York, p. 223 (1976)

22. Mason, E. A. and Spurling, T. W.; The Virial Equation of State, Pergamon Press, Oxford (1969)

23. Wilson, A. H.; Thermodynamics and Statistical Mechanics, Cambridge, London, p. 225 (1966)

24. Gear, C. W.; Numerical Initial Value Problems in Ordinary Differential Equations, Prentice Hall, Englewood Cliffs, New Jersey, (1971)

APPENDIXES

APPENDIX A

Eikonal Equation

The eikonal equation is given by

$$d/ds\left(n(d\vec{r}/dx)\right) = \vec{\nabla}n$$

where in cylindrical coordinates

$$\vec{r} = \rho\hat{\rho} + z\hat{k} \quad .$$

Using the paraxial ray approximation which requires that the $\tan \alpha \approx \alpha$ where α is the interaction angle, this becomes

$$d/dz\left(n(d\vec{r}/dz)\right) = \vec{\nabla}n$$

For the cylindrically symmetric thermal lens,

$$\vec{\nabla}n = (\partial n/\partial \rho)\hat{\rho} + (\partial n/\partial z)\hat{k}$$

and

$$d\vec{r}/dz = (d\rho/dz)\hat{\rho} + \rho(d\hat{\rho}/dz) + (dz/dz)\hat{k} = z(d\hat{k}/dz) \quad .$$

Since $d\hat{\rho}/dz = \hat{\theta}(d\theta/dz)$ and $d\hat{k} = 0$,

$$d\vec{r}/dz = d\rho/dz\hat{\rho} + \rho(d\theta/dz)\hat{\theta} + \hat{k}$$

$$d/dz\left(n(d\vec{r}/dz)\right) = (d^2\rho/dz^2)\hat{\rho} + (d\rho/dz)(d\theta/dz)\hat{\theta} + (d\rho/dz)(d\theta/dz)\hat{\theta}$$

$$+ \rho(d^2\theta/dz^2)\hat{\theta} - \rho(d\theta/dz)^2\hat{\rho}$$

Consequently,

$$n\left[(d^2\rho/dz^2)\hat{\rho} + 2(d\rho/dz)(d\theta/dz)\hat{\theta} + \rho(d^2\theta/dz^2)\hat{\theta} - \rho(d\theta/dz)^2\hat{\rho}\right]$$

$$+ dn/dz\left[(d\rho/dz)\hat{\rho} + \rho(d\theta/dz)\hat{\theta} + \hat{k}\right] = (dn/d\rho)\hat{\rho} + (dn/dz)\hat{k}$$

which yields the following relations

$$n(d^2\rho/dz^2) - n\rho(d\Theta/dz)^2 + (dn/dz)(d\rho/dz) = dn/d\rho$$

$$n(d\rho/dz)(d\Theta/dz) + \rho n(d^2\Theta/dz^2) + (dn/dz)\rho(d\Theta/dz) \equiv 0$$

$$dn/dz = dn/dz \quad \text{(identity)}$$

Since $n = n_o + \delta n$ where $\delta n = -\Lambda\left((n_o - 1)/T\right)\delta T$ for isobaric heating of a gas sample of constant composition, with an imperfect gas coefficient Λ, the index of refraction, n, becomes

$$n = n_o - \Lambda\left((n_o - 1)/T\right)\delta T$$

giving the two gradients,

$$dn/dz = -\Lambda\left((n_o - 1)/T\right)\left(d(\delta T)/dz\right)$$

$$dn/d\rho = -\Lambda\left((n_o - 1)/T\right)\left(d(\delta T)/d\rho\right) \quad .$$

The two eikonal relations then become

$$\left[n_o - \Lambda\left((n_o - 1)/T\right)\delta T\right](d^2\rho/dz^2) - \Lambda\left((n_o - 1)/T\right)\left(d(\delta T)/dz\right)(d\rho/dz)$$

$$- \left[n_o - \Lambda\left((n_o - 1)/T\right)\delta T\right]\rho(d\Theta/dz)^2 + \left(\Lambda\left((n_o - 1)/T\right)\left(d(\delta T)/d\rho\right) = 0\right.$$

and

$$\left[n - \Lambda\left((n - 1)/T\right)\delta T\right]\rho(d^2\Theta/dz^2) + 2\left[n_o - \Lambda\left((n_o - 1)/T\right)\delta T\right]\left(\partial\rho/\partial z\right)(d\Theta/dz)$$

$$- \rho\Lambda\left[(n_o - 1)/T\right]\left(d(\delta T)/dz\right)(d\Theta/dz) = 0$$

To obtain the first-order, coupled differential equations required for the use of the GEAR routine let,

$$f_\rho = d\rho/dz \qquad f_\Theta = d\Theta/dz$$

$$A(\delta T) = \left[\Lambda\left((n_o - 1)/T\right)\left(d(\delta T)/dz\right)\right]/\left[n - \Lambda\left((n - 1)/T\right)\delta T\right]$$

and

$$B(\delta T) = \left[\Lambda\left((n_o - 1)/T\right)\left(d(\delta T)/d\rho\right)\right]/\left[n_o - \Lambda\left((n_o - 1)/T\right)\delta T\right].$$

Inclusion of f_ρ, f_Θ, $A(\delta T)$, and $\beta(\delta T)$ yields the following set of 1st order differential equations

$$df_\rho/dz = A(\delta T)f\rho + \rho f_\theta^2 - B(\delta T)$$

$$df_\theta/dz = A(dT)f_\theta - (2/\rho)f_\rho f_\theta$$

$$d\rho/dz = f_\rho$$

$$d\Theta/dz = f_\theta$$

which is of the form required for use in the GEAR routine.

APPENDIX B

Green's Function

I. The Green's Function for finite boundaries.

The inhomogeneous heat conduction equation is given by

$$\partial T/\partial t - (1/a^2)\nabla^2 T = \Theta(r,z,t)$$

where T is the temperature = T(r,z,t) and $\Theta(r,z,t)$ is the source function. If T is taken to be

$$T = T_\infty + \delta T$$

then the heat conduction equation becomes Bailey's equation 6

$$\partial \delta T/\partial t - (1/\alpha^2)\nabla^2 \delta T = \Theta(r,z,t) \quad .$$

To determine the general form of the Green's function used in the solution of the inhomogeneous heat conduction equation, first set up the homogeneous equation as

$$\partial \delta T/\partial t - (1/a^2)\nabla^2 \delta T = 0$$

For a cylinder with finite radius, b, and length, L, the homogeneous heat conduction equation in cylindrical coordinates is (letting $\psi = \delta T$)

$$\partial^2\psi/\partial r^2 + (1/r)(\partial\psi/\partial r) + \partial^2\psi/\partial z^2 = (1/\alpha)(\partial\psi/\partial t)$$

the boundary conditions of interest are

(1) $\partial\psi/\partial r + H_r\psi = 0$ at $r = b$ $t > 0$

(2) $-(\partial\psi/\partial z) + H_{z1}\psi = 0$ at $z = 0$ $t > 0$

(3) $\partial\psi/\partial z + H_{z2}\psi = 0$ at $z = L$ $t > 0$

(4) $\psi = f(r,z)$ at $t = 0$

The boundary conditions are of the third kind and may be reduced to the first kind by letting $H_i \to \infty$ or to the second kind by letting $H_i \to 0$. The most general case is the third kind which is convection by a surface into a region of constant temperature.[1]

Using separation of variables gives the solution in t, r, and z as

$$\psi(r,z,t) = R_o(\beta_m r)Z(n_p,z)e^{-\alpha(\beta_m{}^2 + n_p{}^2)t}$$

β_m and n_p are discrete because r and z boundaries are finite. Then

$$\psi(r,z,t) = \sum_{m=1}^{} \sum_{p=1}^{} Cmp\ R_o(\beta_m r)Z(n_p z)e^{-\alpha(\beta m^2 + n_p 2)t}$$

Using condition #(4) (t = 0) gives

$$f(r,z) = \sum_{m=1}^{} \sum_{p=1}^{} Cmp\ Ro(\beta_m r)Z(n_p,z)$$

now use the operators

$$\int_o^b rR_o(\beta_m r)dr$$

$$\int_o^L Z(n_p,z)dz$$

which gives

$$C_{mp} = \frac{1}{[N(\beta_m)N(n_p)]} \int_o^b dr \int_o^L dzrR_o(\beta_m r)z(n_p,z)f(r,z)$$

---

[1]The heat conduction problem as stated here is problem 6-13, page 243 in Osisik, M. N., Heat Conduction, John Wiley and Sons, N. Y. (1980). The solution is the author's.

to give

$$\psi(r,z,t) = \sum_{m=1}^{\infty} \sum_{p=1}^{\infty} \left(e^{-\alpha(\beta m^2 + np^2)t}/N(\beta_m)N(n_p)\right) R_o(\beta_m r) Z(n_p,z) \quad (x)$$

$$\int_o^b \int_o^L r\, R_o(\beta_m r') Z(n_p z') f(r',z') dr' dz' \quad .$$

Now use table 3-1 in Ozisik case 1 ($\nu = 0$) to get

$$R_o(\beta_m r) = J_o(\beta_m r)$$

and

$$1/\left(N(\beta_m\right) = 2/\left(J_o^2(\beta_m b)\right)\left[\beta_m^2/b^2(H^2 + \beta_m^2)\right]$$

with β_m being the roots of

$$\beta_m J_o'(\beta_m b) + H_r J_o(\beta_m b) = 0 \quad .$$

In a similar manner, use Ozisik's table 2-2 case 1

$$Z(n_p z) = n_p \cos n_p z + H_{z1} \sin n_p z$$

with

$$1/(N(n_p) = 2\left[(n_p^2 + H_{z1}^2)\left(L + H/(n_p^2 + H_{z2}^2)\right) + H_{z1}\right]^{-1}$$

and the roots n_p are

$$\tan n_p L = \left(n_p(H_{z1} + H_{z2})\right)/(n_p^2 + H_{z1}H_{z2}) \quad .$$

From equation 6-19 the homogeneous part of the equation is written as

$$\psi(\vec{r},t) = \int_A G(\vec{r},t \mid \vec{r}'\tau) \mid f(\vec{r}')dA' \quad .$$

In cylindrical coordinates $dA = drdz$ giving

$$\psi(r,z,t) = \int_o^b dr' \int_o^L dz'\ G(r,z,t \mid r',z',\tau) \mid \quad f(r',z') \quad .$$

Comparing the $\psi(r,z,t)$ gives

$$G(r,z,t \mid r',z',\tau) = \sum_{\tau=1}^{\infty} \sum_{m=1}^{\infty} \sum_{p=1}^{\infty} \frac{e^{-\alpha(\beta_m^2 + n_p^2)t}}{N(\beta_m)N(n_p)} R_o(\beta_m r) z(n_p z) r' R_o(\beta_m r') z(n_p z')$$

or the general green's function

$$G(r,z,t \mid r',z',\tau) = \sum_{m=1}^{\infty} \sum_{p=1}^{\infty} \frac{r' e^{-\alpha(\beta_m^2 + n_p^2)(t - \psi)}}{N(\beta_m)N(m_\rho)} R_o(\beta_m r) R_o(\beta_m r') \quad (x)$$

$$Z(n_p z) Z(n_p z') \quad .$$

Assuming that homogeneous boundary conditions apply (i.e. no variation in the boundary temperatures) and taking $f(r,z)$ to be 0 throughout the region $(T \rightarrow T - T_\infty)$.

$$\delta T(r,z,t) = \frac{\alpha}{k} \int_o^t dt' \int_o^b \phi\theta' \, \& \int_o^L dz' \; G(r,z,t \mid r',z',t') \theta(r',z',t') \quad .$$

Now placing the Green's function value into $\delta T(r,z,t)$ gives the expression

$$\delta T(r,z,t) = \frac{\alpha}{k} \sum_m \sum_p \frac{R_o(\beta_m r) Z(n_p z)}{N(\beta_m)N(n_p)} \int_o^t dt' \int_o^b r' dr' \int_o^L dz' R_o(\beta_m r') Z(n_p, t') \quad (x)$$

$$e^{-\alpha(\beta_m^2 + n_p^2)(t - t')} g(r',z',t') \quad .$$

Using the relations

$$R_o(\beta_m r) = J_o(\beta_m r)$$

$$Z(n_p z) = n_p \cos n_p z + H_z \sin n_p z$$

$$\frac{1}{N(\beta_m)} = \frac{2}{J_o^2(\beta_m b)} \left[\frac{\beta_m^2}{b^2(H^2 + \beta_m^2)} \right]$$

$$\frac{1}{N(n_p)} = \frac{2}{\left[(n_p^2 + H_{z1}^2)\left(L + H_{z2}/(n_p^2 + H_{z2}^2)\right) + H_{z1}\right]}$$

the temperature rise, $\delta T(r,z,t)$, for a finite cylinder becomes

$$\delta T(r,z,t) = \frac{\alpha}{k} \sum_m^{\infty} \sum_p \frac{4J_o(\beta_m r)(n_p \cos n_p z + H_{z1} \sin n_p z)\beta_m^2}{[J^2(\beta b)b^2 E(H^2+\beta^2)]\left[(n^2+H^2)\left(L+\frac{z2}{(n_p^2+H_{z2}^2)}\right) + H_{z1}\right.}$$

$$(x) \int_o^t \phi\tau' \int_o^b r' dr \int_o^L dz' \left[J_o(\beta_m r')[n_p \cos n_p z' + H_{z1} \sin n_p z'\right] \quad (x)$$

$$e^{-\alpha(\beta_m^2 + n_p^2)(t - t')} \theta(r', z', t')]$$

II. The Green's function for semi-infinite boundaries.

From Section I the general Green's function is

$$G(r,z,t \mid r',z',t') = \sum_{m=1}^{\infty} \sum_{p=1}^{\infty} \frac{r' e^{-\alpha(\beta_m^2 + n_p^2)(t - t')}}{N(\beta_m)\, N(n_p)} \quad . \quad (x)$$

$$R_o(\beta_m r) R_o(\beta_m r') Z(n_p z) Z(n_p z') \quad .$$

For Bailey's Green's function the limits on r and z must become semi-infinite; i.e. $0 < r < \infty$ and $0 < z < \infty$. As r and z become semi-infinite, the Fourier component goes from discrete to continuous,[2] so that

$$G(r,z,t \mid r',z',t') = \int_o^{\infty} d\beta \int_o^{\infty} dn \left[\frac{r' e^{-\alpha(\beta^2 + n^2)(t - t')}}{N(\beta)N(n)} \quad (x)\right.$$

$$R_o(\beta r) R_o(\beta r') Z(nz) Z(nz')]$$

---

[2] Ozisik, M. N.; Heat Conduction, John Wiley & Sons, N.Y., p. 113, (1980).

The radial solution $R_o(\beta r)$ requires that at r = 0 no singularities occur, therefore

$$R_o(\beta r) = J_o(\beta r)$$

and the solution along the z axis becomes for the semi-infinite case using Ozisik's table 2-3, case 3

$$Z(n,z) = \sin nz \quad \text{with} \quad \frac{1}{N(n)} = \frac{2}{\pi}$$

the z axis integration becomes

$$F(z) = \frac{2}{\pi}\int_o^\infty e^{-\alpha n^2(t - t')} \sin nz \sin nz' dn$$

or

$$F(z) = \frac{1}{(4\pi\alpha(t - t'))_{1/2}}\left[\exp\left(-\frac{(z - z')^2}{4\alpha(t - t')}\right)\right.$$

$$\left.\exp\left(-\frac{(z + z')^2}{4\alpha(t - t')}\right)\right] \quad .$$

Rearranging terms yields

$$F(z) = \frac{1}{(4\pi\alpha t)^{1/2}}\exp\left[-\frac{(z - z')^2}{4\alpha(t - t')}\right]\left[1 - \exp\left[-\left(\frac{1}{4\alpha t}\right)\left(\frac{1 + z'/z}{1 - z'/z}\right)\right]\right] \quad .$$

The normalization of the radial $N(\beta)$ yields

$$N(\beta) = \int_o^\infty r' J_o(\beta r') J_o(\beta r') dr' \equiv \frac{1}{\beta}$$

to give for the radial portion of the Green's function

$$F(r) = \int_o^\infty \beta e^{-\alpha\beta^2(t-t')} J_o(\beta r) J_o(\beta r') d\beta$$

where $R_o(\beta i)$ is replaced by $J_o(\beta i)$ to insure non-singular behaviour at $\beta = 0$. This integral is standard; evaluating it yields

$$F(r) = \frac{1}{4\pi\alpha(t-t')} e^{-(r^2 + r'^2)/4\alpha(t - t')} I_o\left(\frac{rr'}{2\alpha(t - t')}\right) .$$

For semi-infinite limits, the Green's function then becomes

$$G(r,z,t \mid r',z',t') = \frac{1}{(4\pi\alpha(t - t')^{3/2}} \exp\left[-\left(\frac{z - z'}{4\alpha(t - t')}\right)^2\right]$$

$$\left\{1 - \exp\left[-\frac{1}{4\alpha(t - t')}\left(\frac{1 + z'/z}{1 - z'/z}\right)\right]\right\}\exp\left\{-\frac{(r^2 + r'^2)}{4\alpha(t - t')}\right\} I_o\left(\frac{rr'}{2\alpha(t - t')}\right) .$$

In the narrow region around $z \approx z'$ and with

$$\frac{rr'}{2\alpha(t - t')} >> 0$$

the Green's function then becomes

$$G(r,z,t \mid r',z',t') = \frac{1}{\left(4\pi\alpha(t - t')\right)^{3/2}} \exp\left[-\frac{(z - z')^2}{4\alpha(t - t')}\right] \quad (x)$$

$$\exp\left[-\frac{(r - r')^2}{4\alpha(t - t')}\right]$$

which is Bailey's Green's function.

APPENDIX C

Voight profile and Laser Lineshape

I. Normalization of the Voight Laser Convolution.

As stated in the text the normalized laser/Voight convolution is given by

$$F(\nu_{o\ell},\nu_{og}) = \frac{\Delta\nu_s}{\Delta\nu_L\Delta\nu_g\pi^2}\int_{-\infty}^{\infty}\int \frac{\exp\left(-\left(\frac{\nu-\nu_{o\ell}}{\Delta\nu_L}\right)^2\right)\exp\left(-\left(\frac{\nu'}{\Delta\nu_g}\right)^2\right)d\nu' d\nu}{[\Delta\nu_s{}^2 + (\nu - \nu_{og} - \nu')^2]}$$

To see that this is a normalized convolution, rearrange the integrals as

$$F(\nu_{o\ell},\nu_{og}) = \frac{a}{\Delta\nu_g\pi^2}\int_{-\infty}^{\infty}\int \frac{\exp(-y^2)\exp(-x^2)}{\left[a^2 + \left(\frac{\Delta\nu_L}{\Delta\nu_g}y - \frac{\beta_{LG}}{\Delta\nu_g} - x\right)^2\right]}\,dxdy$$

where $a = \frac{\Delta\nu_s}{\Delta\nu_g}$ $\quad x = \frac{\nu'}{\Delta\nu_g}$ $\quad y = \frac{\nu - \nu_{o\ell}}{\Delta\nu_L}$ $\quad \beta_{LG} = \nu_{og} - \nu_{o\ell}$

this double integral is the overlapping area of the two functions being convoluted. Figures 7, 8, and 9 are plots of the integral showing the gas line functions and the laser lineshape. Areas overlapping represent $F(\nu_{o\ell},\nu_{og})$.

To check that the entire area from $-\infty$ to $+\infty$ is actually normalized to 1.0 integrate over Z where $Z = \beta_{LG}/\Delta\nu_g$ and $b = \Delta\nu_L/\Delta\nu_g(y - x)$,

$$\frac{a}{\pi^2}\int_{-\infty}^{\infty}\int_{-\infty}^{\infty}\int_{-\infty}^{\infty} \frac{\exp(-y^2)\exp(-x^2)dxdydZ}{[a^2 + (Z - b)^2]}$$

Following the Z integration which is a standard integral, this becomes

$$\frac{1}{\pi}\int_{-\infty}^{\infty}\int_{-\infty}^{\infty}\exp(-x^2)\exp(-y^2)dxdy$$

the value of which is 1.0; the Voight/Laser convolution is properly normalized.

B. Approximations for the Voight/Laser Function.

Using Kielkopf's arrangement of the Voight[1] the laser/Voight looks like

$$F(\nu_{o\ell},\nu_{og}) = \int_{-\infty}^{\infty} d\nu\ \exp\left(-\left(\frac{\nu-\nu_{o\ell}}{\Delta\nu_L}\right)^2\right)\int_{-\infty}^{\infty} d\nu'\ \frac{\Delta\nu_s/\pi}{[\Delta\nu^2+(\nu-\nu_{og}-\nu')^2]}\ (x)$$

$$\left(\frac{1}{\Delta\nu_g\sqrt{\pi}}\right)\exp\left(-\left(\frac{\nu'}{\Delta\nu_g}\right)^2\right)$$

Kielkopf derives an approximation to the Voight function

$$g(\nu,\nu_{og}) = I(a)\left[(1-y)\exp\left(-\left(\frac{\nu\nu_{og}}{\Delta\nu_V}\right)^2 1nz\right) + \eta\left(\frac{1}{1+\left(\frac{\nu\nu_{og}}{\Delta\nu_V}\right)^2}\right]\right.$$

where in Kielkopf's notation

$$a = \frac{\Delta\nu_s}{\Delta\nu_g}$$

$$\eta = \frac{\ell}{\ell + g^2}$$

[1] Kielkopf, J. F.; "New Approximation to the Voight Function with Applications to Spectral Line Profile Analysis", Journal of the Optical Society of America, vol 63 no. 8 (1973).

$$I(a) = \frac{a}{\sqrt{\pi}\ \Delta\nu_s} \exp(a^2)\mathrm{erfc}(a)$$

$$\Delta\nu_V = \Delta\nu_{s/\ell}$$

$$g^2 = \frac{(1 - \ell)}{\ln 2}$$

$$\ell = 2/\{1 + \varepsilon\ln 2 + [(1 - \varepsilon\ln 2)^2 + (4\ln 2/a^2)]\ \}^{1/2}$$

$$\varepsilon = 0.0990$$

According to the evaluation of Hui,[2] Kielkopf's approximation is valid only for regions where $a < 2.5$ or near the peak of the Voight curve. Six significant figures can be obtained in this region, but when $a \geq 6.0$ or $\nu \geq |\beta_{LG} \mp 6\Delta\nu|$ (near the wings of the Voight), accuracy drops to only one significant figure. Using a Hermite integration for the $d\nu$ integral yields a highly accurate solution for small a or near the peak of the curve. This will be referred to as the Hermite-Kielkopf integration (H-K).

For those regions where $a > 2.5$ or in the wing regions of the curve, a straight-numerical integration works quite well. This solution using Hermite-Gaussian for both integrations will be referred to as Hermite-Hermite (H-H) integration.

Using these two methods, the Voight/Laser convolution may be accurately determined for each spectral line center.

---

[2]Hui, A. K. et al; "Rapid Computation of the Voight and Complex Error Functions," JQSRT, 19, 513 (1978).

III. Determining the Linewidths

The linewidths entering the Voight/laser convolution are the Doppler linewidth, $\Delta\nu_g$, the natural linewidth, $\Delta\nu_N$, the pressure linewidth, $\Delta\nu_p$, and the laser linewidth, $\Delta\nu_L$. Of the four, only $\Delta\nu_L$ is considered to be known a priori. The other three are functions of the temperature.

The doppler linewidth is given by the full width of the doppler lineshape at half maximum (FWHM). Utilizing a doppler lineshape as[3]

$$g_d(\nu,\nu_{og}) = \exp\left[-\frac{(\nu - \nu_o)^2 mc^2}{2\nu_o{}^2 kT} \right]$$

where ν_o is the linecenter of the profile, m is the mass of the gas molecules, c is the speed of light, k is Boltzman's constant and T is the temperature. Setting this equal to 0.5 and solving for $(\nu - \nu_o)^2$ gives

$$(\nu - \nu_o)^2 = 8\left(\frac{\nu_o{}^2 kt}{mc^2}\right)\ln 2$$

which is $\Delta\nu_g$, the doppler linewidth

$$\Delta\nu_g = 2(\nu_o/c)(kT/m)^{1/2}2\ln 2$$

evaluating the constants with $M = (6.0223 \times 10^{23})m$ where M is the molecular weight of the molecule gives

$$\Delta\nu_g = 7.1615 \times 10^{-7}(T/M)^{1/2}$$

---

[3]Mitchell, Allan G. and Zenansky, Mark W.; Resonance Radiation and Excited Atoms, Cambridge Press, London (1961).

Similarly, the pressure linewidth can be evaluated by calculating the Lorenz function at half maximum. The pressure linewidth is given by

$$g_p(\nu,\nu_o) = \frac{1}{[1 + [2\pi\tau(\nu - \nu_o)]^2]}$$

or

$$1 + [2\pi\tau(\nu - \nu_o)]^2 = 2$$

gives

$$2\pi\tau(\nu - \nu_o) = 1$$

and

$$\Delta\nu = \frac{1}{2\pi\tau} \quad (hz)$$

The mean time between collisions, τ, may be evaluated using Davidson's treatment,[4]

$$1/\tau = (2.753 \times 10^{12})(T/M)^{1/2}D^2N_i$$

where N_i is the mole fraction of the i^{th} species and D^2 is the collision cross section. Campbell and Lewis[5] give the cross section as 6.708×10^{-8}cm and 4.47×10^{-8}cm for N_2 at 300K and 2,000K respectively. For the Na-N_2 mixture $N_{N_2} \simeq 1.0$ and $N_{Na} \simeq 0.0$.

For Na, the Einstein A coefficient for the doublet 3^2P states is given by ref. 5 as $A = 6.13 \times 10^7$ sec $^{-1}$. Natural broadening is the

---

[4]Davidson, N.; Statistical Mechanics, pp. 162-164, McGraw Hill, New York (1962).

[5]Campbell, D. H. and Lewis, J. W. L.; "Detailed Temporal Behavior of Laser Excited Sodium Tracer in Nitrogen and Application to Nitrogen Number Density Measurements at Low Densities", Applied Optics, vol. 20 pp. 4102-4109 (1981).

lifetime of the 3^2P states given by the lorentzian function above with

$$1/\tau = A$$

so that

$$\Delta\nu_N = A/2\pi = 9.756 \times 10^6 \quad \text{(hz)}$$

The lorentzian linewidth, $\Delta\nu_s$, is then simply

$$\Delta\nu_s = \Delta\nu_N + \Delta\nu_p$$

Since $\Delta\nu_g$ and $\Delta\nu_p$ are both dependent on the square root of the temperature it is necessary to see what change in the linewidths accompany a change in the temperature. As shown in Figs. 29a and 29b neither $\Delta\nu_p$ nor $\Delta\nu_g$ vary more than 5% over a temperature range of 250K to 2000K. The temperature dependent linewidths may then be taken as constant for the deflection calculation.

Figure 29. Lorentzian and Doppler Linewidths vs Temperature. (a) $\Delta\nu_s$ (Lorentzian) for (solid) $n(N_2) = 10^{21}$ cm^{-3},(long broken) $n(N_2) = 10^{20}$ cm^{-3}, (mixed broken) $n(N_2) = 10^{19}$ cm^{-3} and (short broken) $n(N_2) = 10^{18}$ cm^{-3} vs Temperature, (b) $\Delta\nu_g$ (Doppler) linewidth

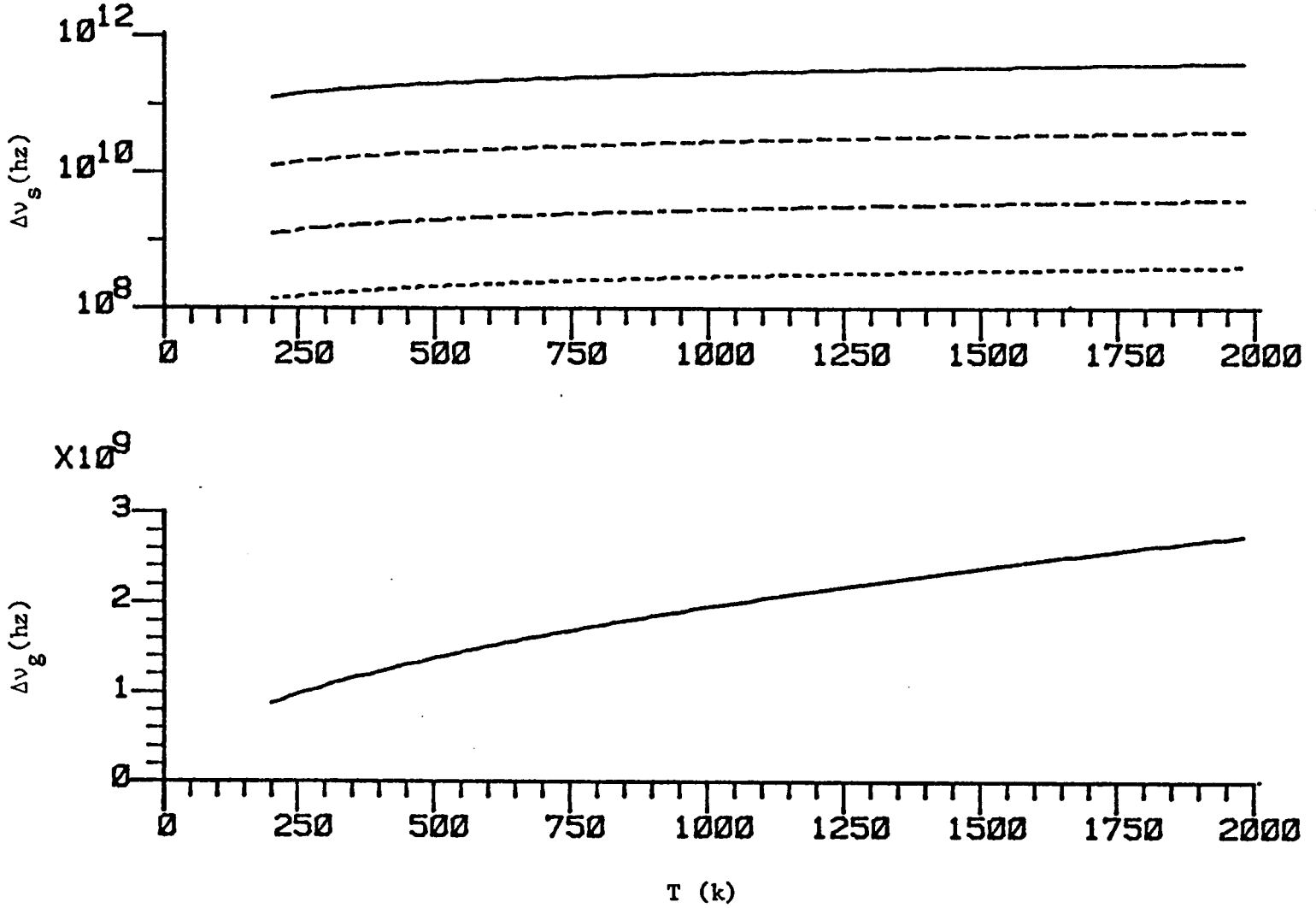
10^{12}
10^{10}
10^{8}
$\Delta\nu_s$ (hz)
0
250
500
750
1000
1250
1500
1750
2000
X10^{9}
3
2
1
0
$\Delta\nu_g$ (hz)
0
250
500
750
1000
1250
1500
1750
2000
T (k)

Figure 29.

APPENDIX D

Pulse Shape Function

Formation of the pump laser pulse is accomplished by using the difference between two Heaviside functions. The basic functional form is

$$A(t) = \tanh\left(\frac{Wt}{10\tau_p}\right) - \tanh\left(\frac{W(t - \tau_p)}{10\tau_p}\right)$$

where τ_p is the pulse width at FWHM in seconds, t is the time in the pulse, and W is a weighting function used to alter the pulse shape. Direct calculation of A(t) is not satisfactory, however, since the values are centered about t = 0 and are not usefully normalized. Since the solution for $\delta T(r,z,t)$ is numerical, array $\tilde{A}(t)$ is generated and stored to provide the proper shaping for a single pulse.

If X_{max} and X_{min} represent the calculated maximum and minimum values of A(t), then $\tilde{A}(t)$ may be formed by first normalizing with,

$$\tilde{A}(t) = 1 - \frac{\left(X_{max} - A(t)\right)}{\left(X_{max} - X_{min}\right)} \quad .$$

Numerical shifting of the array such that the first non-zero value of $\tilde{A}(t)$ falls at t = 0 is then accomplished. The result is a pulse shape dependent on the value of W. Gaussian-like pulse shapes may be obtained for $20 \simeq W \simeq 100$ while square waves are generated for $W > 100$. FWHM of the waveform remains constant for a given τ_p. Linear interpolation between $\tilde{A}(t_i)$ and $\tilde{A}(t_{i-1})$ are used to calculate values of t such that $t_{i-1} < t < t_i$. Use of $\tilde{A}(t)$ in the δT derivation

in section IIB assumes this numerical interpolation procedure. Figures 30a, b, c, and d show the resulting waveform for various values of W, and τ_p = 1 msec.

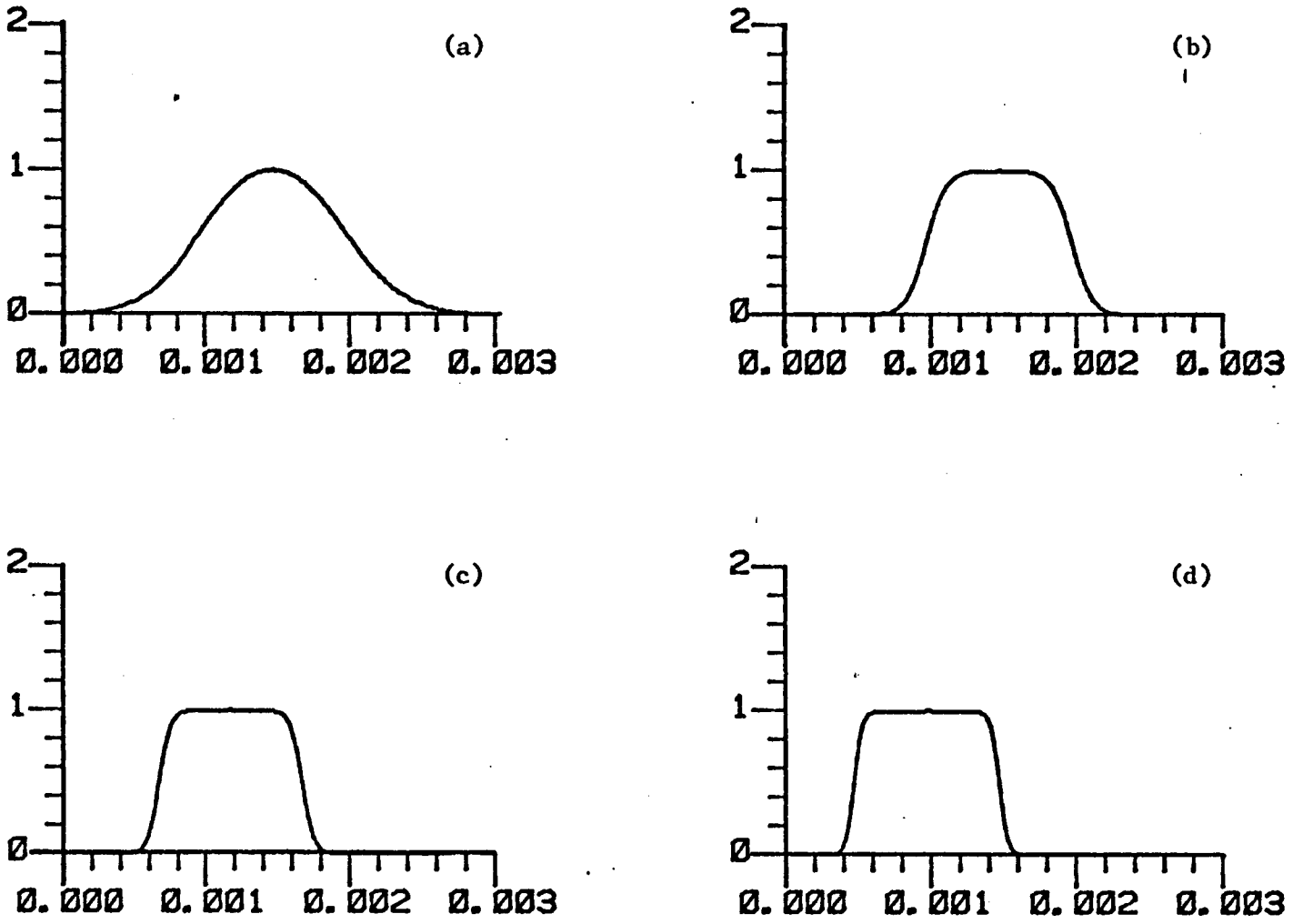

Figure 30. Pulse Shape Function for τ_p = 1 mS (a) W = 25, (b) W = 75, (c) W = 125, (d) W = 175

VITA

James D. Selman, Jr. was born in Chattanooga, Tennessee on November 15, 1950. He graduated from Huntsville High School in Huntsville, Alabama, in May 1969. In December 1973 he was commissioned as a Second Lieutenant in the U.S. Army upon his graduation from Jacksonville State University in Jacksonville, Alabama. During his tour with the U.S. Army, Mr. Selman earned a Master of Engineering Degree from Boston University. After six years with the Army, he entered the Graduate School of The University of Tennessee, Knoxville.

He is married to the former Pamela Ann Byrom of Jacksonville, Alabama, and has two children, Jason and Jesse.

Mr. Selman is a member of Sigma Pi Sigma and the American Physical Society. After graduation he will continue to pursue graduate studies with The University of Tennessee.